geodiversitas

2022 • 44 • 30

The discovery of a Balaenomorpha (*Persufflatius renefraaijeni* n. gen., n. sp.) from the upper Miocene of the Netherlands sheds new light on the cranial anatomy of archaic rorqual relatives

Mark BOSSELAERS & Dirk K. MUNSTERMAN

art. 44 (30) — Published on 27 October 2022
www.geodiversitas.com

PUBLICATIONS SCIENTIFIQUES

MUSÉUM NAL HIST NATURELLE

Geodiversitas est indexé dans / Geodiversitas *is indexed in:*
– Science Citation Index Expanded (SciSearch®)
– ISI Alerting Services®
– Current Contents® / Physical, Chemical, and Earth Sciences®
– Scopus®

Geodiversitas est distribué en version électronique par / Geodiversitas *is distributed electronically by:*
– BioOne® (http://www.bioone.org)

Les articles ainsi que les nouveautés nomenclaturales publiés dans *Geodiversitas* sont référencés par / *Articles and nomenclatural novelties published in* Geodiversitas *are referenced by:*
– ZooBank® (http://zoobank.org)

Geodiversitas est une revue en flux continu publiée par les Publications scientifiques du Muséum, Paris
Geodiversitas *is a fast track journal published by the Museum Science Press, Paris*

Les Publications scientifiques du Muséum publient aussi / *The Museum Science Press also publish:* ***Adansonia***, ***Zoosystema***, ***Anthropozoologica***, ***European Journal of Taxonomy***, ***Naturae***, ***Cryptogamie*** **sous-sections** ***Algologie***, ***Bryologie***, ***Mycologie, Comptes Rendus Palevol***

Diffusion – Publications scientifiques Muséum national d'Histoire naturelle
CP 41 – 57 rue Cuvier F-75231 Paris cedex 05 (France)
Tél. : 33 (0)1 40 79 48 05 / Fax : 33 (0)1 40 79 38 40
diff.pub@mnhn.fr / http://sciencepress.mnhn.fr

ISSN (imprimé / *print*) : 1280-9659/ ISSN (électronique / *electronic*) : 1638-9395

The discovery of a Balaenomorpha (*Persufflatius renefraaijeni* n. gen., n. sp.) from the upper Miocene of the Netherlands sheds new light on the cranial anatomy of archaic rorqual relatives

Mark BOSSELAERS
O. D. Aarde en Historie van het Leven, Koninklijk Belgisch Instituut voor Natuurwetenschappen.
Vautierstraat, 29, B-1000 Brussel (Belgium)
and Koninklijk Zeeuwsch Genooschap der Wetenschappen,
Koudsteensedijk 7, NL-4331 JE Middelburg (the Nederlands)
mark.bosselaers@telenet.be (corresponding author)

Dirk K. MUNSTERMAN
Toegepast Natuurwetenschappelijk Onderzoek
(TNO-Netherlands Organization for Applied Scientific Research),
Geological Survey of the Netherlands, Utrecht (the Netherlands)

Submitted on 24 December 2021 | accepted on 2 April 2022 | published on 27 October 2022

urn:lsid:zoobank.org:pub:DC16419D-DD62-4E4E-B713-A0A18553302B

Bosselaers M. & Munsterman D. K. 2022. — The discovery of a Balaenomorpha (*Persufflatius renefraaijeni* n. gen., n. sp.) from the upper Miocene of the Netherlands sheds new light on the cranial anatomy of archaic rorqual relatives. *Geodiversitas* 44 (30): 933-973. https://doi.org/10.5252/geodiversitas2022v44a30. http://geodiversitas.com/44/30

ABSTRACT
A basal member of Balaenomorpha (Cetacea, Mysticeti), *Persufflatius renefraaijeni*, n. gen., n. sp., is described based on cranial material discovered in upper Miocene deposits of Liessel (the Netherlands). Thanks to the palynological analysis of an associated sediment sample, the specimen is dated from the late Tortonian (Dinozone SNS M14: *c.* 8.2-7.6 Ma). Our phylogenetic analysis recovers the new taxon at the base of the successful crown mysticete clade leading to modern rorquals. Though the holotype is only partially preserved (it consists of the partial right side of the neurocranium), it provides new data on the cranial anatomy of these early relatives of extant rorquals, which are poorly represented in the global fossil record. Several skull parts (postglenoid process of the squamosal, base of the zygomatic process of the squamosal, the anteromedioventral portion of the squamosal bone, and the exoccipital) show unusual swelling due to pachyostosis, giving the whole lateral basicranial region an inflated aspect.

KEY WORDS
Tortonian,
Liessel,
the Netherlands,
early Balaenomorpha,
phylogeny,
rorqual lineage,
pachyostosis,
cranial endocast,
new genus,
new species.

RÉSUMÉ
*La découverte d'un Balaenomorpha (*Persufflatius renefraaijeni *n. gen., n. sp.) du Miocène supérieur des Pays-Bas apporte un éclairage nouveau sur l'anatomie crânienne de parents anciens des rorquals.*
Un Balaenomorpha (Cetacea, Mysticeti) basal, *Persufflatius renefraaijeni* n. gen., n. sp., est décrit à partir de matériel crânien découvert dans des dépôts du Miocène supérieur à Liessel (Pays-Bas). Grâce à l'analyse palynologique d'un échantillon de sédiment associé au spécimen, celui-ci est plus précisément daté du Tortonien supérieur (Dinozone SNS M14: *c.* 8.2-7.6 Ma). Dans notre analyse phylogénétique, le nouveau taxon se positionne à la base du clade diversifié menant aux rorquals modernes. Malgré son état fragmentaire (seule la partie droite du basicrâne est préservée), l'holotype améliore notre connaissance de l'anatomie crânienne de ces parents anciens des rorquals actuels, qui sont relativement mal représentés dans le registre fossile. Plusieurs régions du crâne (le processus post-glénoïde du squamosal, la base du processus zygomatique du squamosal, la portion antéro-médioventrale du squamosal, et l'exoccipital) montrent un renflement inhabituel (pachyostose) qui donne à l'ensemble de la partie latérale du basicrâne un aspect boursouflé.

MOTS CLÉS
Tortonien,
Liessel,
Pays-Bas,
Balaenomorpha basaux,
phylogénie,
lignée des rorquals,
pachyostose,
moulage endocrânien,
genre nouveau,
espèce nouvelle.

INTRODUCTION

In the easternmost parts of the Netherlands, Miocene strata are present just below the surface. Many cetacean remains have been found especially during the 19th and 20th century, but collecting fossils from these outcrops is hardly possible at present. Luckily, construction sites and trailing or mining activities regularly bring Dutch (whale) fossils to the surface. One of the most famous sites that produced many important whale fossils over a long period of time, was the Hoogdonk brick and cement factory at the border of the communities of Liessel and Deurne (Fig. 1). Many Dutch amateur palaeontologists collected fossils there during the period 1970-2002 (Peters 2009). The site is known for its well-preserved fossils of cetaceans and over the last few years, some of these earlier finds have finally been published (e.g. the cetotheriid *Metopocetus hunteri* Marx, Bosselaers & Louwye, 2016 and the balaenopterid *Archaebalaenoptera liesselensis* Bisconti, Munsterman, Fraaije, Bosselaers & Post, 2020). In this article, we describe one of the more early branching, non balaenid, diminutive balaenomorpha from the southern North Sea Basin, based on a specimen uncovered at the same locality. Even though the neurocranium of the type and only known specimen representing this new genus and species is only partially preserved, it clearly represents a type of baleen whale from a poorly represented group of basal non-balaenid mysticetes. Furthermore it is noteworthy that some skull bones show pachyostosis. The cranial side of the braincase is well preserved. This aspect is often overlooked and rarely dealt with in studies of fossil whales. We decided to make a cranial endocast in order to study the brain imprint and anatomy more in detail.

Non-pathological pachyostosis is common in marine mammals, especially during the first stages of their evolution, when their adaption to life in the water is incomplete (Houssaye *et al.* 2015). In later stages, for example in crown cetaceans, the skeleton often becomes lighter. Most research on pachyostosis was performed on postcranial material (de Buffrénil *et al.* 1990; de Buffrénil *et al.* 2000; de Ricqlès & de Buffrénil 2001; Thewissen *et al.* 2007; de Buffrénil & Lambert 2011; Lambert *et al.* 2011; Amson *et al.* 2014; Houssaye *et al.* 2015; Amson *et al.* 2018; Dewaele *et al.* 2019, 2021), although some publications have addressed secondary skull adaptations (de Ricqlès & de Buffrénil 2001; de Buffrénil & Lambert 2011; Gol'din 2014; Amson *et al.* 2018). In first instance, pachyostosis is an adaptation to the aquatic environment and no doubt the extra weight helps to keep the animals submerged and balanced. But even crown cetaceans often display some kind of bone swelling and/or densification, the function of which is not clear in many cases; for example, thickening of rostral bones is common in ziphiids (beaked whales) and could be linked to deep diving or even to species, sex and/or age recognition (de Buffrénil & Casinos 1995; de Buffrénil *et al.* 2000; Lambert *et al.* 2011; Gol'din 2014). In addition to the bone thickening in the new genus and species described in this work, we also report on and discuss bone thickening in a series of extinct mysticetes.

MATERIAL AND METHODS

Institutional abbreviations

CASG	California Academy of Sciences, San Francisco, California, United States;
GMNH	Gunma Museum of Natural History, Gunma, Japan;
HMN	Hiwa Museum for Natural History, Hiroshima, Japan;
IGPS	Institute of Geology and Paleontology, Faculty of Science, Tohoku University, Sendai, Japan;
IRSNB	Institut royal des Sciences naturelles de Belgique – Koninklijk Belgisch Instituut voor Natuurwetenschappen, Brussels, Belgium;
MAB	Oertijdmuseum, Boxtel, the Netherlands;
MFM	Mizunami Fossil Museum, Mizunami City, Gifu, Japan;
MLP	Museo de La Plata, La Plata, Argentinia;
MNHN	Muséum national d'Histoire naturelle, Paris, France;
MSM	Museum Sønderjylland, Department Natural History and Palaeontology, Gram, Denmark;
SMNH	Saitama Museum of Natural History, Chichibu District, Saitama, Japan;
SMNK	Staatliches Museum für Naturkunde Karlsruhe, Karlsruhe, Germany;
TNU	Taurida National University, Simferopol, Crimea, Ukraine;
UL	Universidade de Lisboa, Lisboa, Portugal;
USNM	National Museum of Natural History, Smithsonian Institution, Washington, D.C., United States.

Taxonomical note

Because a diverse group of basal Balaenomorpha, [partly corresponding to Cetotheriidae '*sensu latu*' auctorum; commonly referred to (in part) as basal Plicogulae (clade; Geisler *et al.* 2011) or basal Thalassotherii (Superfamily: Bisconti *et al.* 2013)] does not have a specific taxonomic name as its members often fail to form a clade in cladistic reconstructions, here we refer to these species as "basal non Balaenid Balaenomorpha" (BnBB). BnBB thus refers to the following species: *Atlanticetus patulus* (Kellogg, 1968); *Cephalotropis nectus* Cope,1896; '*Diorocetus*' *chichibuensis* Yoshida, Kimura & Hasegawa, 2003; *Diorocetus hiatus* Kellogg, 1968; '*Diorocetus*' *shobarensis* Otsuka & Ota, 2008; *Heterocetus affinis* (Van Beneden,1886); *Idiocetus longifrons* Van Beneden, 1880; *Isanacetus laticephalus* Kimura & Ozawa, 2002; *Joumocetus shimizui* Kimura & Hasegawa, 2010; *Mesocetus latifrons* Van Beneden, 1880; *Parietobalaena campiniana* Bisconti, Lambert & Bosselaers, 2013; *Parietobalaena laxata* (Van Beneden, 1880); *Parietobalaena palmeri* Kellogg, 1924; *Pelocetus calvertensis* Kellogg, 1965; *Persufflatius renefraaijeni* n. gen., n. sp.; '*Plesiocetus*' *burtinii* (Van Beneden, 1885) (IRSNB M676); '*Plesiocetus*' *dubius* Van Beneden, 1885 (IRSNB M652) and *Uranocetus gramensis* Steeman, 2009. For a list of all mysticete species mentionned in this publication, see Appendix 1.

Cladistic abbreviations

Bisconti: ch. 000; Duboys de Lavigerie: ch. 000: refers to the character (ch.; plural: chs) number(s) of the matrices of Bisconti *et al.* (2020) and Duboys de Lavigerie *et al.* (2020).

Palynological preparation and analysis

The newly defined specimen was dated on the basis of a sample of fine glauconitic sand that was intercalated between the periotic and the squamosal. The preserved sediments were prepared for palynological analysis at Palynological Laboratory Services (hereinafter: PLS) located in the UK, using the standard sample processing procedures, which involve HCl and HF treatment, heavy liquid separation, and sieving over a 15 µm mesh sieve. The organic residue was mounted with glycerin-gelatin on microscopic slides. Two microscopic slides were made: in addition to a non-oxidized kerogen slide, the organic residue was also slightly oxidized with HNO3 in order to concentrate the palynomorphs and reduce the abundant "Structureless Organic Matter" (SOM). The palynological analysis was carried out at the Geological Survey of the Netherlands (TNO) according to standard procedures. The palynomorph association on the microscope slides was counted until approximately a total of 200 sporomorphs (pollen and spores) and marine dinoflagellate cysts was reached. The main miscellaneous categories (e.g. marine acritarchs and test linings of foraminifers) were calculated separately. The remainder of the slide was thereafter scanned for any (rarer) dinocyst species.

Diagnostic species are discussed in the dedicate chapter; a complete distribution chart including all species found is given in the palynofacies and age-assessment paragraph (Figs 2; 3). The age interpretation is based on the Last Occurrence Datum (LOD) and First Occurrence Datum (FOD) of dinoflagellate cysts. For the dinoflagellate cyst taxonomy, the so-called "Lentin and Williams index" is followed (Fensome *et al.* 2019). The palynological interpretation is based on key-references concerning the palynostratigraphy of the Neogene from the North Sea region such as: Dybkjaer & Piasecki (2010), Köthe (2012), Kuhlmann *et al.* (2006), Louwye *et al.* (2004), Louwye & De Schepper (2010), Munsterman & Brinkhuis (2004) and Powell (1992). The Geological Time Scale, version 2016 is here used (Ogg *et al.* 2016). For the dinozones, we refer to Munsterman & Brinkhuis (2004) recalibrated to Ogg *et al.* (2016) in Munsterman *et al.* (2019).

Measurements, photography, making of the cranial endocast and camera lucida drawings

Measurements: all measurements below 17 cm were obtained using a digital calliper; measurements above 17 cm were obtained with an analogue stainless-steel calliper; those above 50 cm with an analogue, self-constructed, wooden, 90-cm-long calliper (nicknamed by prof. Dr 'Dino' Frey "Das Mäusemessgerät") or with a measuring tape.

Due to the incomplete preservation of the studied specimen, many measurements are approximate only. All measurements termed 'bi-' are measured on the preserved half neurocranium and were then doubled. As the exact inclination of the skull relative to the horizontal plane is not clear, several anteroposterior lengths are approximate only, as they often depend on the inclination.

Photographs

Unless specified otherwise, all photographs were taken by the first author. These were taken with a Nikon D3100 camera with a Nikkor 18-105 mm f1:3.5-5.6 lens, (mostly) at aperture f 11 to 13. If necessary, images were treated with Photoshop CC-2018.

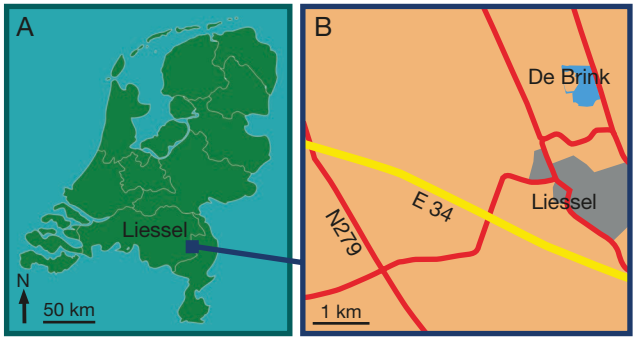

Fig. 1. — Location of the holotype of *Persufflatius renefraajieni* n. gen., n. sp.: **A**, in the Netherlands (green), the blue square indicates the type locality; **B**, the vicinity of Liessel. The holotype of *Persufflatius renefraajieni* n. gen., n. sp. was discovered at 'De Brink' (bright blue spot, 51°25'40"N, 5°49'46"E).

Endocast

Because the internal neurocranium is well preserved and looks different from most neurocrania we know, we decided to make a cranial endocast. The endocast of the braincase was made, using artist quality plasticine (to get the finest detail possible). We sculpted the medial, ventral and posterior shape thus that it approximated the presumed original shape of the right half of the cranial cavity. We made a plaster block-mould from this plasticine endocast and thereafter a plaster cast from this block-mould. By measuring the volume of this cast (by submerging it in a bucket full of water and measuring the volume of the spilled water) and doubling this volume, we could approximate the maximum volume of the brain case. As the brain does not fill the complete brain case, we substracted a 7 mm shell on the external side, to compensate for the volume of the space between the brain and the skull. Because the basicranium, basishpenoid and the presphenoid are missing, this must be considered a rough approximation. We estimate the volume of the brain between 1500 and 1800 cm^3.

Drawings

To assess compactness values for the bone, camera lucida drawings were drawn, on the basis of photos, and then corrected in the presence of the holotype. Naturally polished and flat, eroded or fracture surfaces were selected (not to damage the fossil). These surfaces were randomly oriented. The examined surfaces were minimum 5 × 5 mm and maximum 25 × 10 mm. The bone compactness of eight bone sections was calculated using 'Bone Profiler' (Girondot & Laurin 2003).

To quantify the size of the cavities, the trabecular rods and the trabecular plates (Molino *et al.* 2020), we measured the (approximate) dimensions on the camera lucida corrected photos in Photoshop (with the calibrated Photoshop measuring tool). For the cavities, we measured the maximum width and height; for the trabecular rods the minimum thickness and the maximum length and for the trabecular plates the minimum width and the minimum height.

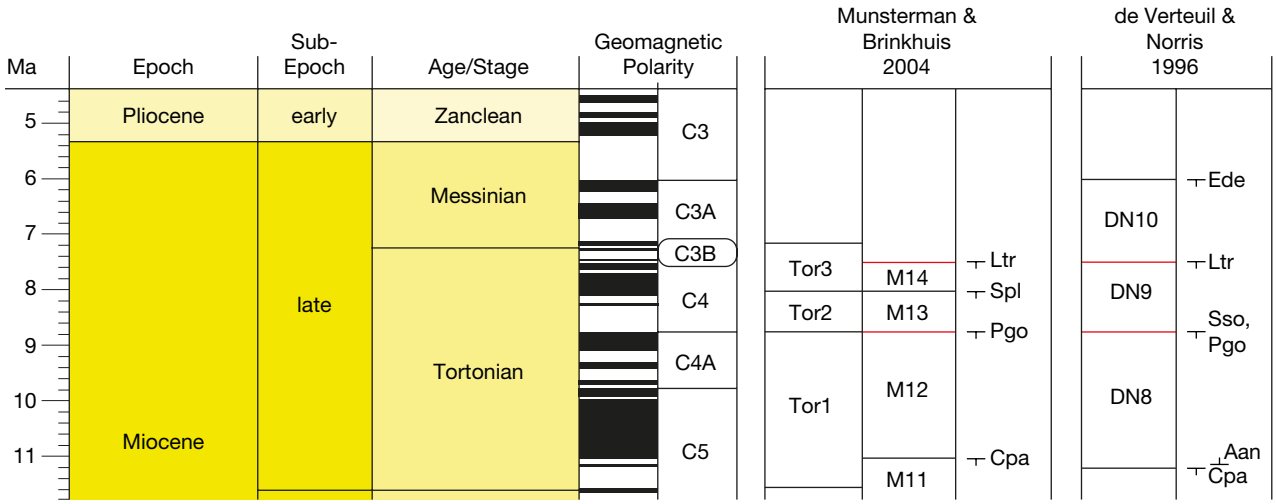

FIG. 2. — Dinoflagellate cyst zonation *cf*. Munsterman *et al*. 2019. Abbreviations: **Ma**, million years ago; **Tor**, Tortonian; **Aan**, *Achomosphaera andalousiensis*; **Cpa**, *Cannospaeropsis passio*; **Ede**, *Erymnodinium delectabile*; **Ltr**, *Labyrinthodinium truncatum*; **Pgo**, *Palaeocystodinum golzowensis*; **Spl**, *Systematophora placacantha*; **Sso**, *Sumatradinium soucouyantiae*. Red lines indicate the limits of the dinozone Southern North Sea DN9, the dinozone the specimen is dated from.

ESTIMATION OF BODY SIZE

The total body length (TL) was estimated based on the estimated bizygomatic width of the skull (BZW), using:

– the general mysticete equation of Lambert *et al.* (2010):

1) TL = 8.209 × (BZW) + 66.69 cm

– and the 'stem mysticete' and 'stem balaenopteroid' equations of Pyenson & Sponberg (2011):

2) log(TL) = 0.92 × (log(BZW) – 1.72) + 2.68 cm

3) log(TL) = 0.92 × (log(BZW) – 1.64) + 2.67 cm

PHYLOGENY

Two phylogenetic analyses were performed, based on the matrices proposed by Duboys de Lavigerie *et al.* (2020) and Bisconti *et al.* (2020), using PAUP 4.0b10 (Swofford 2002); character states were unordered and unweighted under the ACCTRAN character states optimization. The tree-bisection-reconnection (TBR) algorithm, with one tree being held at each step during stepwise addition, was used to find the most parsimonious cladograms (5001 replicates). Bremer support was also calculated (1002 replicates). Character support at the nodes was assessed by a bootstrap analysis with 101 replicates. Bootstrap values below 50 are not shown in the trees.

HOW TO VIEW THE STEREO IMAGES

Render the images 14 cm wide (or less) on a screen or a print; hold a piece of cardboard perpendicular to the surface, such that each of your eyes sees the corresponding image only (this is not necessary, but it makes viewing stereo images a lot easier). Focus a detail with one eye; open the other eye and the stereo image should appear. If not, try to turn your head slightly (rotate it), to align the images. If this doesn't help, use a special stereo image viewer. Not everybody can see stereo images.

INFLATED

Throughout the text we use the term "inflated" a lot. By the term inflated we mean: exposed surfaces of several bones of the neurocranium, especially of the squamosal and the exoccipital, that are seemingly swollen, bulging outwards, more than in any other balaenomorpha species, giving the specimen a rounded, 'inflated' aspect, reminiscent of 'Bibendum', the Michelin man. This 'inflated' bone consists internally of cancellous bone only, having the same structure as the rest of the adjacent bone; externally, it is covered by a thin layer of cortical bone.

SYSTEMATIC PALAEONTOLOGY

Infraorder CETACEA Brisson, 1762
Unranked clade PELAGICETI Uhen, 2008
Unranked clade NEOCETI
Fordyce & de Muizon, 2001
Parvorder MYSTICETI Flower, 1864
Unranked clade CHAEOMYSTICETI Mitchell, 1989
Unranked clade BALAENOMORPHA
Geisler & Sanders, 2003

Genus *Persufflatius* n. gen.

urn:lsid:zoobank.org:act:AFD92E26-6212-47C7-94DF-CD6AE454280E

DIAGNOSIS. — As for the type and only species.

TYPE SPECIES. — *Persufflatius renefraaijeni* n. sp.

ETYMOLOGY. — From the Latin '*sufflatus*', meaning bulbous, inflated and the prefix '*per*' meaning 'very much', 'strongly'. The genus name '*Persufflatius*' relates to the inflated overall aspect of the neurocranium (Figs 4; 5).

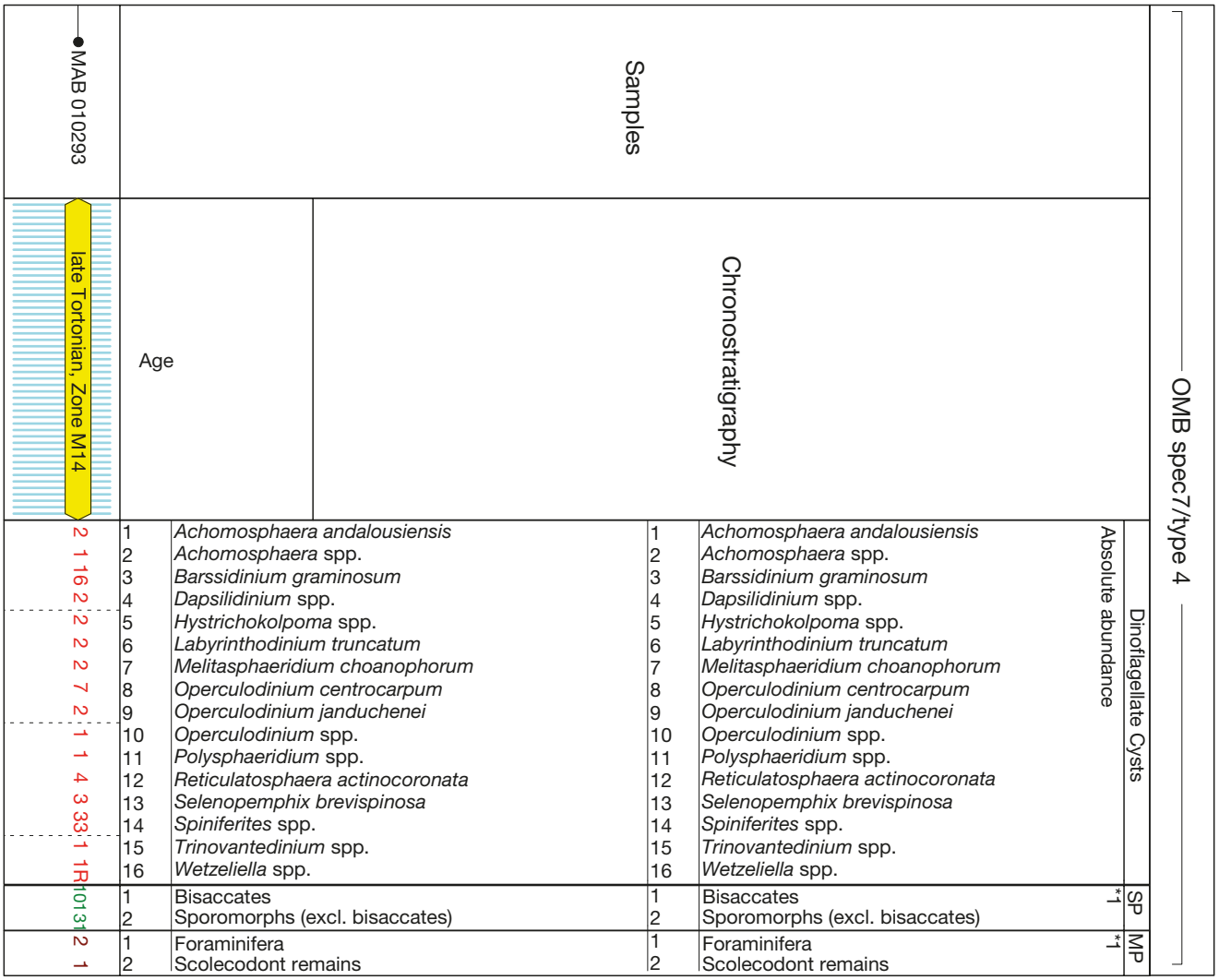

FIG. 3. — Distribution chart of palynomorphs in the sandy sample, the newly defined specimen (MAB 010293) was dated from. The sample, consisting of fine glauconitic sand, was intercalated between the periotic and the squamosal of the holotype. Abbreviations: **SP**, sporomorphs; **MP**, miscellaneous palynomorphs.

Persufflatius renefraaijeni n. gen., n. sp.
(Figs 1-25; Tables 1-6; Appendix 2)

urn:lsid:zoobank.org:act:B1833429-144C-44FF-B7FF-AC45E8552437

HOLOTYPE. — MAB 010293. A partial cranium consisting of the right half of a neurocranium including the squamosal (without the anterior part of the zygomatic process of the squamosal), the supraoccipital, the exoccipital (the medial part, bearing the condyle and the foramen magnum, is missing), the parietal, a small fragment of the pterygoid, the periotic and the compound posterior process of the petrotympanic. Part of the vertex is preserved, although eroded. The bulla tympani, part of the basicranium, the palate, the suborbital region and the rostrum are missing.

TYPE LOCALITY. — The skull MAB 010293 has been discovered on the spoil piles of the Liessel sand mining (brick producing) company Hoogdonk, in the 1980-90s. The factory was situated at 'De Brink', in between the villages Liessel and Deurne, province of Noord Brabant, the Netherlands (51°25'40"N, 5°49'46"E); (Fig. 1).

ETYMOLOGY. — Named after the first and last name of Dr René H. B. Fraaije (Fig. 6), founder and director of the Oertijdmuseum at Boxtel, the Netherlands, who discovered the specimen. In honour of his long-lasting efforts in favour of the study of fossils in general (especially Decapoda) and of the Liessel cetaceans in particular, and for his outstanding efforts to bring particularly (school) children in contact with natural history, *c.q.* fossils and dinosaurs, in the Oertijdmuseum.

TYPE HORIZON AND GEOLOGICAL AGE. — Borehole B52C1978, interval 0-44.5 m, directly adjacent to the sand pit (at RD-coordinates: (X) 185.627 and (Y) 382.024) was drilled in 2001. The results of the lithostratigraphic and palynological interpretations are reported by Munsterman (2007) (see also: Peters 2009: 98-105; Marx *et al.* 2016a: 4; Bisconti *et al.* 2020: 3-5).

LITHOLOGICAL UNIT. — The specimen was dragged from sands assigned to the Diessen Formation. This is a shallow marine deposit consisting of glauconiferous sands, sandy clays and clays. The Diessen Formation is present throughout the Netherlands and includes part of the Dutch late Miocene succession (Tortonian-Messinian) (Munsterman *et al.* 2019).

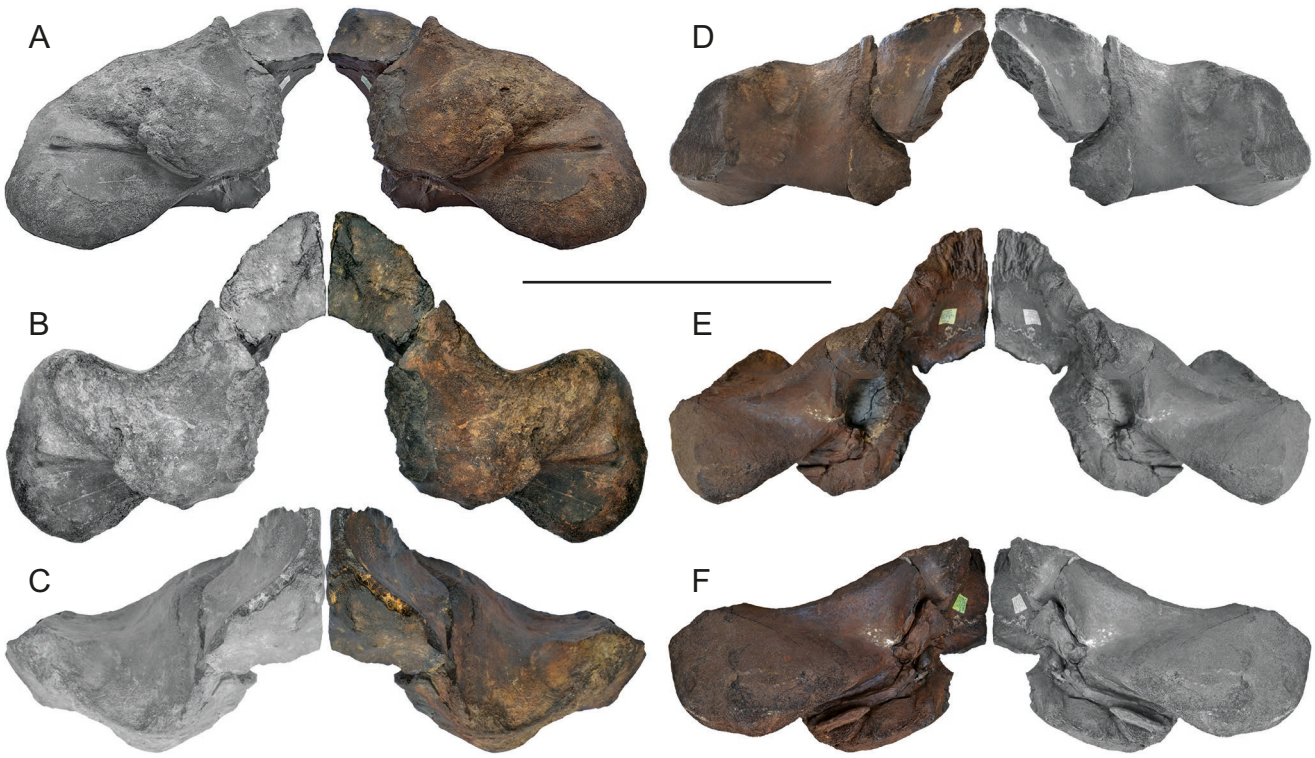

Fig. 4. — *Persufflatius renefraaijeni* n. gen., n. sp., MAB 010293, holotype, partial right neurocranium: **A**, posterior view; **B**, posterodorsal view; **C**, dorsal view; **D**, anterior view; **E**, anteroventral-ventral view (with periotic removed); **F**, anteroventral view (with periotic in place). Colour images: original; grey images: reconstruction of the left side by mirroring the original. Scale bar: 30 cm.

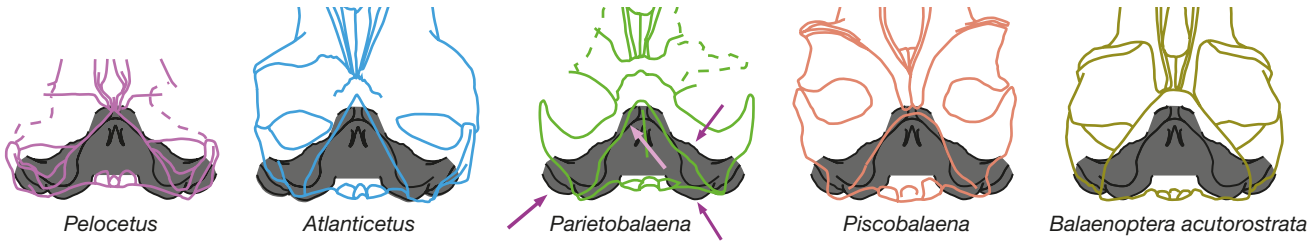

Fig. 5. — *Persufflatius renefraaijeni* n. gen., n. sp.; MAB 010293, holotype. The neurocranium of *Persufflatius* n. gen. compared to the outline drawings of *Pelocetus*, *Atlanticetus*, *Parietobalaena*, *Piscobalaena* (a typical Cetotheriidae) and *Balaenoptera acutorostrata* (a typical derived Balaenopteridae). Notice the rounded, bulbous, 'inflated' shape of the postglenoid process, the exoccipital, the anterior squamosal and the supraoccipital (**arrows**).

Palynofacies and age-assessment (Figs 2; 3)

The assemblage is dominated by continental influence (63% of the total sum palynomorphs, i.e., spores, pollen and dinoflagellate cysts). The non-bisaccate pollen group is in minority (23% of the total sum sporomorphs). Most of the sporomorphs are bisaccate pollen (77% of the total sum sporomorphs). Bisaccate pollen are formed by conifers, gymnosperms (Gymnospermae). Bisaccate pollen have a higher aerial and aquatic buoyancy than other sporomorphs, indicating a relatively distal position from the coast. The relatively distal facies is confirmed by the concentration and composition of marine dinoflagellate cysts. The most common genus, *Spiniferites* (42% of the total dinocyst sum), has a preferential orientation for open marine conditions. *Barssidinium graminosum* on the contrary, is also well-represented (20% of the total sum dinoflagellate cysts). This taxon has a temperate to tropical distribution in neritic (and especially, inner neritic) waters. Heterotrophic genera like *Barssidinium, Selenopemphix* and *Trinovantedinium* (25% of the total dinocyst sum) refer to nutrient-rich water. As a whole, the marine dinocyst assemblage is relatively variegated, indicating nutrient-rich neritic conditions.

An age-diagnostic taxon is *Labyrinthodinium truncatum.* This taxon has a last occurrence datum (LOD) in the late Miocene, late Tortonian, Zone SNSM14 (Munsterman & Brinkhuis, 2004). This event is also used to define the DN9 Zone by de Verteuil & Norris (1996) (originally described for the East Coast of the USA and generally adopted in Belgium), in Germany by Köthe (2012) and for the *Hystrichosphaeropsis obscura* Zone on- and offshore Denmark by Dybkjaer & Piasecki (2010). Marker taxa indicating possible older zones, like e.g. the

FIG. 6. — Dr René H. B. Fraaije, ferociously attacked by one of his dinosaurs at the entrance of the 'Oertijdmuseum' at Boxtel, the Netherlands. Anterior view. **u**, up; **ll**, left lateral. Scale bar: 15 cm.

dinocysts *Systematophora placacantha* (LOD in Zone SNSM13) and *Palaeocystodinum golzowensis* (LOD in Zone SNSM12) are absent. The presence of *Operculodinium janduchenei* with a maximum age range (FOD) in the Tortonian confirms the dating. Also present in the microflora is *Achomosphaera andalousiensis*, having a slightly older FOD. In conclusion the age assessment of the present assemblage is early late Miocene, late Tortonian SNSM14 Zone, *c.* 8.1-7.5 Ma (Munsterman *et al.* 2019) (Figs 2; 3).

DIAGNOSIS

Absolute diagnosis

Small-sized non-balaenid balaenomorph mysticete, differing from all other basal non-balaenid Balaenomorpha (BnBB) in having i) a notably inflated squamosal, in particular the posteriorly oriented postglenoid process, which is also large compared to the size of the neurocranium; ii) a rounded bulbous exoccipital that is confluent with the posterior portion of the zygomatic process of the squamosal (Duboys de Lavigerie 2020: ch. 74), resulting in an anteroposteriorly long squamosal-exoccipital complex; iii) a bell-shaped supraoccipital without an external occipital crest (Bisconti, chs 140, 141, 142; Duboys de Lavigerie: ch. 112), that anteriorly overhangs the temporal fossa; and iv) a very wide, rounded posterior temporal crest (anterior width *c.* 15 cm). The periotic is *Pelocetus*-like in general aspect, in having v) a small pars cochlearis, that is not cranially elongated, in having vi) an overall inflated aspect, vii) having a strong and wide, dorsally protruding tuberosity, continuously running over the whole length of the dorsal surface of the pars petrosa and the anterior process. But contrary to the latter, it has (amongst others), viii) the rod-like compound posterior process widely exposed laterally (L: 34 mm) and ix) the cochlear aqueduct, the dorsal vestibular area and the endocranial opening of the facial canal aligned. The estimated bizygomatic width, including the anterior zygomatic process of the squamosal (missing in the holotype) is about 720 mm (Table 1).

Differential diagnosis (Fig. 7)

Persufflatius renefraaijeni n. gen., n. sp. is closely related to *Pelocetus calvertensis*, *Uranocetus gramensis* and *Parietobalaena palmeri* in having a rod-like posterior process of the petrotympanic. It differs from eomysticetids, balaenids, *Atlanticetus patulus*, *Diorocetus hiatus* and the cetotheriids *Brandtocetus chongulek* Gol'din & Startsev, 2014, *Cetotherium rathkii* Brandt, 1843, *Heterocetus affinis* and *Piscobalaena* Pilleri & Siber, 1989 in having a squamosal cleft (Bisconti: ch. 114; Duboys de Lavigerie: ch. 107), and from all known mysticetes except *Parietobalaena*, in this cleft being 'smiley'-shaped (semi-circular, dorsally concave). It further differs from eomysticetids in having a more anteriorly projected supraoccipital and parietal; from balaenids in having a concave anterior supraoccipital dorsally (Bisconti: ch. 135; Duboys de Lavigerie: ch. 113), a small but prominent attachment surface ('paired tubercles') for the neck muscles on the anterior supraoccipital (Bisconti: ch. 85; Duboys de Lavigerie: ch. 109), a posterodorsally inclined superior part of the posterior wall of the squamosal fossa, and a wide temporal fossa (Bisconti: ch. 110); from '*Balaenoptera*'

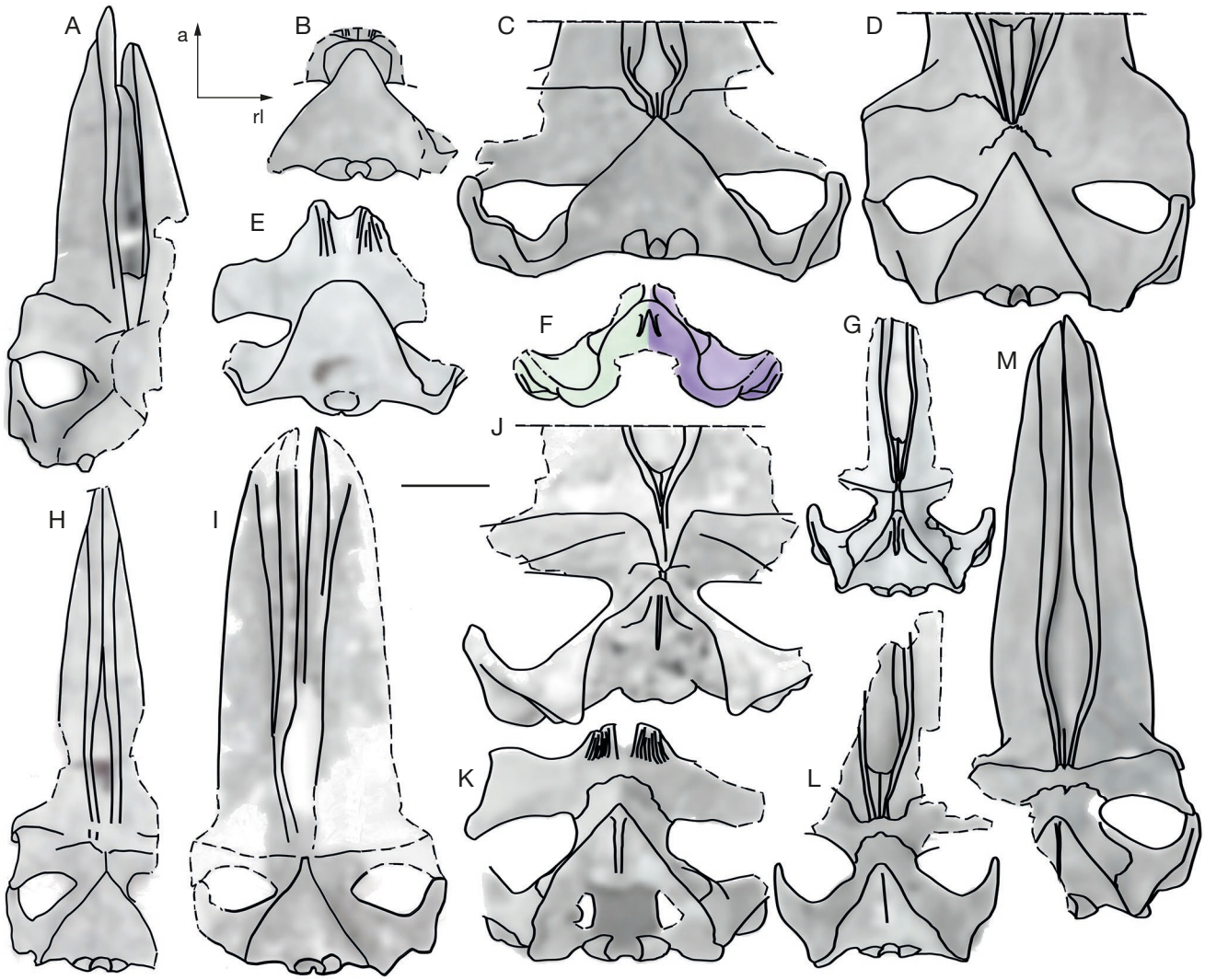

FIG. 7. — *Persufflatius renefraaijeni* n. gen., n. sp.; MAB 010293, holotype and some closely related species. Line drawings in dorsal view, on the same scale. **a**, anterior; **rl**, right lateral. **A**, *Isanacetus laticephalus* MFM 28501, holotype; **B**, '*Balaenoptera*' *ryani* CASG 1733, MFM 28501; **C**, *Pelocetus calvertensis* USNM 11976, holotype; **D**, *Atlanticetus patulus* USNM 23690, holotype; **E**, *Morenocetus parvus* MPL 5-11, holotype; **F**, *Persufflatius renefraaijeni* n. gen., n. sp., MAB 010293, holotype (original: right, purple-grey side; mirrored: left, green side); **G**, *Tiucetus rosae* MNHN.F.PPI261, holotype; **H**, '*Diorocetus*' *chichibuensis* SMNH-VeF-68, holotype; **I**, '*Diorocetus*' *shobarensis* HMN-F00005, holotype; **J**, *Uranocetus gramensis* MSM p 813, holotype; **K**, *Parietobalaena palmeri* USNM 10668, holotype; **L**, USNM 16119, referred specimen; **M**, *Diorocetus hiatus* USNM 16783, holotype. Scale bar 20 cm.

ryani Hanna & McLellan, 1924 in having a wide semi-circular posterior temporal crest (Bisconti: ch. 107), a posterodorsally inclined superior part of the posterior wall of the squamosal fossa (Bisconti: ch. 113), a parietal that anteriorly overhangs the temporal fossa (Bisconti: ch. 78), and a relatively large periotic having a prominent, deep groove for the tensor tympani muscle (Bisconti: ch. 196; Duboys de Lavigerie, chs 160, 161), the cochlear aqueduct being not confluent with the fenestra cochlearis (Bisconti, chs 215, 216; Duboys de Lavigerie: ch. 174), and a small, not-inflated pars cochlearis (Bisconti: ch. 213); from balaenopterids and eschrichtiids in having the parietal broadly exposed at the vertex (Bisconti, chs 82, 83) and a *Pelocetus*-like periotic with a pars cochlearis that is not cranially elongated (Bisconti: ch. 211; Duboys de Lavigerie: ch. 144); from *Parietobalaena palmeri* and *P. laxata* by the large, strongly inflated and ventrally expanded postglenoid process; from *Atlanticetus patulus*, *Diorocetus hiatus*, *Pelocetus calvertensis*, *Tiucetus rosae*, '*Diorocetus*' *shobarensis*, '*Diorocetus*' *chichibuensis*, *Isanacetus laticephalus* and *Parietobalaena* in having a bell-shaped supraoccipital (Bisconti, chs 140, 141, 142; Duboys de Lavigerie: ch. 112), large inflated postglenoid processes and wide rounded exoccipitals, confluent with the squamosal (Duboys de Lavigerie: ch. 74); from *Uranocetus gramensis* in having a large inflated postglenoid process, anteroposteriorly much longer squamosals (squamosal + exoccipital length: 170 mm) and wide rounded exoccipitals; from *Isanacetus*, *Parietobalaena* and '*Diorocetus*' *chichibuensis* in them having a narrow body of the periotic with no sign of lateral inflation; from *Diorocetus hiatus* in lacking a ridge posteriorly bordering the facial sulcus on the compound posterior process (Duboys de Lavigerie: ch. 185); from all cetotheriids except *Cephalotropis nectus* and *Joumocetus shimizui* in having parietals that are well exposed on the skull vertex (Bisconti, chs 82, 83); from *Diorocetus*, *Uranocetus*, *Tiucetus* and *Parietobalaena*

TABLE 1. — *Persufflatius renefraaijeni* n. gen., n. sp.; MAB 010293, holotype. Measurements (in mm) of the cranium, the periotic and the bulla tympani. Abbreviations: **e**, estimate; **ee**, rough estimate; **m**, measurement; **H**, height; **W**, width; (List after Marx 2017; adapted).

Neurocranium		
condylobasal length, as preserved (min. *c.* 260 – max. *c.* 350; depending on the inclination)	–	*c.* 330 (ee-m)
bizygomatic width at widest zygomatic process (half as preserved: 330)	(estimated half: 360)	720 (e-m)
bicondylar width (maximum width, rough estimate)	(half: 70-93; *c.* 2 × 85)	*c.* 170 (ee-m)
maximum width across exoccipitals (half: *c.* 285; approximate as it merged almost completely)	–	570 (e-m)
maximum bilateral width across lateral surfaces of the periotic's posterior process (half: 305)	–	610 (e-m)
maximum bilateral width across the lateral paroccipital process	(half: *c.*145)	290 (e-m)
maximum anteroposterior length (thickness) of the exoccipital	–	*c.* 73 (m)
maximum length of the supraoccipital (posteroventral exoccipital to anterior vertex)	–	360 (m)
maximum anteroposterior length of the squamosal + the exoccipital	–	170 (m)
estimated height of neurocranium (vertex-ventral postglenoid)	266-360	*c.* 340 (m)
maximum height medially at anterior pseudoval foramen	–	*c.* 250 (m)
width of supraoccipital at posterior parietal	(*c.* 125)	*c.* 250 (m)
anteroposterior length of external acoustic meatus at its medial border	–	18.8 (m)
maximum width of the pseudoval foramen anteriorly (right)	–	*c.* 30 (m)
maximum width of the pseudoval foramen posteriorly (right)	–	*c.* 39 (m)
mediolateral width of the paroccipital fossa, as preserved	–	*c.* 42 (m)
anteroposterior length of the paroccipital fossa	–	30 (m)
width of the jugular notch (right)	(min. 16, max. 22)	*c.* 19 (m)
maximum height of the postglenoid process (as preserved)	–	97 (m)
maximum mediolateral width of the postglenoid process at its base	–	188 (m)
maximum length of the parietal exposure on the vertex (measured along medial axis)	–	58 (m)
maximum width of the parietal on the vertex (at anterior supraoccipital) (half: 35)	–	*c.* 70 (m)
maximum width of the parietal on the vertex (at centre of curvature)	(half: *c.* 14)	*c.* 30 (m)
anteroposterior length of squamosal (posterior postglenoid-foramen pseudovale)	–	*c.* 230
Distance from the posteromedial corner of the falciform process of the squamosal to the innermost portion of the dorsal vestibular area	–	30.5 (m)
anteroposterior length of the ventral squamosal fossa at the medial EAM	–	87.5 (m)
maximum width of condyles through bimedial-jugular notch	*c.* 2 × 83 mm	166 (ee m)
Periotic		
length of the anterior process anterior to the mallear fossa	(42.3 mm as preserved)	*c.* 59 (ee)
length of the pars cochlearis anterior to the fenestra cochleae (rotunda) ventrally	–	24.6 (m)
width of the pars cochlearis medial to the fenestra vestibuli (ovalis)	–	18.6 (m)
length of the fenestra cochleae (rotunda)	(H: 2.86)	7.0 (m)
length of the fenestra vestibuli (ovalis)	(H: 2.60)	5.20 (m)
maximum anteroposterior length of pars cochlearis, up to medial border of fenestra rotunda	–	27.3 (m)
maximum diameter of the lateral (distal) opening of the facial canal	(H: 2.5)	3.6 (m)
maximum diameter of the aperture for the cochlear aqueduct	(W: 1.6)	9.4 (m)
maximum diameter of the aperture for the vestibular aqueduct	–	7.1 (m)
maximum anteroposterior length of the endocranial opening of the facial canal (proximally)	–	9.3 (m)
maximum dorsoventral height of facial sulcus (cranially)	–	4.3 (m)
mediolateral width (long axis) of the posterior process	(H: *c.* 39)	122.5 (m)
maximum anteroposterior length of the external surface of the posterior process	–	35.0 (m)
maximum anteroposterior length of the lateral end of the facial canal at lateral exoccipital	–	40-45 (m)
maximum length of periotic (posterior cochlear crest-anterolateral AP as preserved)	–	71.5 (m)
maximum length of periotic (posterior cochlear crest-anterior tip AP, estimated)	–	83-87 (ee)
maximum width of periotic	–	62.0 (m)
maximum height of periotic	–	48.8 (m)
maximum length of pars cochlearis including posterior cochlear crest	–	32.7 (m)
maximum width of the hypertrophied medial process dorsally, dorsal to the vestibular area	–	26.4 (m)
maximum anteroposterior length of ventral surface of compound posterior process medially	–	22.9 (m)
maximum mediolateral diameter of the posterior pedicle of periotic	–	19.1 (m)
Bulla tympani		
Distance between the anterior and the posterior pedicle	(max. 32.4; min. 18.9)	25.5 (m)
anteroposterior length of the anterior pedicle	–	6.7 (m)
anteroposterior length of the posterior pedicle	–	7.2 (m)

in lacking an external occipital crest on the anterior supraoccipital (Bisconti: ch. 81; Duboys de Lavigerie: ch. 114); from all BnBB in having a bell-shaped supraoccipital (except maybe for *Uranocetus* (Steeman 2009); due to breakage the exact shape of the latter's supraoccipital is not very clear) (Bisconti, chs 140, 141, 142; Duboys de Lavigerie: ch. 112); differs from *Atlanticetus patulus* by the deeply excavated tensor tympani fossa (Bisconti: ch. 196; Duboys de Lavigerie: ch. 160), the different rod-like posterior process (Duboys de Lavigerie: ch. 188), slit-like aqueducts (Bisconti: ch. 217; Duboys de Lavigerie: ch. 172) and the strongly inflated postglenoid process of the squamosal and from '*Plesiocetus*' *dubius* (IRSNB M 652), '*Plesiocetus*' *burtinii* (IRSNB M 676), *Mesocetus latifrons* (IRSNB M 567) and *Idiocetus longifrons* (IRSNB M 719) in having a small cochlea, a slit-like cochlear aqueduct foramen (except '*P*'. *dubius*) (Bisconti: ch. 217; Duboys de Lavigerie:

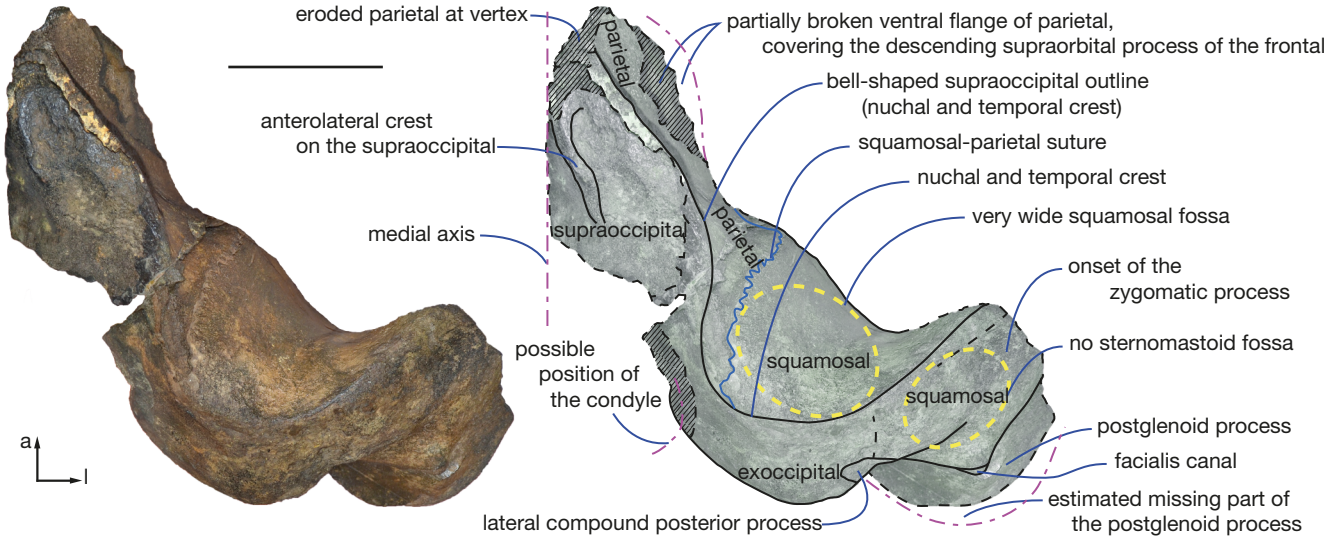

Fig. 8. — *Persufflatius renefraaijeni* n. gen., n. sp., MAB 010293, holotype. Posterodorsal view. **a**, anterior; **l**, lateral. Scale bar: 10 cm.

ch. 172), a very different rod-like compound posterior process (Duboys de Lavigerie: ch. 188) and a strongly inflated postglenoid process of the squamosal. Differs from *Atlanticetus patulus*, *Heterocetus affinis* and *Cephalotropis nectus* in that all three taxa have a (sub-)diamond-shaped compound posterior process of the petrotympanic in ventral view; in addition, the shape of the anterior process of the periotic and the cranial openings of the promontorium also differ (Duboys de Lavigerie, chs 168, 169). The species is smaller than *Pelocetus calvertensis*, *Uranocetus gramensis* and *Atlanticetus patulus*, and larger than *Tiucetus rosae* (Fig. 7).

Description of the holotype

A (partial) reconstruction of the holotype MAB 010293 was performed by mirroring the preserved part along the medial axis. Compared to almost all other mysticetes, the postglenoid process, the shape of the exoccipital, the anteromedioventral squamosal and the supraoccipital are more rounded, bulbous and, 'inflated' (Figs 4; 5).

Preservation, taphonomy, ontogenetic stage, body size estimate, faunal assemblage

The specimen shows several recent fractures, most likely the result of dredging. These are: the fractures at the base of the zygomatic process and, anteroventrally, at the squamosal (Figs 8-10) and the pterygoid (Fig. 11B), at the posteromedial supraoccipital, and across the cranial cavity, just in front of the squamosal-parietal suture, in the middle of the supraoccipital (Fig. 8). All other damage seems to be due to natural processes. The fossil shows erosion at all edges (all of them being rounded and many of them are polished, exposing deep blue-black apatite). Erosional features are particularly strong at the vertex (Fig. 8), at the posterodorsolateral side of the squamosal, at the supramastoid crest (lateral temporal crest) on the posterior part of the zygomatic process (Figs 10-14) and along the ventral and lateral edge of the postglenoid process (Figs 12; 13).

The specimen is to be considered a young adult, judging from the state of merging/fusion of the cranial sutures (see below) (Marx *et al.* 2016a: 21; Walsh & Berta 2011; Bouetel & de Muizon 2006: 11; MB pers. obs. of several ontogenetic stages of *Balaenoptera acutorostrata* Lacépède, 1804). Moreover, the periotic has impressive medial and anteromedial secondary (hypertrophied) bone growth medial to the dorsal vestibular area. The posterior process of the petrotympanic is mediolaterally wide (Fig. 12). Some sutures on the squamosal surface are not fully merged yet. On the contrary, the "smiley"-shaped squamosal cleft is hard to observe externally, unless viewed in grazing light (Figs 10; 14). It is definitely at an advanced stage of merging; in addition this cleft is no longer discernible in internal view. Likewise, the dorsal part of the parietal-squamosal suture and the parietal-supraoccipital suture are in an advanced state of merging, both being almost completely merged (though still discernible as a fine line) (Fig. 11A, B, D). In turn, the ventral part of the parietal-squamosal suture, which is exposed due to breakage of the ventral part of the parietal, is not in an advanced state of merging yet (Fig. 11B; 14). The parietal-frontal suture shows a fragment of merged frontal of about 26 × 26 mm posteroventrally, but the rest of the suture is certainly not merged (Fig. 11C). As the parietal-frontal suture is filled with sediment, it looks like the frontal detached (i.e. broke off) prior to fossilization (Fig. 11C). The posteromedial part of the squamosal-pterygoid suture is preserved. This suture is well merged and is locally hard to discern (Fig. 14).

The zygomatic width of the specimen, as preserved and thus without the anterior zygomatic process, is about 330 mm. Based on superpositions of photos of *Persufflatius renefraaijeni* n. gen., n. sp. and of three closely related species (*Pelocetus calvertensis*, *Uranocetus gramensis* and *Atlanticetus patulus*), we estimated the full bizygomatic width to be about 720 mm (Table 1). Based on this estimated bizygomatic width, the body size has been calculated, using the general mysticete equation of Lambert *et al.* 2010 (equation '1'), the 'stem mysticete equation' (equation '2') and the 'stem balaenopterid equation' (equation '3') of Pyenson & Sponberg (2011)

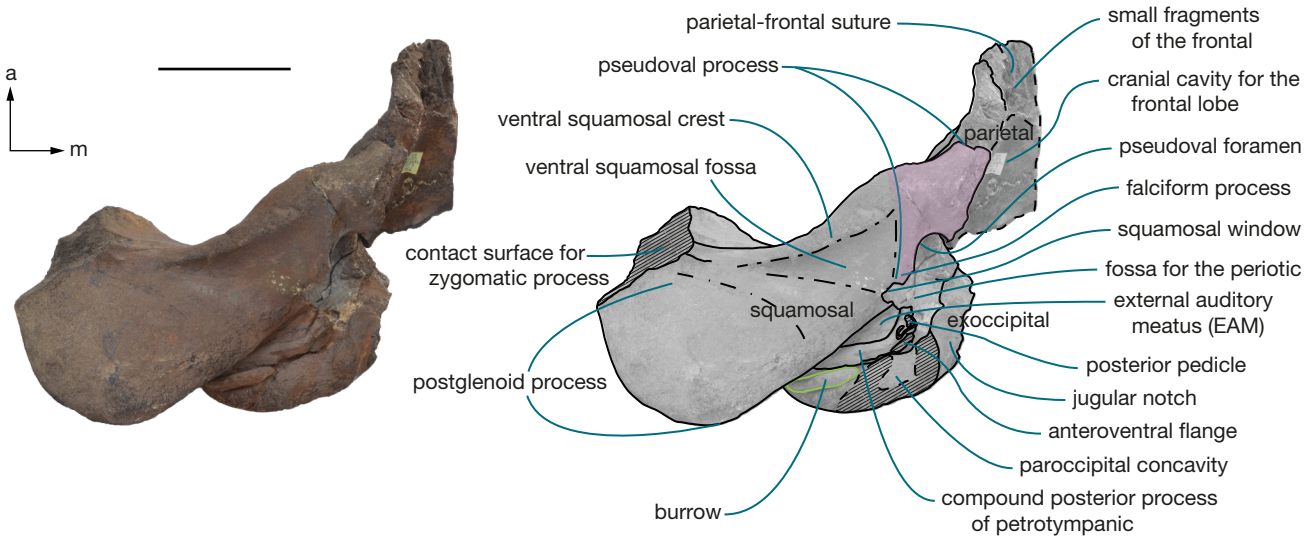

FIG. 9. — *Persufflatius renefraaijeni* n. gen., n. sp., MAB 010293, holotype. Anteroventral view. **a**, anterior; **m**, medial. Scale bar: 10 cm.

(Table 2). This resulted in an estimated body size of roughly 650 cm, somewhat larger than in adults of the pygmy right whale *Caperea marginata* (Gray, 1846), the smallest extant mysticete (Baker 1985; Kemper 2008; Reidenberg & Laitman 2008; MB pers. obs. 2008; Appendix 4).

The type and only specimen exhibits clear, specific characters, that are quite different from all other BnBB-species. More in particular, the neurocranium exhibits an inflated general aspect. Especially the postglenoid process of the squamosal, the exoccipital and the posterolateral base of the zygomatic process are swollen. Also, the bell-shaped supraoccipital gives the neurocranium a more inflated aspect than all of the other BnBB that have a narrow triangular supraoccipital (Figs 4; 5; 8; 24). The anterior third of the supraoccipital is dorsoventrally thick (Table 3) and consists of dense bone (compactness about 0.83) (Table 4).

Frontal (Figs 4; 8; 9; 11; 14)

The frontal is almost completely missing. The parietal-frontal suture preserves a remnant of merged frontal of about 26 × 26 mm posteroventrally in the top of the curvature. The lower part of the suture is missing in most places, apparently as it was already fused when the frontal broke off (Fig. 4D, E). The parietal-flange that covers the posterodorsal corner of the descending supraorbital process of the frontal has broken off. Most of the parietal-frontal suture is preserved and the missing flange covering the posterodorsal corner of the supraorbital process of the frontal must have been small; judging from the preserved adjacent bone, it is estimated to have been maximum a few centimetres long (Figs 8; 9; 11A-C; 13; 14).

Parietal (Figs 4; 8-11; 13-15)

The right parietal is almost completely preserved. Only the ventral part of the anteroventral flange that was covering the descending supraorbital process of the frontal and its anterodorsal part at the skull vertex are missing. The parietal bulges slightly into the temporal fossa posterolaterally; anterolaterodorsally it is strongly concave (Figs 10; 11A). Anteriorly, the dorsal border of the parietal supports the supraoccipital; it is slightly inflated and projects laterally, forming the ventral component of the temporal crest that overhangs the temporal fossa for about 25 mm as preserved, but the size of the overhang is estimated to have been originally maximum 40 mm wide (based on the preserved adjacent bone) (Figs 10; 11A). The parietal's internal structure is exposed on a roughly 40 × 70 mm (fracture) surface anterodorsomedially (Fig. 11A); it consists of spongy bone with large, elongated cavities (mean H: 1.586 mm; mean W: 0.636) (Appendix 2) and a relatively low compactness (about 0.55) (Table 4).

At the level of the dorsal part of the squamosal-parietal suture, the temporal crest does no longer overhang the temporal fossa. The dorsal part of the parietal-squamosal suture is dorsoventrally broadly straight and runs vertically. The suture is crenate (wavy and rough). It is in an advanced state of fusion (Fig. 11A, B; 14). The ventral part is missing (due to breakage). It runs inclined in anteroventral direction (at an angle of 135° with respect to the vertical part), contacting the preserved squamosal side of the suture. This lower part of the suture is not fused (Fig. 11B). The anterior part of the parietal is anteroventrally inflated and bulges (inverse U-shaped) to accommodate for the missing dorsally convex descending supraorbital process of the frontal (Figs 10; 11B; 13; 14).

TABLE 2. — *Persufflatius renefraaijeni* n. gen., n. sp.; MAB 010293, holotype. Body size estimates (in cm), based on the general mysticete equation of Lambert *et al.* 2010 (equation '1'), the 'stem mysticete equation' (equation '2') and the 'stem balaenopterid equation' (equation '3') of Pyenson & Sponberg 2011.

Estimated body length for bizygomatic width 72 cm	
Equation 1	658 cm
Equation 2	658 cm
Equation 3	741 cm

TABLE 3. — Dorsoventral height of the anterior supraoccipital versus the bizygomatic width, in mm, measured centrally (medially) on the anterioposterior axis. The last column gives the relative thickness, indicating the bone is very thick anterocentrally in the *Persufflatius renefraaijeni* n. gen., n. sp. holotype. *Persufflatius* n. gen. and *Metopocetus* Cope, 1896 are both late Miocene genera; *Caperea* Gray, 1864 and *Balaenaoptera* Lacépède, 1804 are extant genera.

Collection number	Species	Bizygomatic width in mm	Anterior supraoccipital height, medially at the vertex (in mm)	Relative supraoccipital height (in mm) per 1000 mm of bizygomatic width
MAB 010293	*Persufflatius renefraaijeni* n. gen., n. sp.	760-720	25	33-35
NMR 99917729	*Metopocetus hunteri*	580	*c*. 11.6	*c*. 20
NMR 99901449	*Caperea marginata*	440	4.7-5.7	10.7-13.0
NMR 99902727	*Balaenoptera borealis*	980	*c*. 15	*c*. 15.3
NMR 99903024	*Balaenoptera acutorostrata* (juvenile)	527	12	22.8

TABLE 4. — Compactness measured at several sections of the type neurocranium (see Fig. 25).

	Anatomical position of the sections illustrated in Figures 24 and 25	Compactness
1	anterior parietal at vertex	0.545
2	pterygoid-squamosal suture	0.631
3	anteroventral squamosal border	0.594
4	posterior fracture of supraoccipital	0.836
5	posterior postglenoid process	0.348
6	jugular notch	0.461
7	medial side of anterior supraoccipital, Top:	0.808
	Middle:	0.509
	Bottom:	0.775
8	posterodorsal base of zygomatic process	0.391
9	lateral exoccipital	0.413

Parietal on vertex

In dorsal view, the parietal is broadly exposed on the vertex (Figs 8; 11A, B; 13; 14), but the exact shape and length of the exposure is unknown, as the dorsal-most part of the vertex is missing (due to fracture and/or erosion). The preserved part is posteriorly about 30 mm wide; in the middle 10 mm and anteriorly about 15 mm wide, as preserved; the maximum length is about 58 mm.

Parietal-frontal (coronal) suture

The dorsal part of the parietal-frontal suture on the vertex is preserved (*c*. *q*. the parietal overlapping the posterodorsal frontal). It is (half) inverse U-shaped in anteroventral view. At the (curved) top 6 cm it features about nine irregular rough and deep lamellae (Figs 11C; 14). As this part of the suture is locally covered by sediment, it looks like the frontal broke off prior to fossilisation. The lowermost (ventrolateral) 6 cm of the suture are damaged in most places (probably as it was already fused when the frontal broke off). Where it is still preserved, it shows a much finer interdigitation (Figs 11C; 14). The suture was generally not fused anterodorsally, but locally remnants of a fused fragment of the frontal are present (over a 26 × 26 mm surface).

Dorsal border/anterior nuchal crest

The dorsal parietal border contacting (supporting) the supraoccipital is bell-shaped in dorsoposterior view. Anterolaterally, the dorsal border overhangs the temporal fossa. Below this border, the parietal is rather deeply concave (Figs 10; 11A). Anteroventrally, it becomes strongly convex and inflated (the ventral-most part of the flange that was covering the descending supraorbital process of the frontal is missing), providing the anterior part of the parietal with a saddle-like shape in anterior view. Anteriorly, the parietal-supraoccipital suture is V-shaped, due to a wide and deep sutural lamella (Figs 10; 11A). Dorsally, the anterior 9 cm of this suture are irregular, wavy and widely open (up to 13 mm separation). The anterolaterodorsal extremities of both the supraoccipital and the parietal (estimated to be less than 15 mm wide) have broken off and are missing (Figs 10; 11A, B). Medially, the parietal-supraoccipital suture has completely merged, resulting in a fine line, running parallel to the dorsal supraoccipital surface. The supraoccipital is about 28 mm thick at this medial surface, and as such is very robust (Table 3). Internally (posteriorly), in the cranial cavity (imprint of the frontoparietal lobe of the brain), the suture is visible as a fine, very irregular wavy white line (Figs 11D; 15). Here also the suture has completely merged.

Squamosal (Figs 4; 8-14)

The squamosal is massive and inflated, especially laterally and anteriorly. It is generally robust, and together with the exoccipital, this part of the skull is anteroposteriorly relatively longer (170 mm) than in most other BnBB (such as *Pelocetus* and *Uranocetus* (Fig. 7C, F, J). The dorsal edge of the squamosal (temporal crest) gently slopes downwards in lateral direction; centrally, it slopes down in anterior direction, to form the dorsal squamosal fossa (similar to *Pelocetus*, *Uranocetus*, *Parietobalaena* and *Tiucetus*, but it is, especially posteriorly, a lot wider in *Persufflatius* n. gen. (Figs 7; 8; 10; 14). This posterior wall ('floor') of the temporal fossa is continuously convex and bulges into the temporal fossa. Basally and medially, at the level of the pseudoval foramen, the squamosal is anteroposteriorly short (57 mm). The squamosal fossa is anteroposteriorly elongate. Its floor is concave, especially anteriorly, though it becomes less concave posteriorly as it approaches the posterior apex of the temporal crest. The zygomatic process of the squamosal has broken, exposing its robust tear-shaped transverse section (ventral width: 87 mm; height: 141 mm). It is ventrally and laterally inflated and rounded, and consists entirely of spongy bone with, very small cavities (mean mediolateral W: 0.354; mean H: 0.478) (Appendix 2), covered externally by a thin layer of cortical bone (Figs 13; 14). The compactness of the bone at this section is *c*. 0.39 (Table 4). The temporal crest

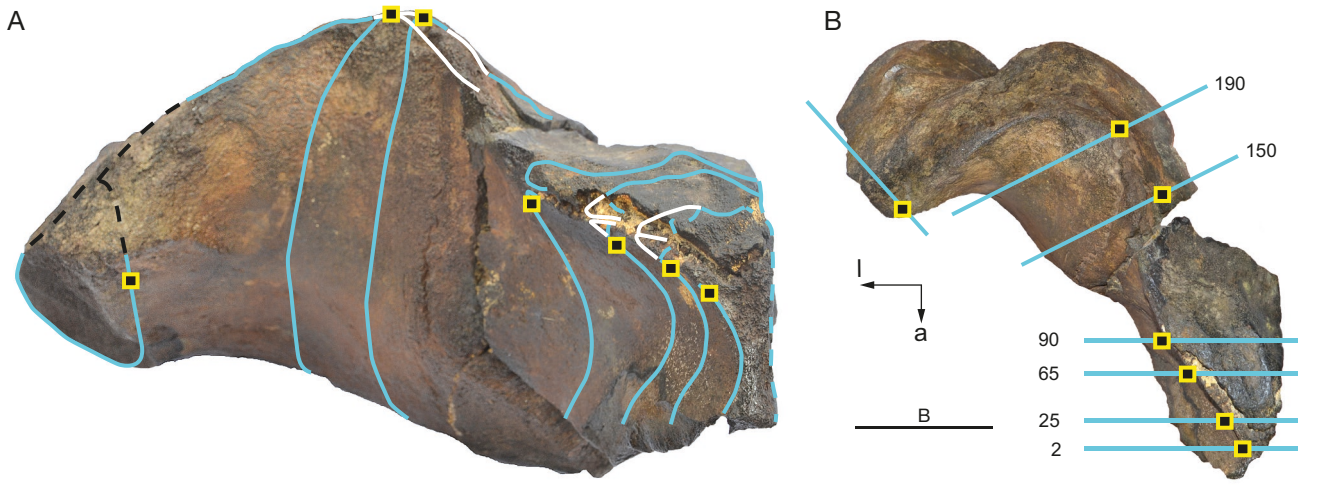

FIG. 10. — *Persufflatius renefraaijeni* n. gen., n. sp., MAB 010293, holotype: **A**, sections from right to left at 2, 25, 65, 90, 150 and 190 mm from the anterior tip, superimposed on an anterolateral view of the neurocranium. **B**, the same sections, superimposed on a posterodorsal view, from bottom to top at 2, 25, 65, 90, 150 and 190 mm from the anterior tip. **Clear blue lines**, sections as preserved; **dotted clear blue lines**, fractures as preserved; **white lines**, estimated shape of missing parts based on adjacent preserved parts; **dotted black lines**, estimated shape of the lateral temporal crest dorsal to the base of the zygomatic process. **a**, anterior; **l**, lateral. Scale bar: A, not to scale; B, 10 cm.

is strong, obtuse and rounded dorsal to the parietal; on the squamosal it gradually becomes a 90° edge. Laterodorsally, at the base of the zygomatic process of the squamosal, the supramastoid crest (lateral temporal crest) is eroded over the 70 lateral-most millimetres, judging by the curvature of the remaining surfaces, about 2 cm of bone is missing dorsally at this lateral-most point (Figs 10; 13; 14[dotted purple/green line at the left]). Laterally, only the posterior 71 mm of the zygomatic process of the squamosal are preserved. This posterior remnant of the zygomatic process of the squamosal is unusually high (Table 5A, B). On this surface, contrary to other BnBB, there is no sign of a supramastoid crest or fossa; the surface is laterally smooth over the dorsal 60 mm and is possibly abraded by erosion (Figs 8; 13). Anteroventrally, the pseudoval process protrudes relatively far into the temporal fossa (Figs 4E; 9; 12). The bone is spongy, with big mediolaterally elongated cavities (mean mediolateral W: 2.142; mean H: 0.824) (Appendix 2), having a compactness of *c.* 0.54 (Table 4). The anteroventral part of the dorsal squamosal fossa (= the posterior wall of the temporal fossa) bulges into the temporal fossa rising upwards at about 65° with respect to the horizontal plane; the posterodorsal part rises in posterior direction at some 45° to form the squamosal fossa. Posteriorly, the dorsal squamosal fossa is notably wider than in all other BnBB. Ventral to the dorsal squamosal-parietal suture, on the lateral wall of the temporal fossa, the ventral squamosal bulges more strongly into the temporal fossa, being somewhat inflated at this point. The bone has a *c.* 20 mm thick layer, composed of alternating thin layers of spongy and compact bone. More dorsally, along the dorsal part of the squamosal-parietal suture, the surface slopes in dorsomedial direction at about 120° with respect to the horizontal plane. In ventral view, the periotic fossa is deeply excavated and it is anteriorly abruptly restricted by a steep wall at the level of the posterior side of the pseudoval foramen (Fig. 12).

Pseudoval process, squamosal window and falciform process

We use the new term 'pseudoval process' (Figs 9; 12; 14) to indicate the anteromedial process of mysticete squamosals, that projects medioventrally and that bears the pseudoval foramen (Figs 9; 12) and the falciform process (Figs 9; 12; 20); In ventral view, the pseudoval process is laterally limited by the medial border of the ventral squamosal fossa; posteriorly it is limited by the anterior border of the periotic fossa. Anterodorsally, the pseudoval process is confluent with the squamosal body; the imaginary line running from the medial squamosal cleft to the medial border of the ventral squamosal fossa delimits the pseudoval process there. Medially and medioventrally the pseudoval process has a big sutural contact surface for the pterygoid (Fig. 14); mediodorsally it (most probably) contacted the (missing) alisphenoid. The pseudoval process is quite robust but anteroposteriorly short (71.8 mm high at the anterior side of the pseudoval foramen and 56.4 mm long anteroposteriorly). The pseudoval foramen is about 35 mm wide transversally (widening to 42 mm posteriorly). It is weakly curved ventrodorsally (about 9 mm high in the middle, as preserved; both the falciform process and the anterior process being damaged ventrally). The pseudoval process is mediolaterally relatively short (roughly 85 mm including the pseudoval foramen but excluding the falciform process). Only the dorsal part (roof) of the pseudoval foramen is preserved (Figs 4E, F; 9; 12). This preserved dorsal part is exclusively formed by the squamosal. As the ventral part is missing, it is unclear whether the foramen was entirely formed by the squamosal or whether the pterygoid made up part of the ventral side. Medially, a small fragment of the pterygoid is preserved. The preserved bone fragment is firmly fused with the squamosal (Fig. 14); it does not contact the pseudoval foramen. The falciform process is about 15 mm thick. It is at least 39 mm long (anteroposteriorly), but the exact dimen-

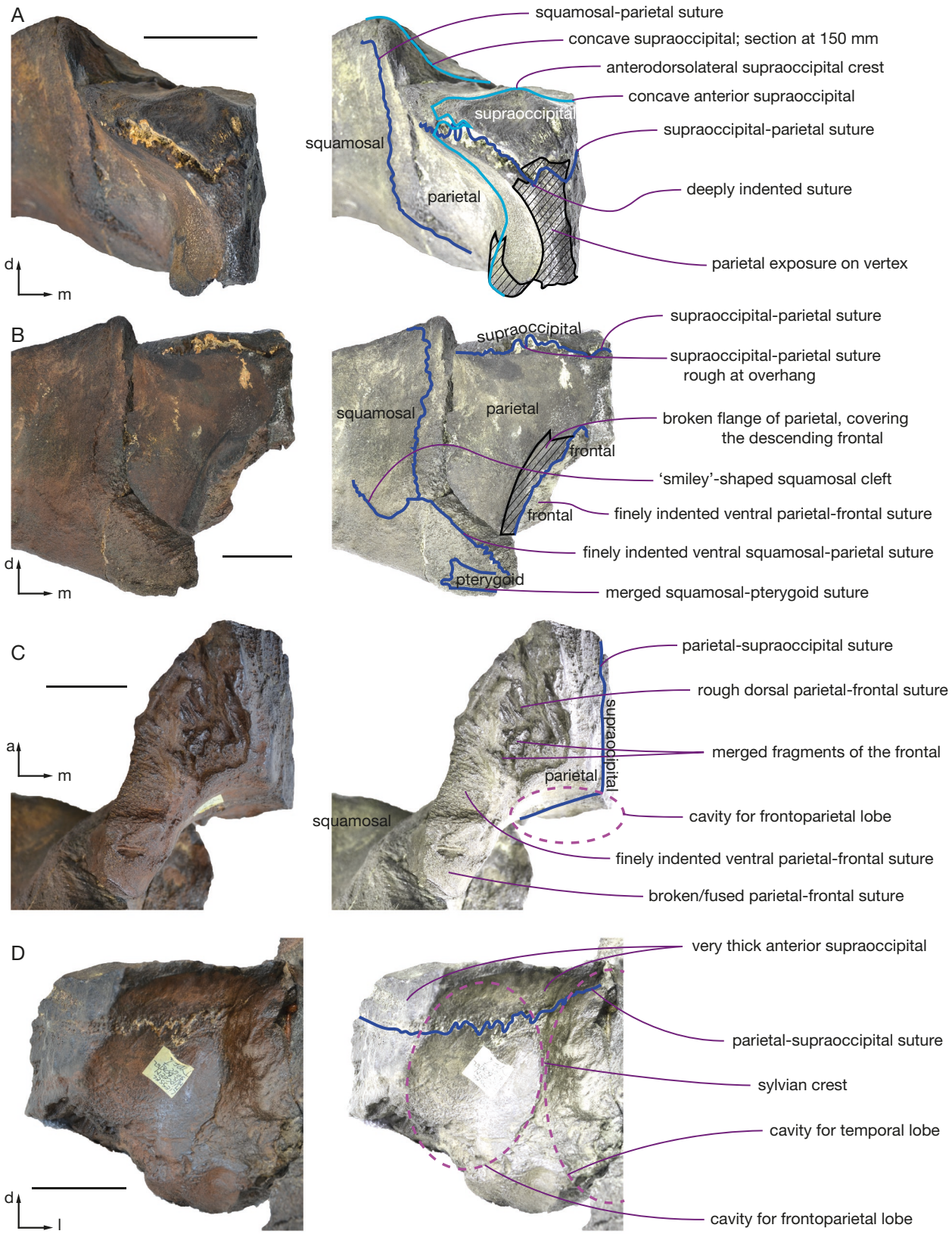

FIG. 11. — *Persufflatius renefraaijeni* n. gen., n. sp., MAB 010293, holotype. Detailed views of the parietal and the anterior supraoccipital: **A**, anterodorsal view; **B**, anterior view; **C**, ventral view; **D**, posteromedial view. **Dark blue lines**, sutures; **clear blue lines**, sections; **dotted magenta lines**, zones; **black hatched surface**, broken surfaces of the parietal. **a**, anterior; **d**, dorsal; **l**, lateral; **m**, medial. Scale bars: 5 cm.

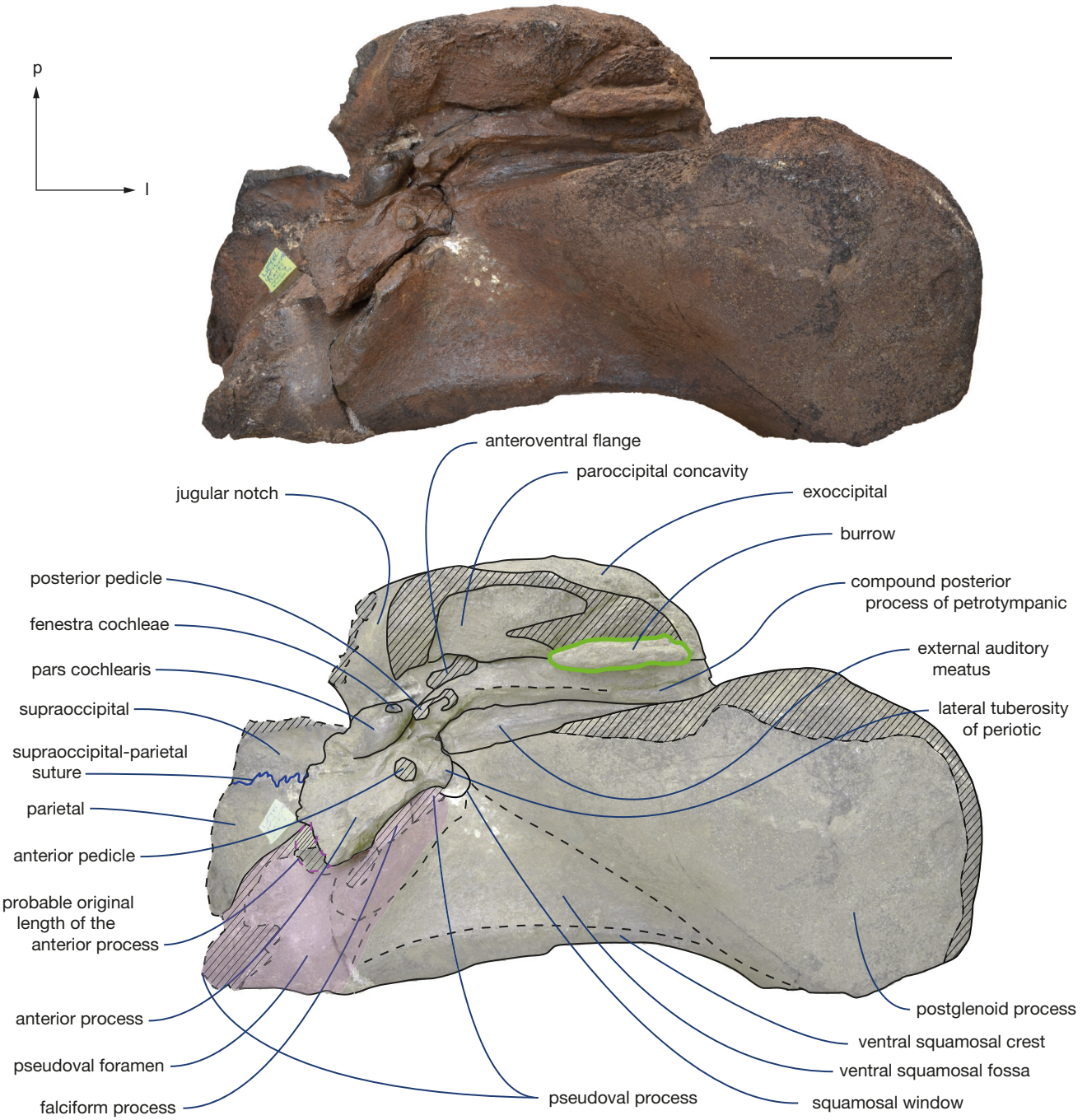

Fig. 12. — *Persufflatius renefraaijeni* n. gen., n. sp., MAB 010293, holotype. Ventral view, with the periotic in place. **l**, lateral; **p**, posterior. **Dashed magenta line**, (maximum) estimated shape of the missing tip of the anterior process, based on the limited room left by the posterodorsal part of the pseudoval foramen and the shape and curvature of the preserved part of the anterior process of the periotic; **pink surface**, pseudoval process. Scale bar: 10 cm.

sions are uncertain, as it is damaged at both the anterior and posterior sides. We designate the concave surface of the squamosal between the posterior falciform process and the anterior border of the external meatus as 'squamosal window' (new term; Figs 4E, F; 9; 12; 20). The squamosal window exposes part of the lateral side of the anterior process of the periotic. In ventral view, the squamosal window is anteroposteriorly short (about 28 mm long, which is shorter than in *Parietobalaena*) and continuously curved (contrary to the condition in *Metopocetus hunteri* Marx, Bosselaers & Louwye, 2016, where the squamosal window is squared (Marx *et al.* 2016a: 12-13, fig. 5/6a); it is rounded also in (most) other BnBB mysticetes like *Parietobalaena palmeri* (Kellogg 1968: 182, fig. 83, 84, pl. 67), *Diorocetus hiatus* (Kellogg 1968: plate 50), *Parietobalaena campiniana* (Bisconti *et al.* 2013: 111, RBINS M 399, fig. 19 [hiat]), '*Parietobalaena*' *laxata* (IRSNB M 712, 713 and 727) and *Idiocetus longifrons* (IRSNB M 718) (MB pers. obs.).

TABLE 5. — **A**, **B**, Comparison of *Persufflatius* n. gen. with some other mysticetes: **A**, measurements; **B**, values relative to bizygomatic width. All measurements in mm. Abbreviations: **EAM**, extarnal auditory meatus; **H**, height; **L**, length; **W**, width.

A: species Absolute values	(estimated) W bi-zygomatic	bilateral EAM	mediolateral W squamosal	Antero-posterior L squamosal	H squamosal fossa	anteroposterior L postglenoid process base	mediolateral W postglenoid process- EAM	ventrodorsal H zygomatic onset
Persufflatius renefraaijeni n. gen., n. sp. MAB 010293	740	630	238	170	166	111	188	130
Parietobalaena campiniana IRSNB M399	440	310	175	92	70	47	102	47
Herpetocetus sendaicus IGPS 78423	380	240	140	143	-	34	83	70
Piscobalaena nana SAS1617	404	286	125	123	-	47	87	55
Balaenoptera acutorostrata juvenile NMR 99903024	575	508	205	130	86	55	147	80

B: species Relative values	(estimated) W bi-zygomatic	bilateral EAM	mediolateral W squamosal	Antero-posterior L squamosal	H squamosal fossa	anteroposterior L postglenoid process base	mediolateral W postglenoid process- EAM	ventrodorsal H zygomatic onset
Persufflatius renefraaijeni n. gen., n. sp. MAB 010293	1000	851	322	230	224	150	254	175
Parietobalaena campiniana IRSNB M399	1000	704	397	209	159	107	231	107
Herpetocetus sendaicus IGPS 78423	1000	631	368	376	-	99	229	144
Piscobalaena nana SAS 1617	1000	707	309	304	-	116	215	136
Balaenoptera acutorostrata Juvenile NMR 99903024	1000	884	357	226	150	96	257	135

Squamosal-parietal suture

The dorsal part of the squamosal-parietal suture descends anteroventrally from the temporal crest and is almost perfectly straight (Figs 8; 10; 11A, B; 13; 14). In this dorsal part, the suture-line itself is crenate, still visible as a 3 to 4 mm wide furrow externally; internally, the suture is not discernible anymore. slightly below mid-height the suture inclines about 135° in anteroventromedial direction. The squamosal side of this lower part of the suture is preserved, but the opposite parietal side has broken off and is missing. This ventral part of the squamosal-parietal suture (anterodorsal border of the squamosal) is slightly curved (concave anterodorsally). This part of the suture is not fused and, contrary to the upper part, is finely denticulate. At the point where the squamosal-parietal suture changes direction, it also contacts the squamosal cleft (laterally).

Squamosal cleft

The squamosal cleft is 'smiley'-shaped (dorsally concave); the suture is irregular, shallow and in places only visible in grazing light due to an advanced state of merging (Figs 11B; 14). It looks similar to the squamosal cleft of *Parietobalaena* sp. (*Parietobalaena laxata* (IRSNB M 712 and M 727); MB pers. obs.). It is mediolaterally 70 mm wide. Internally, on the anterior border and on the anteromedial border of the periotic fossa, the remnant of the internal squamosal cleft suture is visible as a sharp edge, medially terminating in a narrow furrow, running upwards from the anteromediodorsal edge of the periotic fossa. It seems to continue in anterior direction, to 'surface' as a narrow foramen (8.5 mm) at the posteroventrolateral corner of the parietal flange covering the dorsal supraorbital process of the frontal (white arrows in Fig. 14).

Postglenoid process

The postglenoid process is wide and semi-circular to half-teardrop-shaped in posterior view (Figs 4A, B; 9), protruding far ventrally (about 100 mm high, as preserved posteriorly; another *c.* 15 mm is missing ventrally, based on the shape, curvature and orientation of the preserved surfaces, totalling about 115 mm

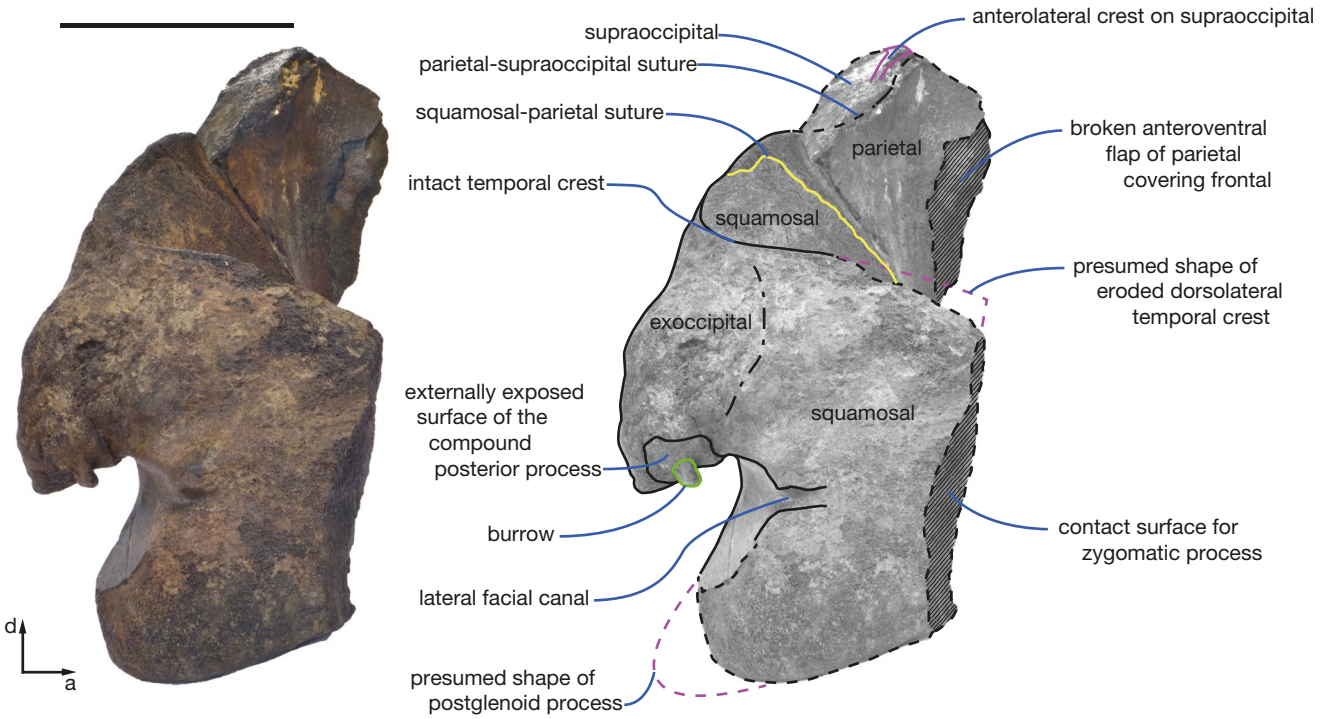

FIG. 13. — *Persufflatius renefraaijeni* n. gen., n. sp., MAB 010293, holotype. Posterolateral view. Scale bar: 10 cm.

dorsoventral height). Posteriorly, it is flat to slightly concave; anteriorly, it is globose and inflated (a strange condition for the surface that articulates with the convex mandibular condyle). Lateroventrally, the postglenoid process is also strongly inflated (Figs 12; 13). This is somewhat similar to the condition observed in *Atlanticetus patulus*, but the anterior surface is more inflated and is mediolaterally wider, being massive and large compared to the size of the skull. The postglenoid process consists entirely of spongy bone (its internal compactness is about 0.35; Table 4) with medium-sized cavities (mean W: 1.01 mm; mean H: 0.765 mm; Appendix 2). Externally, it is covered by a thin layer of cortical bone. The posterodorsal base of the postglenoid process, the central edge in the external auditory meatus (EAM), is 188 mm wide mediolaterally (medial border of the cranial hiatus till the lateral U-shaped edge of the foramen for the facial nerve). The base-line is mediolaterally continuously curved.

Ventral squamosal crest

The anteroventral border of the squamosal fossa is delimited by a ventrally protruding, sharply edged bony crest (ventral squamosal crest) that separates the ventral surface of the squamosal (ventral squamosal fossa) from the temporal fossa, thus limiting the manoeuvrability of the mandibular condyle medial to the postglenoid contact surface (Figs 4E; 9; 12).

External auditory meatus (EAM)

The EAM is narrow (medially, 17 mm; centrally, 15 mm; laterally, at the level of the lateral exoccipital, *c.* 31 mm), slightly widening medially, recaling the condition in *Cephalotropis nectus* and *Heterocetus affinis*, giving it the appearance of a slender elongated spoon. Far laterally the borders of the EAM are not well defined and it widens fan-shaped (Fig. 21). Anterolaterally, a furrow continues far on the posterior side of the postglenoidal process, terminating laterodorsally in a distinct narrow U-shaped sulcus (11.2 mm wide and 8.22 mm deep), that most probably accommodated the facial nerve (Figs 4A, B; 12; 13; 21).

Sternomastoid fossa

Dorsolaterally, above the postglenoid process, there is no deep well-defined sternomastoid fossa. This fossa is very pronounced in *Parietobalaena*, but in the same position on the squamosum, there is no sign of a fossa in *Persufflatius renefraaieni* n. gen., n. spec. Instead, there is an inflated protrusion, having an irregular, coarse, somewhat eroded surface, not covered externally by cortical bone. The sternomastoid fossa may have been completely abraded, or, the sternomastoid fossa was positioned more anteriorly, on a part of the squamosal that is missing due to fracturing (Figs 8; 13).

Ventral squamosal

The periotic fossa (the anterolateral, lateral and laterodorsal border of the cranial hiatus) is deeply excavated and ovoid (anteroposteriorly oblong) and anteriorly steeply restricted by the dorsal wall of the pseudoval foramen (width 52.5 mm; length: 47 mm; deep: 20.1 mm with respect to the EAM border; 33 mm with respect to the lateral border). Whereas the periotic fossa is long, the pseudoval foramen is shorter than usual (Fig. 12).

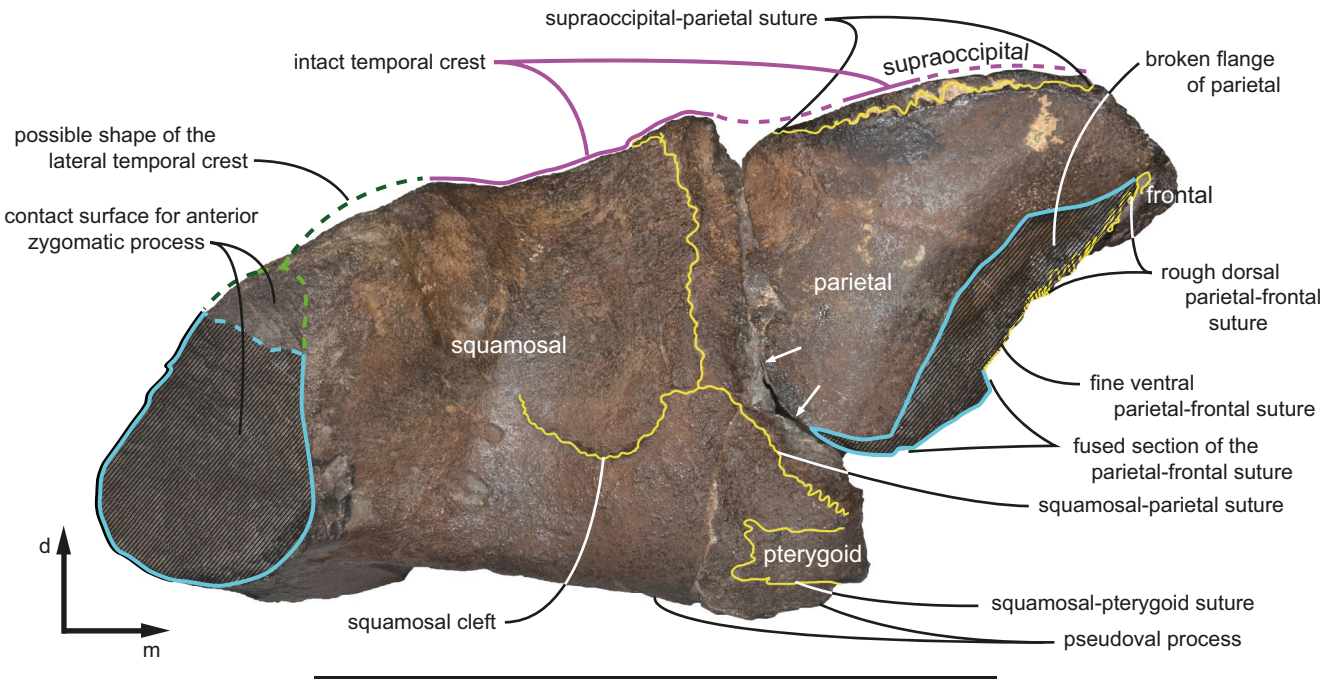

FIG. 14. — *Persufflatius renefraaijeni* n. gen., n. sp., MAB 010293, holotype. Anterolateral view with all preserved sutures indicated (**yellow lines**). **White arrows**, narrow posteroventrolateral parietal foramen. **d**, dorsal; **m**, medial. Scale bar: 30 cm.

Pterygoid

The anteromedioventral part of the squamosal-pterygoid suture is preserved on the squamosal. Medioventrally, this suture seems to be in an advanced state of fusion and its shape is difficult to observe in full detail. The preserved part of the fused bone is 35 mm wide and 25 mm high. On the posterior side the bone has broken and the trapezoid suture, delimiting this roughly 50 × 30 mm sized bone is clearly visible (Figs 11B; 14). The bone is spongy with a compactness of *c.* 0.59 (Table 4).

Occipital

The occipital is (half) bell-shaped in posterodorsal view. The medioventral part of the supraoccipital, the exoccipital and the basioccipital are missing (Figs 4B, C; 7F; 8; 10; 11A; 14; 15). The lateral exoccipital is well preserved.

Supraoccipital

Part of the right half of the supraoccipital is preserved. Judging from the right half, the complete supraoccipital shield must have been (sub-)bell-shaped, with a sigmoid temporal crest (somewhat similar to *Uranocetus* but more rounded and bell-shaped), the supraoccipital being transversely compressed along its anterior half. The anterodorsal surface of the supraoccipital is slightly to strongly concave. The medial part of the exoccipital, bearing the condyles and the foramen magnum, is missing, but the approximate position of the right occipital condyle can be reconstructed (Fig. 8).

The exact shape of the apex is unclear, due to erosion of this part of the skull. It was most probably pointed (triangular) or narrowly trapezoid. Medially, the suture between the supraoccipital and the parietal is visible as a fine straight line, about 25 mm below the dorsal edge of the supraoccipital. Centrally, in the *c.* 25 mm-thick-supraoccipital, a layer of spongy bone, about 7 to 9 mm thick, is present (compactness *c.* 0.51; Table 4). The bone above and below this strip consists of dense, hypermineralized bone (compactness *c.* 0.81; Table 4), which is most probably redeposited (Figs 11D; 15). Such a thick anterior supraoccipital with two thick layers of dense bone is unusual. The anterior supraoccipital can be equally thick or even thicker in *Herentalia nigra* Bisconti, 2014-like cetotheriids, such as *Metopocetus hunteri* (with the same bizygomatic width), but the bone is internally uniformly spongy and becomes quickly thinner in posterior direction, while in *Persufflatius* n. gen. it stays equally thick over 85 mm (Table 3) and becomes even more dense posteriorly (compactness *c.* 0.84; Table 4). In extant Balaenopteridae the anterior supraoccipital is thin. In specimens of *Balaenoptera acutorostrata* with the same bizygomatic width, the supraoccipital is anteriorly about 12 mm thick and becomes slightly thinner posteriorly (MB pers. obs.; Table 3).

Anterolaterally, the supraoccipital is roughly indented with the parietal. This anterolateral part of the supraoccipital overhangs the temporal fossa laterally; posteriorly, it does not overhang this fossa (similar to *Titanocetus* Bisconti, 2006, but in the latter it also overhangs the temporal fossa posteriorly). The lateral overhanging edge is *c.* 25 mm wide as preserved. The anterolaterodorsal extremities (estimated to have been about 15 mm wide) of both the supraoccipital and the parietal broke off and are missing (Figs 8; 10[white lines]). The width of the overhang is thus estimated to have been maximum *c.* 40 mm wide origi-

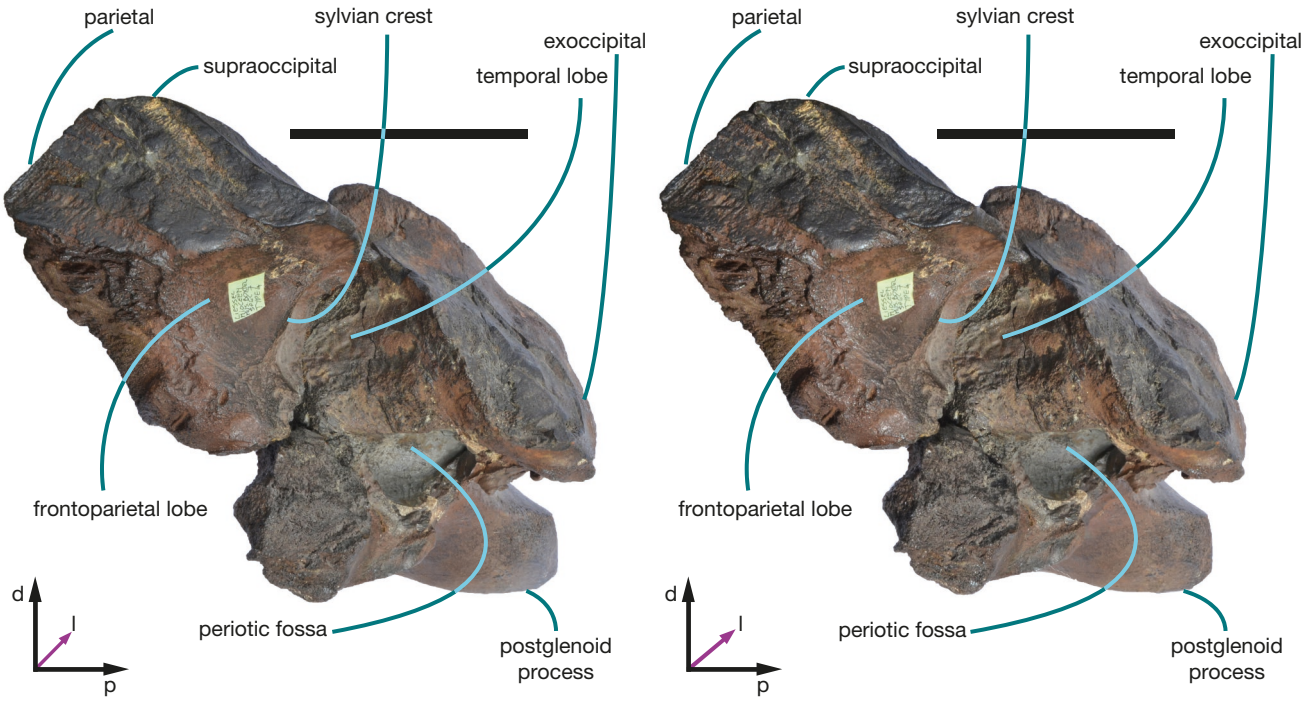

FIG. 15. — *Persufflatius renefraaijeni* n. gen., n. sp., MAB 010293, holotype. Medial view without periotic. **d**, dorsal; **l**, lateral; **p**, posterior. Stereo image. Scale bars: 10 cm.

nally, based on the orientation and curvature of the preserved surfaces of the lateral supraoccipital and the parietal adjacent to the fracture. The parietal-supraoccipital suture is rough at the level of the overhang; anteriorly, it is deeply indented with a triangular descending V-shaped point (Figs 10; 11A; 14).

Anterodorsolaterally on the supraoccipital there is a prominent, broad, oblique crest, running from the central axis in posterolateral direction, roughly parallel to the lateral border of the bone (Figs 8; 10; 11A). Dorsally, the crest is eroded, polished and obtuse. This crest is quite peculiar and does not, to our knowledge, occur in any other mysticete. Apart from this crest there is no other obvious attachment surface for neck musculature preserved. The preserved part of the supraoccipital has no external occipital crest; the anteromedial part of the supraoccipital is concave (the external occipital crest is missing also in *Pelocetus calvertensis* and *Atlanticetus patulus*, contrary to *Parietobalaena*, *Tiucetus*, *Uranocetus and Diorocetus hiatus*).

Cranial endocast (Figs 15-17)

Medioventrally, the imprints of the frontoparietal and the temporal lobes of the cerebrum are clearly visible (Figs 11C, D; 15; 16; 17). Because the internal neurocranium is well preserved and looked different from most neurocrania we know, we decided to make a cranial endocast (see Material and methods). We estimate the volume of the brain between 1500 and 1800 cm³. The imprint of the temporal lobe of the cerebrum is short and deeply excavated (extending about 35 mm more lateral than the lateral-most point of the frontoparietal lobe). The temporal lobe and the adjacent perisylvian cortex are strongly developed in whales, indicating that the auditory signal processing is important (Fig. 16; Ölschläger & Ölschläger 2002: 137, 138). The temporal lobe is anteroposteriorly compressed (foreshortened; Morgane *et al.* 1980), making it transversely ovoid (L: 63 mm; H: 82 mm; W: *c.* 53 mm). The top 21 mm of this lobe are situated in the supraoccipital. The ventral part is situated in the parietal and the squamosal. The suture between the parietal and the squamosal runs over the middle of the temporal lobe, from the left top corner to the right bottom corner (Figs 16; 17). The surface of the bone near this suture is damaged due to fracturing. It is visible in the stereo-image (Fig. 16) as a diagonal, slightly elevated dark grey strip. The posteroventral part (Fig. 17), just below the centre of the image, which is situated within the squamosal, has a wrinkled surface. The largest tubular imprints are terminal branches of venous sinuses, presumably linked to the inferior anastomotic vein of Labbé (black lines in Fig. 17), some of which are crossed by fine thread-like superimposed imprints, being terminal branches of smaller cortical veins (magenta lines on Fig. 17) (obs. and pers. corr. Dr Yannick Van Ael; MB pers. obs.). At this posterior base of the lobe, surface features are well preserved and more marked than on the rest of the cerebral surface. The anterior side of the temporal lobe and the frontoparietal lobe have a smooth surface, due to the partial ossification of the meninges (Ölschläger & Ölschläger 2002: 133; Marx *et al.* 2016b: 81); therefore, cortical gyri are not present on the imprint/cast. The curved border on the right side of the temporal lobe (Fig. 17[top right, green line]) is the sylvian fissure (Breathnach 1955; Ölschläger & Ölschläger 2002: 135; Bisconti *et al.* 2021b). The deep imprint of the sylvian fissure ventrally, hints at a sizeable superficial sylvian vein. The rectangular part at the bottom left, below the lobe, is not part of the cranial imprint. It is the medial

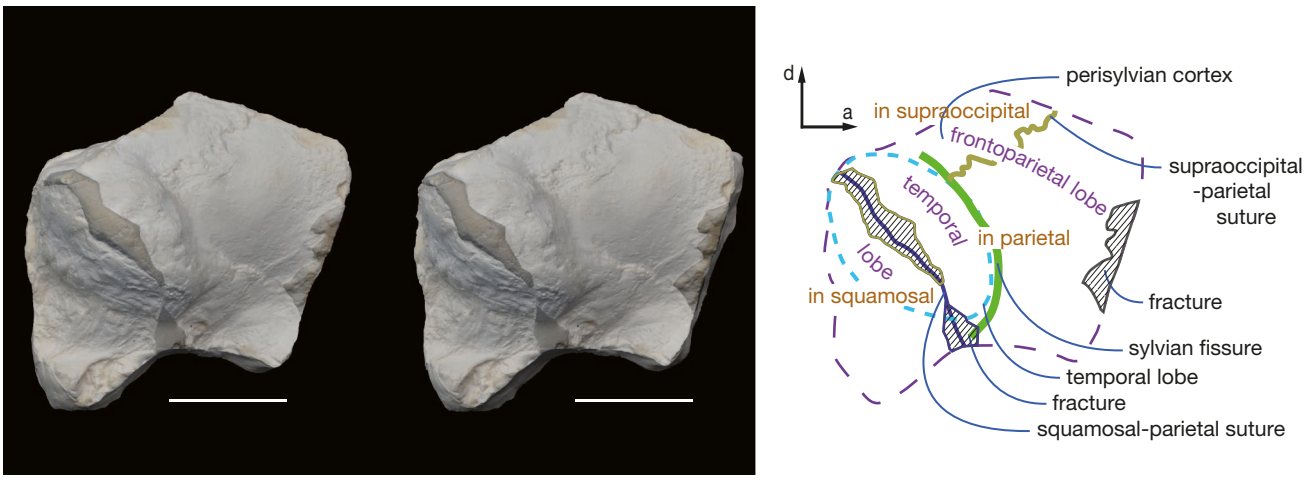

Fig. 16. — *Persufflatius renefraaijeni* n. gen., n. sp., MAB 010293, holotype. Lateral stereo view and annotated line draw of the endocast of the right cerebral imprint as preserved. **d**, dorsal; **a**, anterior. **Grey areas**, missing fragments due to fracture. At the right side is the imprint of the frontoparietal lobe. To the left is the protruding imprint of the laterally protruding temporal lobe. Scale bars: 5 cm.

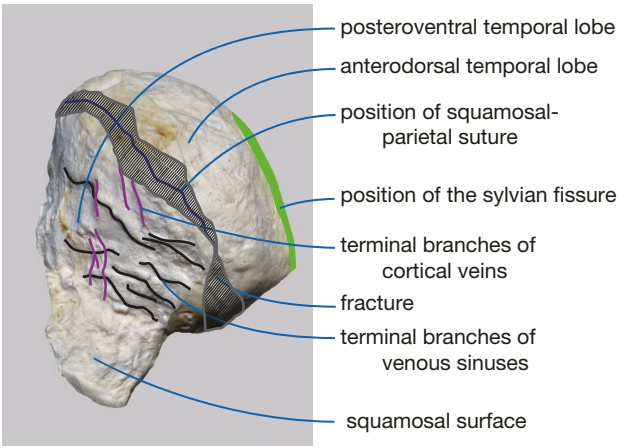

Fig. 17. — *Persufflatius renefraaijeni* n. gen., n. sp., MAB 010293, holotype. Cast of the lateral side of the temporal lobe of the cerebrum: interpretation of the surface structures. Antrolateral view. **a**, anterior; **d**, dorsal. **Bright green line** indicates the position of the almost vertical sylvian fissure (the separation between the frontoparietal and the temporal lobe). The **wavy violet line** in the middle of the lobe indicates the position of the internal parietal-squamosal suture. The **black lines** indicate terminal branches of the venous sinuses (reasonably large blood vessels); they are crossed by smaller cortical veins (**magenta lines**). **Hatched lines**, fracture. Scale bar: 30 mm. (obs. and pers. comm. Dr Yannick Van Ael; MB pers. obs.).

surface of the squamosal that connects the fossa for the periotic (just above the lateral side of the anterior process of the periotic) with the fossa for the temporal lobe. The imprint of the frontoparietal lobe is about 100 mm high and the diagonal length is 80 mm as preserved. The top 30 mm are situated in the supraoccipital; the ventral part is completely situated in the parietal. Mediodorsally, internally, there is no indication of a internal central occipital crest (Fig. 11C, D).

Exoccipital (Figs 4A-C; 8; 12; 13; 15)

The exoccipital is mediolaterally wide compared to all other BnBB; it is strongly inflated, posterolaterally globose and very rounded (anteroposterior length: 43 mm at the paroccipital cavity; 53 mm laterally, just dorsal to the posterior process of the petrotympanic). The lateral and dorsal border of the exoccipital is poorly defined, as it is almost completely merged with the posterior side of the zygomatic process of the squamosal, hinting at a young adult ontogenetic age. In dorsal view its lateral border is just lateral to the level of the medial base of the zygomatic process. This lateral part consists of spongy bone with a low compactness (*c.* 0.41; Table 4). The exoccipital is tapering at the lateral side, dorsal to the posterior process of the petrotympanic. The posterior process of the petrotympanic is laterally confluent with the exoccipital border and it is surrounded by the exoccipital dorsally, posteriorly and posteroventrally. This suture is also merging dorsally, where it is difficult to observe.

Ventrally, the jugular notch and the paroccipital concavity are partially preserved. Only the lateral part of the jugular notch is preserved over *c.* 22 mm (posteriorly). The anteroposterior length of the exoccipital is *c.* 35 mm at the level of the jugular notch, the surface of which is only slightly concave. The jugular notch is laterally constricted by a 19 mm wide and 38.5 mm long robust crest, running over the entire length of the exoccipital, that separates it from the paroccipital concavity. The ventral edge of this crest is missing due to erosion. The jugular notch widens anteriorly, approaching the posterior cranial hiatus, and reaches *c.* 32 mm there, but due to the fracture of the anteromedial part, the real shape can only be estimated. The surface of the jugular notch is strongly inclined in anterodorsal-posteroventral direction (*c.* 30° with respect to the horizontal plane) (Fig. 12). The bone of the jugular notch is spongy, with a compactness of *c.* 0.48 (Table 4). As the jugular notch is adjacent to the occipital condyle, we can roughly estimate the bicondylar width at *c.* 150 - 170 mm. The condyles must have been relatively smaller than in *Tiucetus*, but larger than in *Pelocetus* and probably similar in size to those of *Uranocetus* (Fig. 7C, F, G). The paroccipital cavity is weakly excavated. Its shape is not clear due to erosion, but the concavity was at least 30 mm long at its longest point and about 42 mm wide posteriorly, at its widest point (Fig. 12).

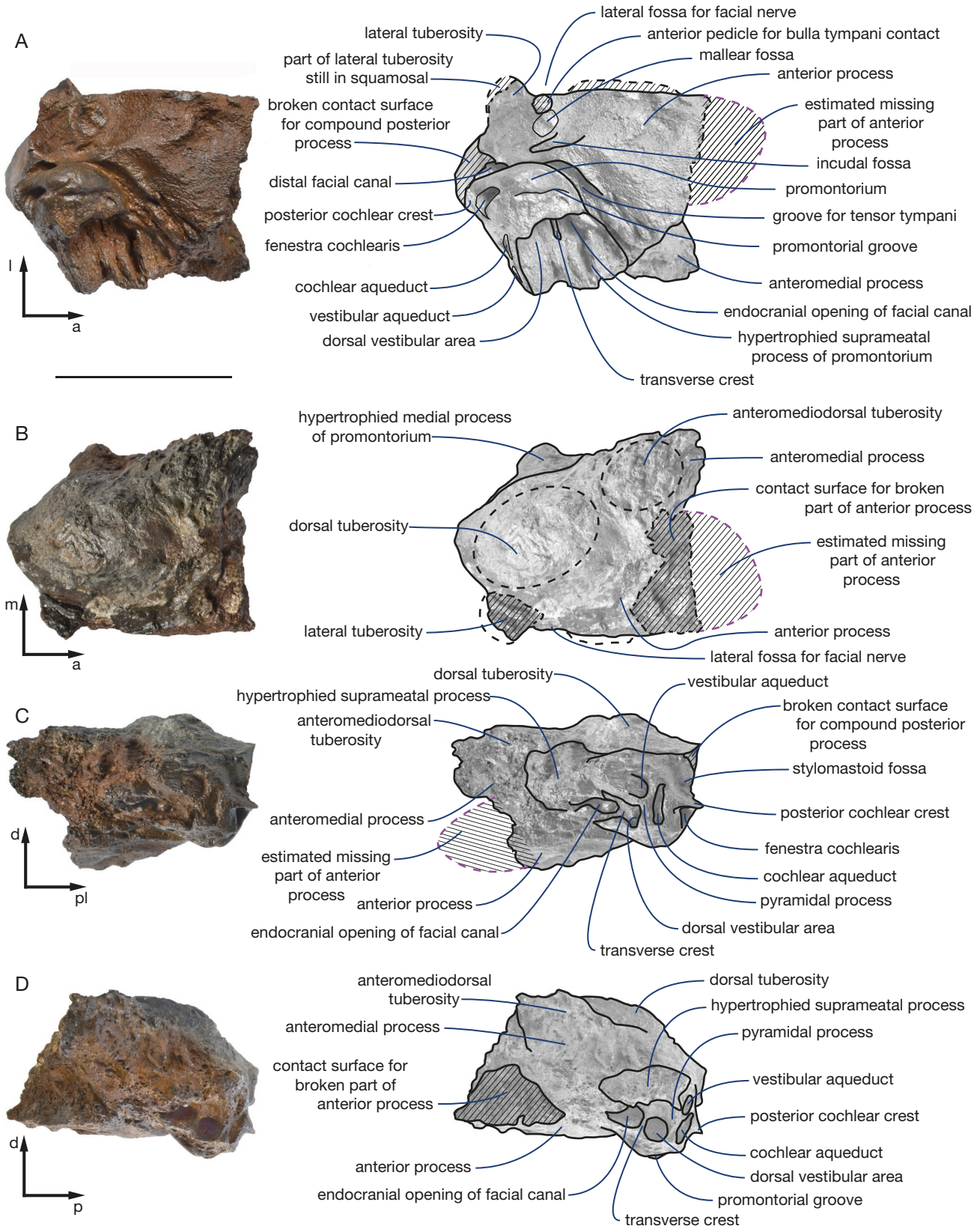

FIG. 18. — *Persufflatius renefraaijeni* n. gen., n. sp., MAB 010293, holotype. Right periotic: **A**, ventral view; **B**, dorsal view; **C**, posteromedial view; **D**, medial view. **a**, anterior; **d**, dorsal; **l**, lateral; **m**, medial; **p**, posterior; **pl**, posterolateral. Scale bar: 5 cm.

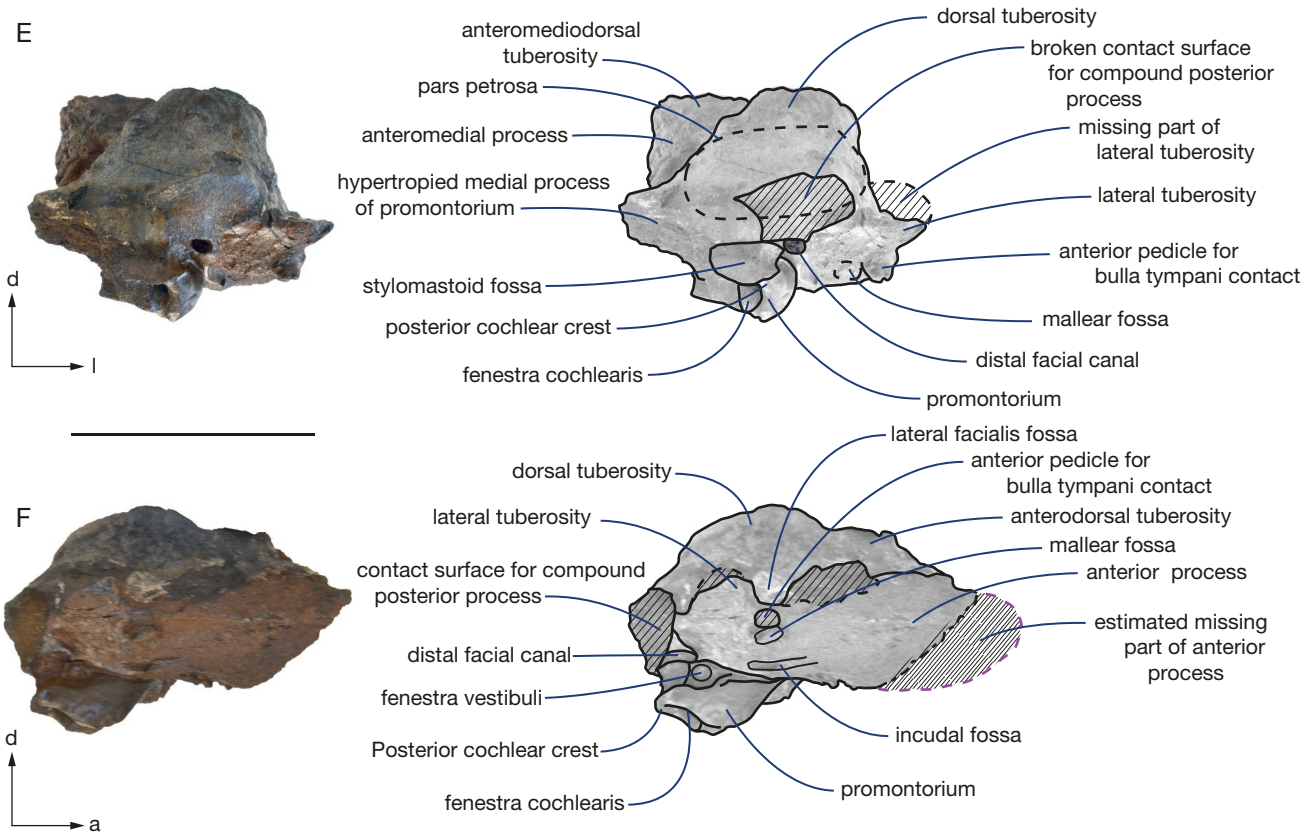

FIG. 19. — *Persufflatius renefraaijeni* n. gen., n. sp., MAB 010293, holotype. Right periotic: **E**, posterior view; **F**, lateroventral view. **a**, anterior; **d**, dorsal; **l**, lateral. Scale bar: 5 cm.

Periotic (Figs 4F; 12; 13; 18-20; 22)

In mysticetes, the periotic often gives an important indication of the species' overall taxonomic affinities (Steeman 2010; Ekdale *et al.* 2011). The periotic of *Persufflatius renefraaijeni* n. gen., n. sp. closely resembles that of *Pelocetus calvertensis* and, to a lesser extent, that of *Atlanticetus patulus*. It resembles *Pelocetus* in having a generally inflated aspect, having a strong and wide, dorsally protruding tuberosity, continuously running over the whole dorsal surface of the pars petrosa (H: 22 mm). It continues (somewhat less inflated) over the anterior process (H: 10 mm). The lateral tuberosity is relatively small compared to the overall volume of the periotic. This process appears blade-like in the images, but it should be noted that a spherical dorsal part that belongs to it, is still attached to the ventral side of the squamosal (the circumference of which is marked with a dashed line in Fig. 18A, B. The full extent of this lateral process can be judged from the reconstruction in (Fig. 22[purple-grey spot at the left]). The lateral tuberosity is positioned very far posteriorly, at the level of the fenestra vestibuli (oval window).

Pars petrosa (Figs 18; 19)

The pars petrosa is mediolaterally wide (W: 62 mm at the level of the lateral process), and especially wide compared to *Parietobalaena palmeri*, *Heterocetus affinis* and *Cephalotropis nectus* (Fig. 19E). A *c.*15 mm long part of the anterior process is missing. The preserved length of the anterior process, anterior to the mallear fossa, is 42.3 mm, so originally it must have been about 57 mm long (Fig. 22[right purple-grey spot]). Ventrodorsally it is very high (about 37 mm anteriorly). The length of the periotic as preserved is 71.5 mm (anterolateral process till posterior cochlear crest). The original length is estimated to have been *c.* 83-87 mm. The periotic is medially and anteromedially hypertrophied, dorsal and anterodorsal to the dorsal vestibular area. This type of bone growth is often due to aging (ontogenetic hypertrophy), indicating the specimen is certainly a young adult at least. At the dorsal side, the dorsal tuberosity is reminiscent of that in *Parietobalaena*, being anteroposteriorly elongated (L: *c.* 38 mm; W: *c.* 27 mm) and inflated, its dorsal surface being irregularly rippled and bumped, without a clear crest. Anteromedially, on the pars petrosa (anteromedial to the promontorium), there is an anteromedially oriented, ventrodorsally thick, relatively long and slender, pointed anteromedial process (Fig. 18A-D), about 36 mm wide (anteromedial to the dorsal bulge); 45 mm long anteromedial to the anteromedial corner of the promontorium and 27 mm thick (apparently as a result of ontogenetic secondary bone growth also).

Mallear fossa

The mallear fossa is poorly defined and has a somewhat rough surface (*c.* 6 mm wide). It is situated just posterior to the anterior pedicle. Medial to this surface, there is a narrow

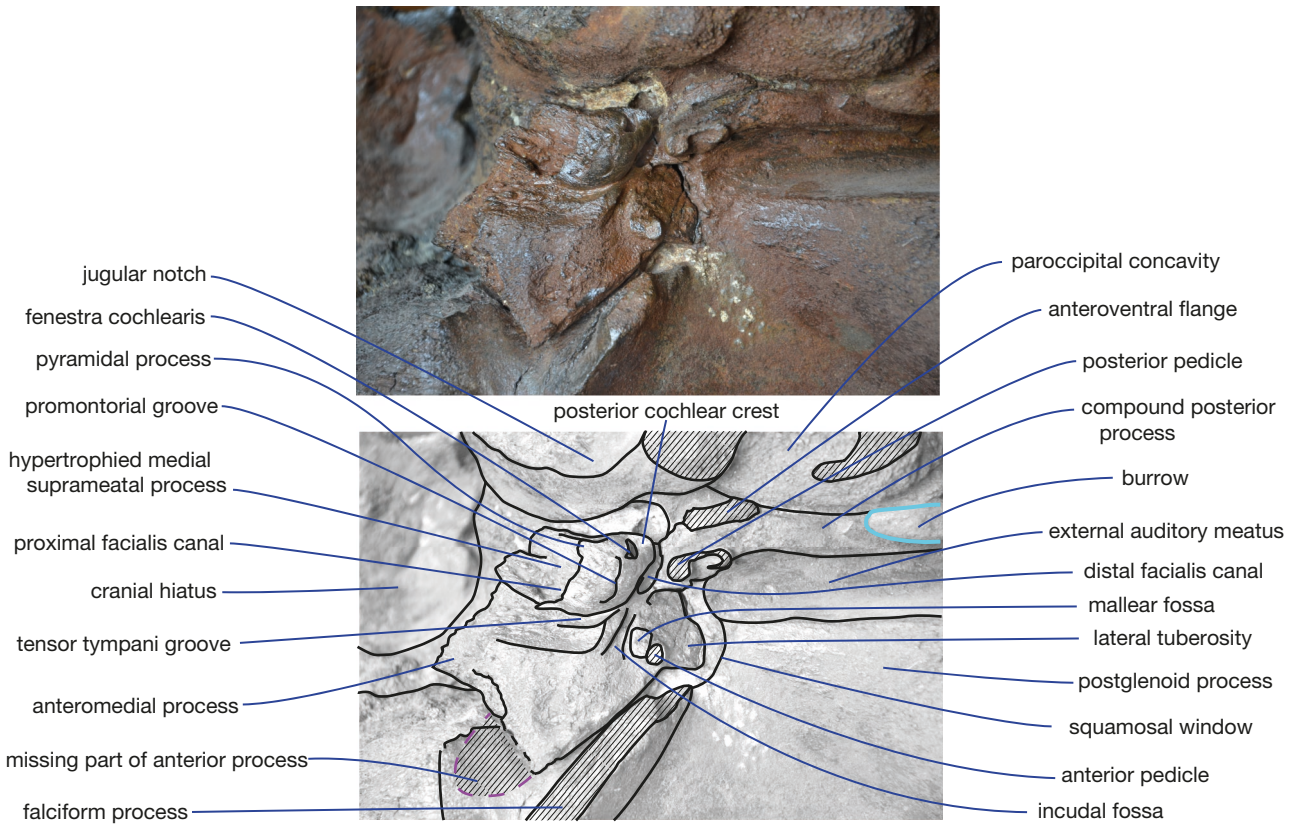

FIG. 20. — *Persufflatius renefraaijeni* n. gen., n. sp., MAB 010293, holotype. Right periotic *in situ* in squamosal. **Light blue line**, burrow. Ventral view.

(L: 11 mm; W: 3.3 mm), relatively deep and well-defined incudal fossa, discernible just lateral to the base of the lateral (distal) facial canal, medially and posteriorly constricted by a clear steep crest (Figs 18A; 19F; 20). This fossa is similar to the one in *Atlanticetus patulus*, but narrower.

Compound posterior process of the petrotympanic

The compound posterior process of the petrotympanic (hereafter posterior process) is mediolaterally wide (long), slender and rod-like. Laterally the posterior process widens a bit to become slightly inflated and sub-rectangular (Figs 13; 21). But its lateroventral border lacks a flange or other protrusions (Figs 12; 20). Posterodorsal to the EAM, dorsal and far lateral to the lateral end of the posterior process, the postmeatal crest forms a deep, prominent, well-defined canal for the transit of the facial nerve laterally (Fig. 13).

Medially, the contact surface between the pars petrosa and the posterior process is large, measuring 26 × 15 mm, and roughly semi-circular, the circular side pointing dorsally. In ventral view, the ventral surface of the posterior process shows a narrow cusp posteriorly, for the transit of the facial nerve, that is anteriorly bounded by a weak, elliptical anteroventral flange (*sensu* Marx *et al.* 2016a: 16). It is *c.* 23 mm wide, *c.* 11.7 mm long and *c.* 6 mm high. Anteriorly, this groove is defined by a robust and distinct upright crest delimiting the lateral facial canal. The groove for the facial nerve disappears more laterally (Fig. 21). Medially, on its posterior edge, the posterior process has an elongated, mediolaterally oriented, kidney-shaped posterior pedicle that contacts the tympanic bulla. The anterior and posterior pedicles to contact the tympanic bulla are closely separated (about 25 mm), hinting at a small (anteroposteriorly short) tympanic bulla (Table 1; Figs 12; 20), possibly similar to that of *Parietobalaena campiniana*.

The shape of the dorsal pars petrosa and of the anterior process and the long, straight and slender posterior process, with just a simple anteroventral flange medially and no protrusions laterally, indicate a close relationship to some BnBB-mysticetes, such as *Pelocetus*, *Uranocetus* and *Parietobalaena*.

Lateroventrally on the posterior process, centrally in the concave depression, there is an elongated tube-like structure. This structure is an ichnofossil, made of very hardened sediment. It is probably a burrow (L: 60 mm; W: *c.* 12 mm), though no clear openings or surface structures are present to confirm this (Figs 9; 12; 13).

Anterior process of the periotic

The anterior process occupies the anterolateral, lateral and anterodorsal borders of the cranial hiatus. It was probably anteroposteriorly short. Anteriorly, the process is damaged: a 19 mm thick flange has broken off. The posterior side of the pseudoval foramen anteriorly limits the possible length of the missing part to maximum 17 mm, thus limiting the maximum original length of the complete anterior process to maximum 59 mm. Posterolaterally, almost adjacent to the posterior process, is a small (diameter about 13 mm), rounded, lateral tuberosity. It appears as blade-like in the

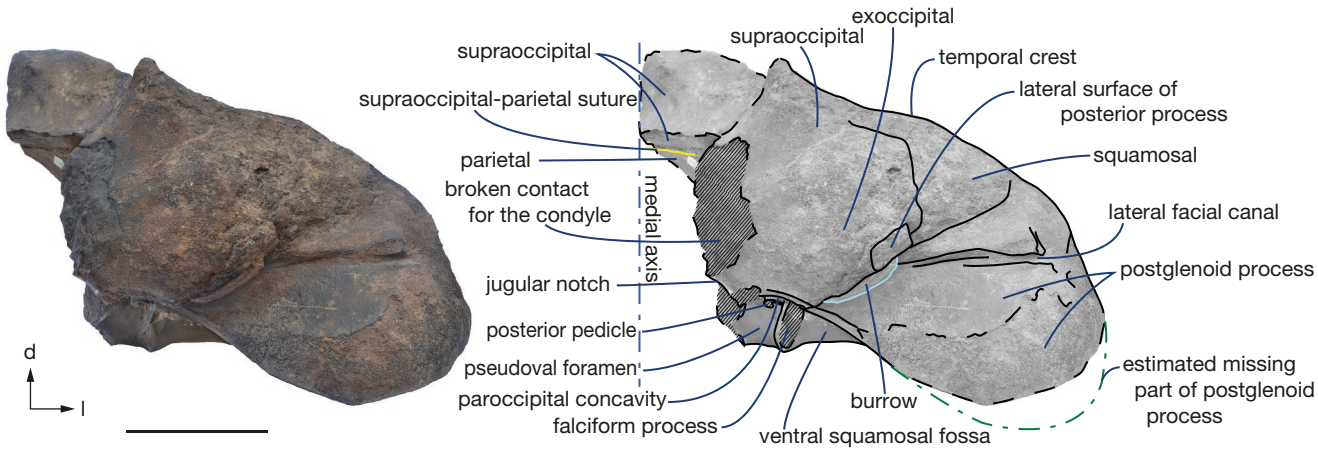

FIG. 21. — *Persufflatius renefraaijeni* n. gen., n. sp., MAB 010293, holotype. Posterior view. **d**, dorsal; **l**, lateral. Scale bar: 10 cm.

TABLE 6. — Measurements of periotic foramina in mm.

	endocranial opening of the facial canal	Dorsal vestibular area	Cochlear aqueduct	Verstibular aqueduct	Fenestra cochleae (rontunda)	Fenestra vestibuli (ovalis)	Lateral facial canal
H	4.3	6.9	9.4	7.1	2.9	2.6	2.5
W / L	9.3	6.9	1.6	1.8	7.0	5.2	3.6

posterior view (Fig. 19E), but is in fact inflated, globular, as the dorsal part of the process broke off and is still embedded in the sediment on the ventral border of the squamosal (H: 11 mm) (Fig. 22[left purple-grey spot]). Anterior to the lateral tuberosity, there is a 2.5 mm deep fossa for the lateral facial nerve (Table 6). More anteriorly, a fragment of the lateral border of the anterior process has broken off and is also still attached to the squamosal body. Therefore, the lateral side is slightly convex (Fig. 22[central purple-grey spot]); the ventral surface is flattened. Anterior to the promontorium, the anterior process bears a distinct groove to accommodate the tensor tympani muscle, separating the pars cochlearis clearly from the anterior process. The anterior pedicle for the bulla contact is slender, anteroposteriorly short and circular (about 6.5 mm diameter; Table 1). It is positioned far posteriorly, just in front of the lateral process and the mallear fossa (and thus about 10 mm anterior to the fenestra vestibuli).

Pars cochlearis

The fenestra vestibuli is sub-circular and small (L: 4.5 and H: *c.* 3 mm). The promontorium (pars cochlearis) is equally small and not inflated, being about 11 mm high (dorsal to the fenestra vestibuli) and about 33 mm long, including the long, shelf-like posterior cochlear crest. Dorsal to the latter, there is a high but anteroposteriorly short stylomastoid fossa; mediolaterally wide, posteriorly restricted by the compound posterior process and dorsally not roofed. Ventrally, there is a prominent promontorial groove (L: 14 mm; at less than 10 mm from the lateral border; H: 3.3 mm). The promontorium is mediolaterally strongly restricted (11 mm wide, ventral to the promontorial groove).

Cranial foramina of the pars cochlearis (Fig. 18C, D; Table 6)

The dorsal vestibular area and the endocranial opening of the facial canal are separated by a thin transverse crest (1.3 mm wide). The endocranial opening of the facial canal is oval and big (almost as big as the dorsal vestibular area) and tapers anteriorly to make it appear tear-shaped. The dorsal vestibular area is circular. The foramen for the vestibular aqueduct (endolymphatic foramen) runs vertical and is slit-like, as well as that for the cochlear aqueduct (perilymphatic foramen). The dorsal vestibular area, the endocranial opening of the facial canal and the cochlear aqueduct are aligned, the vestibular aqueduct being slightly more dorsal. This configuration is exceptional for this type of basal BnBB (diameter dorsal vestibular area: 6.9 mm; endocranial opening of the facial canal: W: 9.3 mm, H: 4.3 mm; H cochlear aqueduct: 9.4 mm, H vestibular aqueduct: 7.1 mm; both slit-like and vertical; Table 6). The fenestra cochlearis (fenestra rotunda) is sub-rectangular and strongly compressed mediolaterally. The cranial openings differ from *Parietobalaena* sp. and *Heterocetus affinis* by being aligned, whereas they form a equilateral triangle in the latter species; moreover, both the cochlear aqueduct and the endocranial opening of the facial canal are slit-like in the latter species. Dorsal to the dorsal vestibular area, the pars cochlearis has a strong, hypertrophied process posteromedially (= process of tegmen tympani of Luo & Gingerich 1999 and Ekdale *et al.* 2011). This extensive medial bone growth indicates we almost certainly deal with a nearly adult speci-

men, even though it must be noted that the frontal was not completely merged to the parietal and also the anterior part of the parietal-squamosal suture was not merged. There is no hole anterodorsal to the endocranial opening of the facial canal and there are no other holes in the dorsal part of the periotic. The cranial openings differ from *Atlanticetus patulus* in the vestibular aqueduct being rounded in the latter and the endocranial opening of the facial canal being circular rather than tear shaped. In addition, the vestibular aqueduct, the dorsal vestibular area and the endocranial opening of the facial canal are not aligned in the latter (Steeman 2010: 66, fig. 1).

Some notes on pachyostosis, osteosclerosis, bone expansion and bone compactness in the neurocranium of *Persufflatius* n. gen. (Figs 23-25; Tables 4, 5; Appendix 2)

Non-pathological pachyosteosclerosis often occurs in postcranial bones during early stages of adaption to life in water of secondarily aquatic tetrapods, such as the ribs in basilosaurids; this condition is typified by dense and inflated bone (de Buffrénil *et al.* 1990; de Buffrénil & Lambert 2011; Houssaye *et al.* 2015; van Vliet *et al.* 2019). In a later evolutionary phase, bone thickening usually diminishes as swimming efficiency and speed increase (Dewaele *et al.* 2021). As the pachyostosis observed in several bones of the neurocranium of *Persufflatius renefraaijeni* n. gen., n. sp. does not display irregular or discontinuous internal transitions, and as the external surfaces are smooth and unaltered, we consider the observed increase in spongy bone volume to be non-pathologic (contrary, for instance, to infectious spondylitis: Fettuccia *et al.* 2013; Kompanje 1999). In several baleen-bearing mysticetes, non-pathological pachyostosis and/or osteosclerosis re-emerged during the Miocene; postcranial osteosclerosis, without pachyostosis, is known from Miocene mysticetes such as *Diorocetus hiatus* Kellogg, 1968 and, to a lesser extent, also in other contemporaneous chaeomysticetes such as *Metopocetus* Cope, 1896 and *Parietobalaena* Kellogg, 1924 (van Vliet *et al.* 2019). The late Miocene *Cetotherium riabinini* Hofstein, 1943, *Brandtocetus chongulek* and other marine mammals from the Paratethys have pachyostotic/pachyosteosclerotic ribs and/or vertebrae, presumably as an adaptation to increased salinity (the Badenian salinity crisis; Gol'din 2014; Dewaele *et al.* 2021). Furthermore, extant mysticetes at least occasionally develop bone thickening. Especially the anterior and anterodorsal parts of the squamosal body (medial to the zygomatic process) form very thick sections of non-remodelled, apparently cyclically deposited multi-layered bone in extant rorquals (MB pers. obs. 2014), consisting of a succession of thin, alternating layers of compact and trabecular bone. Several extinct cetotheriids, such as: cf. *Herentalia nigra* (ZMA.MAM.5069); cf. '*Plesiocetus*' *burtinii* (IRSNB M 676) and *Mesocetus latifrons* (IRSNB 567), show similar sections of multi-layered cortex (MB pers. obs. 2017).

So far, little has been published about the pachyostosis, osteosclerosis and pachyosteosclerosis of cranial elements of mysticetes. To our knowledge, the degree of inflation of the neurocranium of *Persufflatius renefraaijeni* n. gen., n. sp. is more pronounced than it is in any other chaeomysticete discovered so far. The preserved neurocranium of the holotype is relatively intact. Therefore, the internal bone structure is only visible on some eroded surfaces and fracture zones. We could thus preliminarily document several bone structures in the inflated areas of the type skull (Figs 23; 24; 25) and

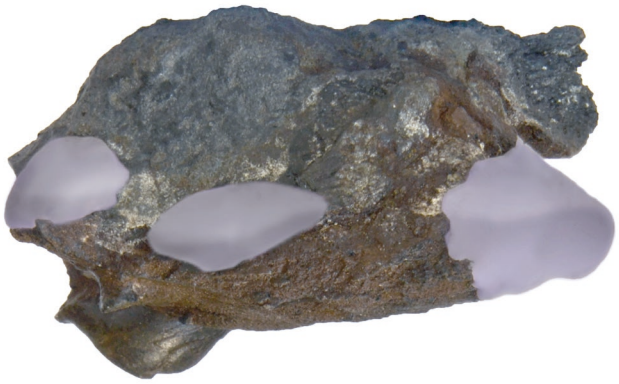

Fig. 22. — *Persufflatius renefraaijeni* n. gen., n. sp., MAB 010293, holotype. Periotic, lateral view (anterior to the right): **additions in purple-grey**; **right purple-grey spot**, reconstruction of the broken anterior process (maximum size possible); **middle purple-grey spot**, the addition of the fragment of the lateral side of the anterior process that is still attached to the squamosal; **left purple-grey spot**, addition of the fragment of the lateral tuberosity that is still attached to the squamosal.

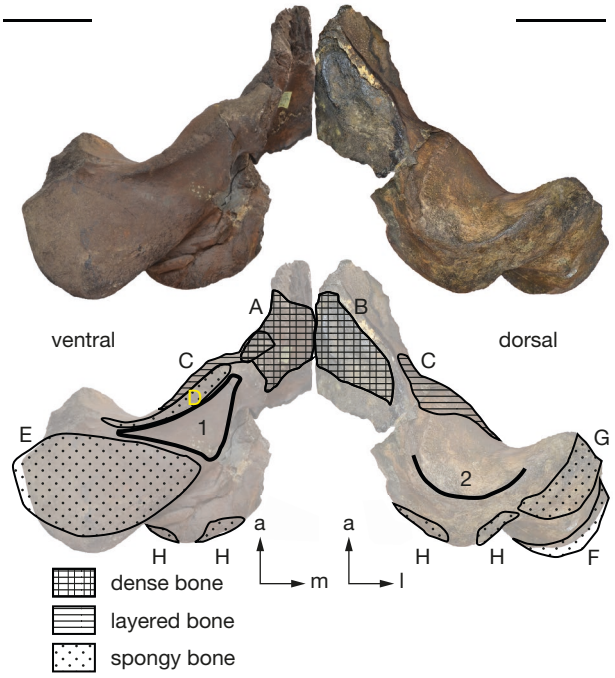

Fig. 23. — Anteroventral (**left**) and posterodorsal (**right**) views of *Persufflatius renefraaijeni* n. gen., n. sp., with a schematic indication of expanded ('inflated') regions (compared to the neurocranium of *Pelocetus*, *Uranocetus* and *Piscobalaena*). Note the sub-triangular ventral squamosal fossa (**1**), with a strong ventrally protruding wall (**D**) and the wide, rounded dorsal squamosal fossa (**2**). **A**, dense mediodorsal parietal; **B**, dense anterodorsal supraoccipital; **C**, layered anteromedioventral squamosal body; **D**, inflated ventral squamosal wall; **E**, inflated and laterally expanded anterior surface of the postglenoid process; **F**, inflated and laterally expanded posterolateral postglenoid process; **G**, inflated laterodorsal squamosal and posterolaterodorsal zygomatic process; **H**, inflated and mediolaterally expanded exoccipital. Scale bars: 10 cm.

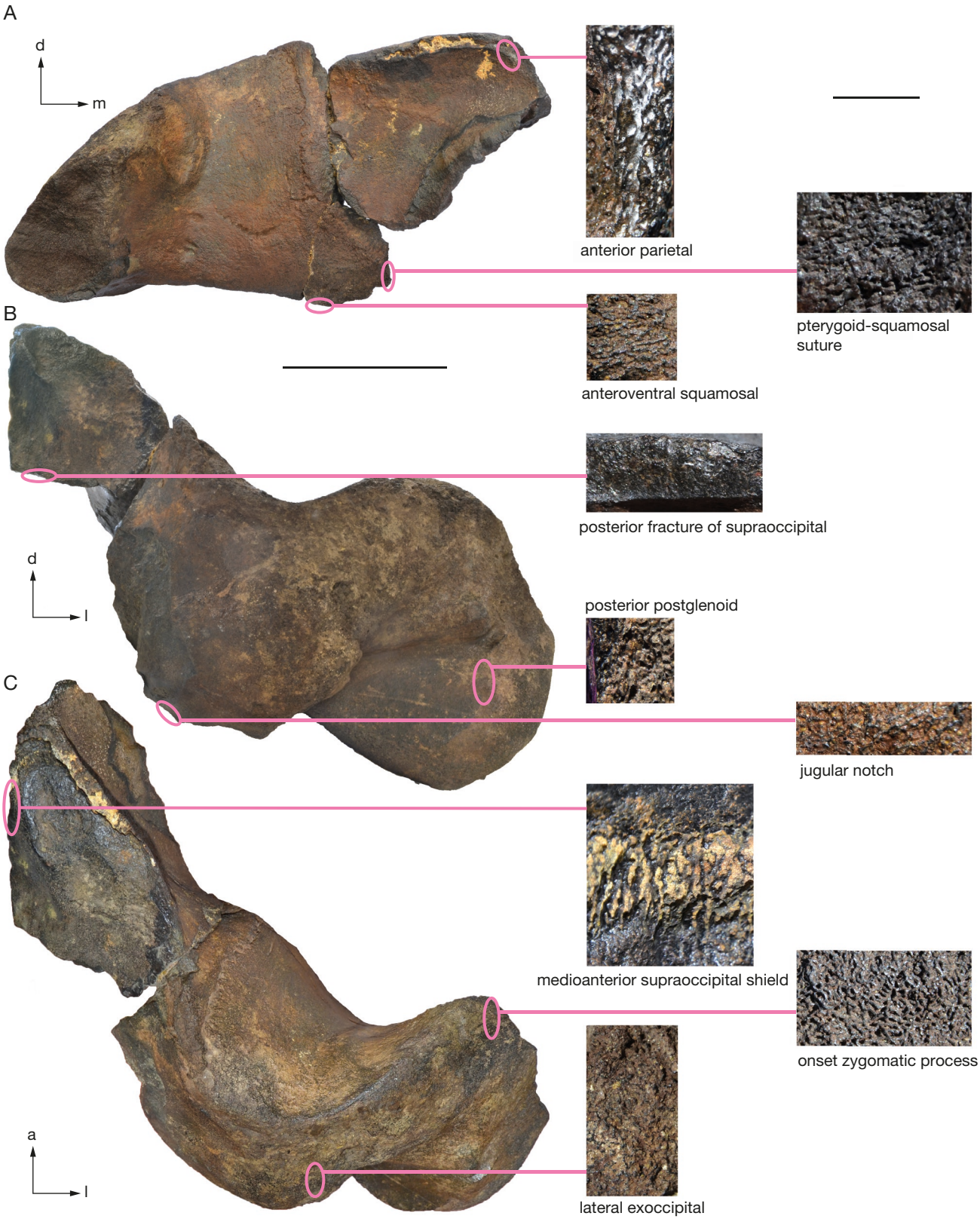

FIG. 24. — Series of bone samples of the neurocranium of the holotype (MAB 010293), showing some different bone structures. **Left**, neurocranium of holotype: **A**, anterior view; **B**, posterior to posterodorsal view; **C**, posterodorsal view. **a**, anterior; **d**, dorsal; **m**, medial; **l**, lateral. **Magenta ovals** show positions where the bone samples were taken. Scale bar: 10 cm exept photos of the bone samples (on the right), to the same scale (10 mm).

calculate the compactness for the locations involved. We further documented the shape and size of the cavities and the thickness of the trabecular rods in the studied areas of spongy bone (Appendix 2). It must be noted however that these areas are randomly oriented and hence these measurements should be treated with caution.

We could discern three different types of bone: 1) very dense bone; 2) "inflated" spongy bone; and 3) layered bone, consisting of alternating thin layers of trabecular and compact bone (Fig. 23). Most of the extra bone volume is due to extra spongy bone with a relatively low to intermediate compactness (0.32 to 0.59; Appendix 2). The anterior supraoccipital consists of ventrodorsally thick, compact bone (compactness 0.81 to 0.84; Tables 3, 4).

The postglenoid process and the posterior zygomatic process are inflated (pachyostotic) in the holotype and consist internally of spongy bone only, externally, they are covered by a thin layer of cortical bone. Anteroposteriorly, the postglenoid process is long (Table 5A, B). It is longer than in many other fossil whales, such as *Herentalia nigra*, *Herpeocetus sendaicus*, *Metopocetus hunteri*, and *Parietobalaena campiniana* (MB pers. obs.; Table 5A, B). At the posterolateral side (as preserved), at the jugular notch, at the exoccipital and below the fossa for the compound posterior process is just spongy bone covered by a thin (sub-millimetric) layer of cortical bone (Fig. 23).

When we look at the sections (Fig. 25), we see a varied picture, with different structures. In some places, the cavities are elongated and run in a specific direction (Fig. 25A, C, G2); in other places we see roughly circular, evenly spaced cavities (Fig. 25B, H, I). It must be noted however that the observed differences could be, at least in part, a side effect of the fact that the sections are randomly oriented. There is also a clear difference in size: in some places we encounter only small structures (Fig. 25H); elsewhere, small and large structures are mixed (Fig. 25A, E, I), and in still other places, large structures prevail (Fig. 25B, C, G2). The size of the trabecular rods and plates varies widely. At the postglenoid process and the posterior base of the zygomatic process, trabecular rods (about 0.14 mm thick and elongated) and plates (smaller than 0.42 × 0.37 mm) are thin and small, resulting in a low compactness (less than 0.40). In other places, the thickness of the trabecular rods varies between 0.3 and 0.7 mm, resulting in a compactness between 0.55 and 0.63 (Table 4; Appendix 2).

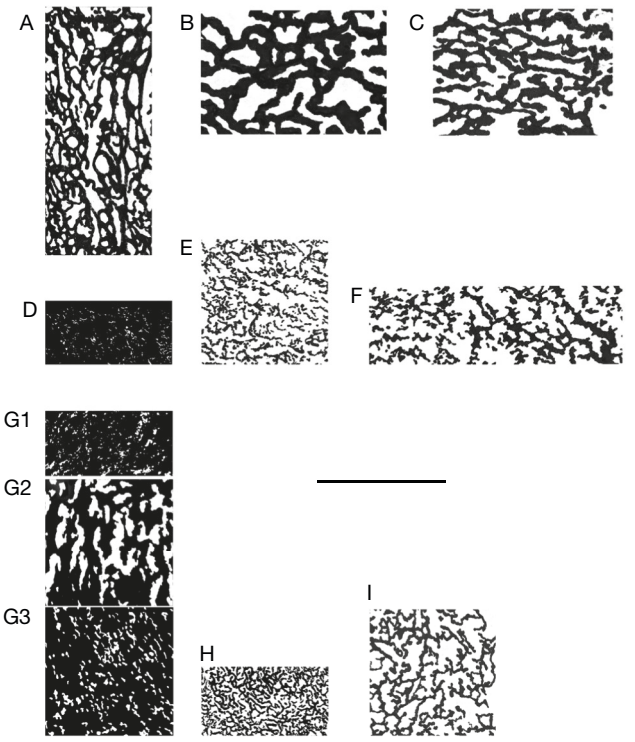

FIG. 25. — Camera lucida drawings of the bone samples shown in Fig. 24: **A**, anterior parietal (at vertex); compactness: 0.545; **B**, pterygoid-squamosal suture; compactness: 0.631; **C**, anteroventral squamosal border; compactness: 0.594; **D**, posterior fracture of anterior supraoccipital; compactness: 0.836; **E**, postglenoid process; compactness: 0.348; **F**, jugular notch; compactness: 0.461; **G**, medial anterior supraoccipital shield; compactness: **G1**, top: 0.808; **G2**, middle: 0.509; **G3**, bottom: 0.775; **H**, base of the zygomatic process; compactness: 0.391; **I**, lateral exoccipital; compactness: 0.413. The bone compactness was calculated using 'Bone ProfileR' (Girondot & Laurin 2003). Scale bar: 10 mm. See also Table 4.

PHYLOGENETIC ANALYSIS (Figs 26; 27)

We performed cladistic analyses based on two matrices that were recently published: Bisconti *et al.* (2020) and Duboys de Lavigerie *et al.* (2020). We performed both analyses in PAUP 4.0b10 (Swofford 2002).

In an effort to ease comparison, we derived from each of the two original matrices a new, modified matrix, limiting the number of species to 39. All of these but two were present in both the original matrices; two more species and *Persufflatius* n. gen. were added to this set, both matrices thus totalling 40 species (Appendices 5; 6). In the modified matrix based on Bisconti *et al.* (2020), we incorporated 'Protocetidae' and the basilosaurid *Cynthiacetus peruvianus*, whereas in the modified matrix based on Duboys de Lavigerie *et al.* (2020), we incorporated the basilosaurid *Zygorhiza kochii* and the odontocete *Waipatia maerewhenua*. These species, together with *Aetiocetus weltoni* and *Eomysticetus whitmorei*, serve as default outgroup(s). Given the partial nature of *Persufflatius renefraaijeni* n. gen., n. sp. and the poor state of preservation of *Uranocetus gramensis* and of the periotic of *Pelocetus calvertensis*, only a relatively small number of characters was available for comparison and analysis. As for the modified matrix of Duboys de Lavigerie *et al.* (2020), 79 of the 278 characters (28%) could be scored for *Persufflatius renefraaijeni* n. gen., n. sp. (Fig. 26). As for the modified matrix of Bisconti *et al.* (2020), 112 of the 335 characters (33%) could be scored (Fig. 27). In the bootstrap analysis, *Persufflatius* n. gen. falls in an unresolved polytomy comprising all balaenomorpha, with the exclusion of the Balaenidae (it must be noted that *Caperea* is included in the Cetotheriidae in the analysys based on Duboys de Lavigerie *et al.* (2020), while the latter is included in the Balaenidae in the analysys based on Bisconti *et al.* (2020)

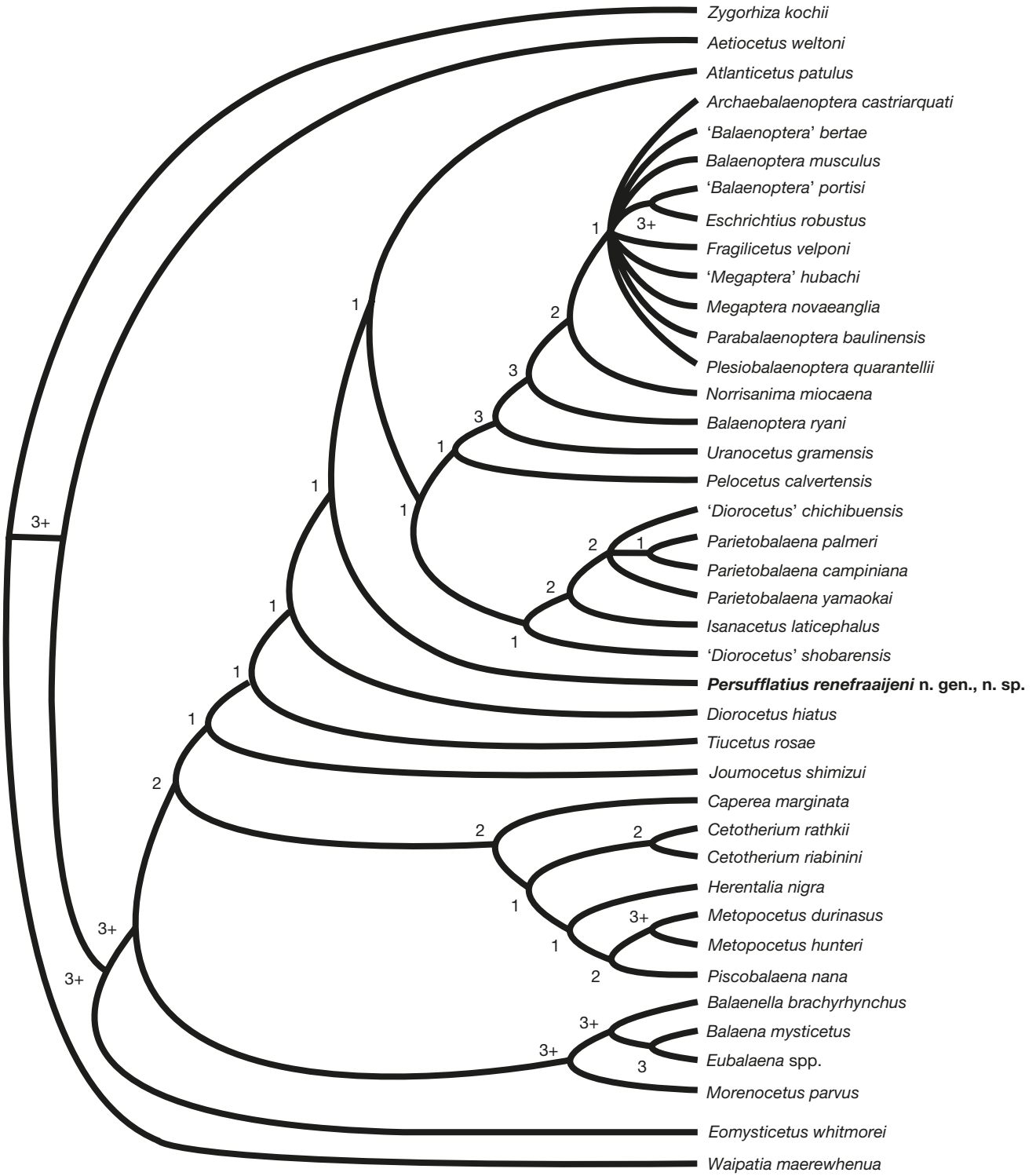

FIG. 26. — **A**, Consensus tree of the matrix based on Duboys de Lavigerie *et al.* 2020. The numbers at the nodes indicate the Bremer support values.

(Figs 26B; 27B). For the modifed matrix based on Bisconti *et al.* (2020), this analysis resulted in 6 trees with a length of 1227 steps (40 taxa, 355 characters; 331 parsimony informative). The bootstrap value for the node leading to the clade including *Persufflatius* n. gen. and (amongst others) extant balaenopterids is low (36%), but the Bremer-support is high (3) and thus its position in the phylogeny is relatively well supported. The modified matrix based on Duboys de Lavigerie *et al.* (2020) resulted in 19 trees with a length of 884 steps (40 taxa, 278 characters; 256 of which are parsimony-informative). In this strict consensus tree (Fig. 26A) *Persufflatius* n. gen. is just crownwards to *Diorocetus hiatus* and just basal to *Atlanticetus patulus*. The latter is just basal to two clades: one clade comprising

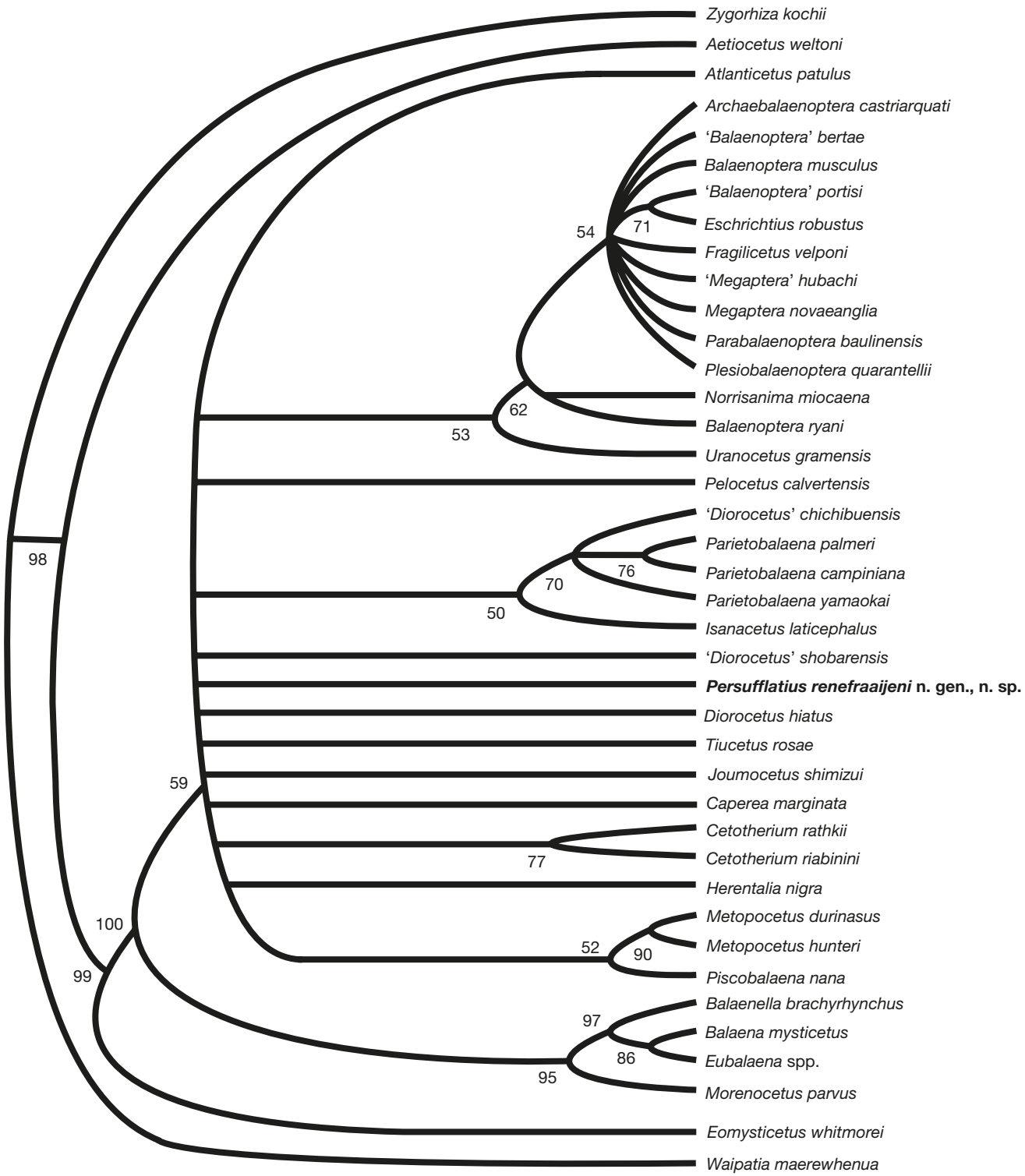

FIG. 26. — **B**, Bootstrap tree of the matrix based on Duboys de Lavigerie *et al.* 2020. The numbers at the nodes are bootstrap values (higher than 50).

'*Diorocetus*' *shobarensis*, '*Diorocetus*' *chichibuensis*, *Isanacetus* and three species of *Parietobalaena*; the other clade, based by respectively *Pelocetus*, *Uranocetus* and '*B.*' *ryani* is leading to the actual balaenopterids also (Fig. 26A). The bootstrap value for the node leading to *Persufflatius* n. gen. is equally low (40 %) as is the Bremer support (1) (Fig. 26A, B), resulting in a low support for the position of *Persufflatius* n. gen. in this analysis.

The strict consensus tree of the matrix based on Bisconti *et al.* (2020) shows a well-supported Balaenoidea clade (including *Caperea marginata*) (Bootstrap value 100 and Bremer support ≥ 6). This clade is just basal to two

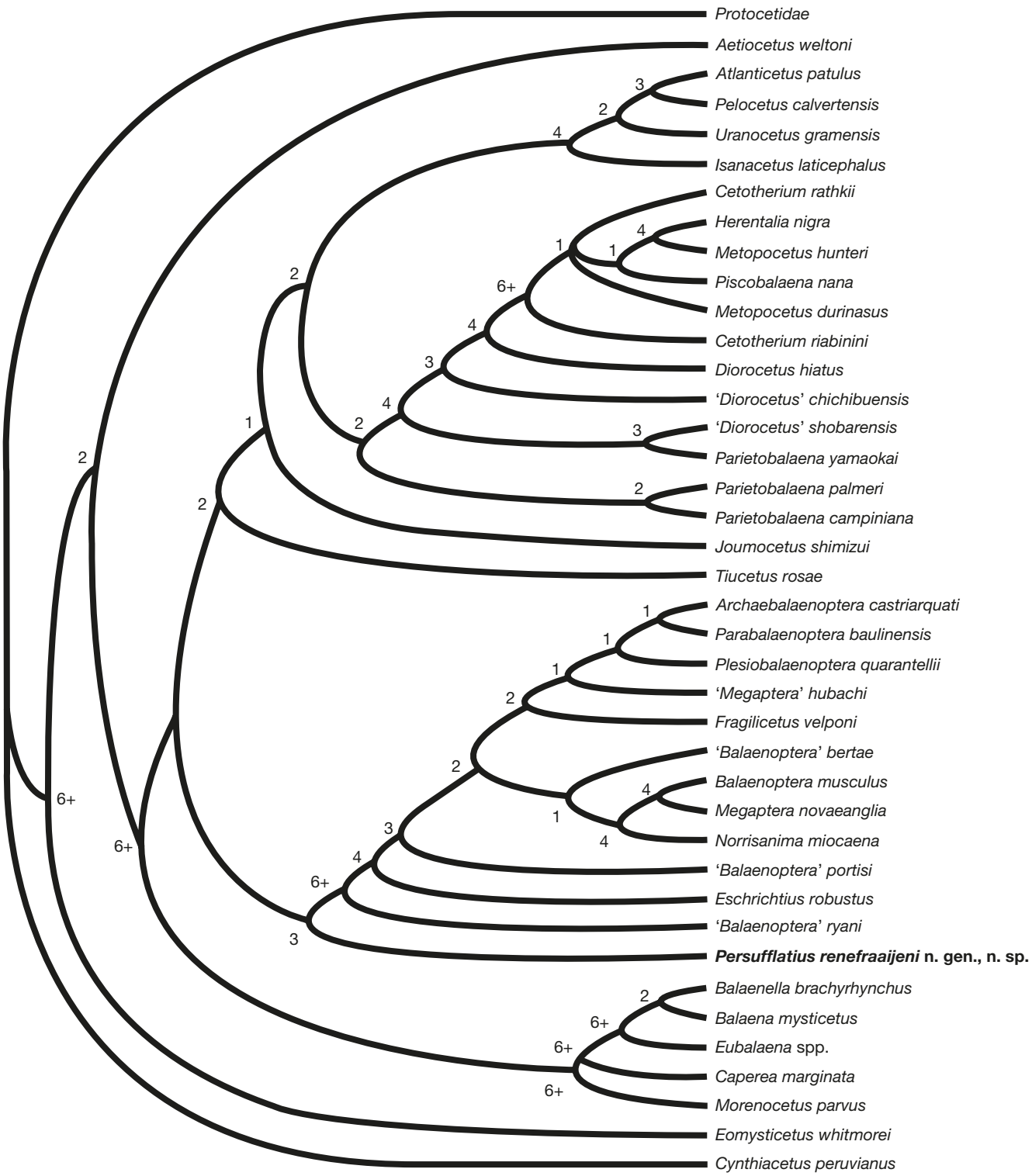

FIG. 27. — **A**, Consensus tree of the matrix based on Bisconti *et al.* 2020. The numbers at the nodes are Bremer support values.

clades: one with a first branch leading to *Tiucetus rosae* and which further comprises *Joumocetus*, *Aglaocetus*, *Pelocetus*, *Uranocetus*, *Parietobalaena*, *Diorocetus* and the cetotheriids (except *Caperea marginata*, which is considered to be a balaenoid in this analysis); the other one, with the first branch leading to *Persufflatius* n. gen. (Bootstrap value 36 and Bremer support 3) and which comprises all balaenopterids, including the extant members of the family. The strict consensus tree based on Duboys de Lavigerie *et al.* (2020) shows a somewhat more complex result. It has an equally well-supported balaenid clade (excluding *Caperea marginata*, which is considered to be a cetotheriid in this

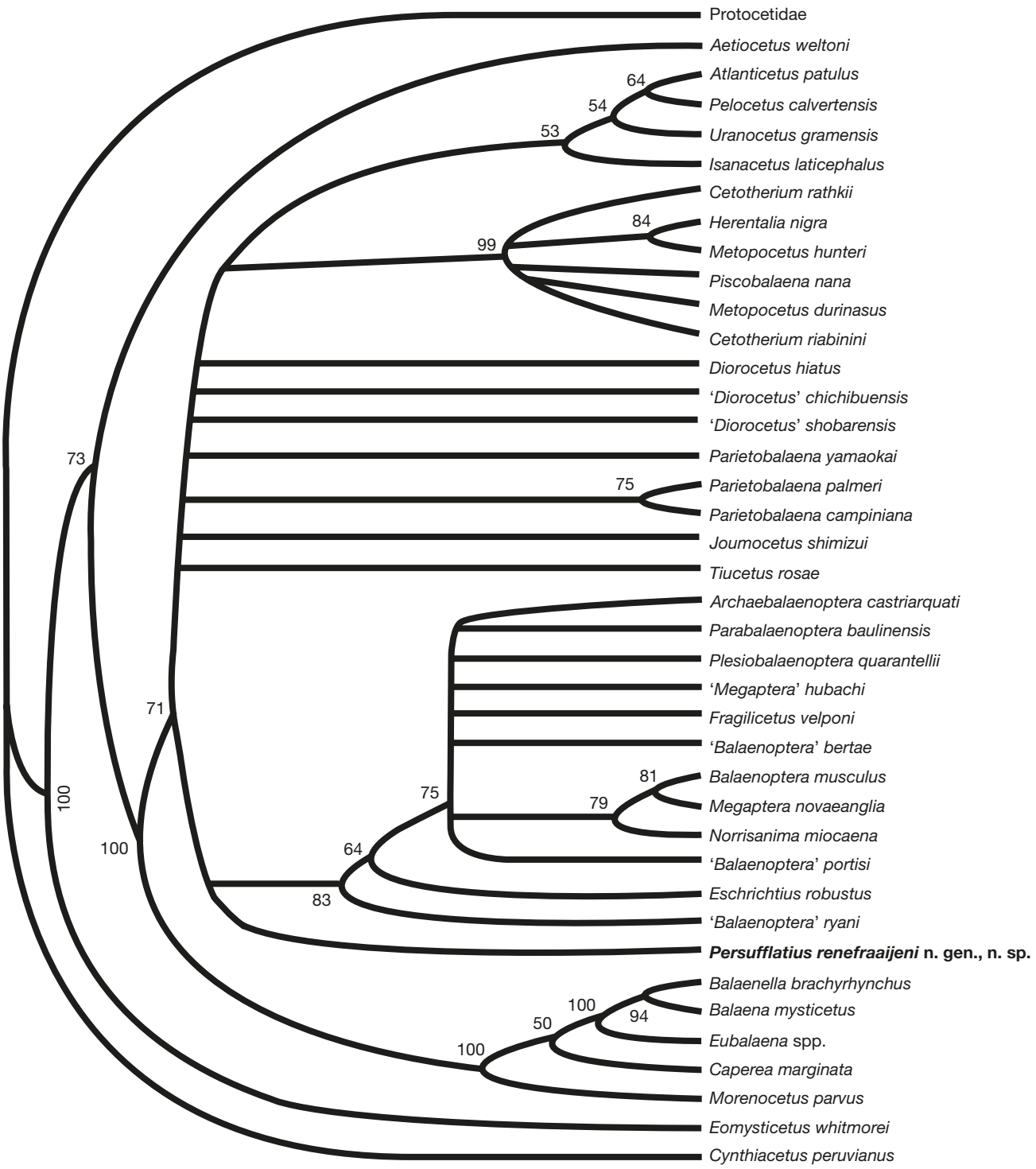

FIG. 27. — **B**, Bootstrap tree for the matrix based on Bisconti *et al.* 2020. The numbers at the nodes are bootstrap values (higher than 50).

analysis) (bootstrap value: 95 and Bremer support ≥ 3). It is just basal to a (weakly supported) clade comprising the cetotheriids (including *Caperea*). In a crownward cascade to this clade we find successively: *Joumocetus*, *Tiucetus*, *Diorocetus hiatus*, *Persufflatius* n. gen. (bootstrap value 40 and Bremer support 1) and *Aglaocetus patulus*. The latter is basal to two clades: one comprising '*Diorocetus*' *shobarensis*, '*D*' *chichibuensis*, *Isanacetus* and *Parietobalaena*; the other with a first branch leading to *Pelocetus calvertensis* (bootstrap < 50 and Bremer support 1). The clade crownward to *Pelocetus* with a first branch leading to *Uranocetus* is well supported (bootstrap value 53 and Bremer support ≥ 3). It comprises all the balaenopterids, including the extant members of the family.

DISCUSSION AND CONCLUDING REMARKS

The new species differs markedly from all other BnBB described so far. In particular, the presence of an anteroposteriorly long squamosal/exoccipital complex; the high degree of pachyostotic, non osteosclerotic 'inflation' of several cranial bones; the bell-shaped supraoccipital that anteriorly overhangs the temporal fossa (Bisconti *et al.* 2020: ch. 78-79); the very anteriorly placed crest-like attachment scars for the neck muscles (Bisconti *et al.* 2020: ch. 136); the huge posteriorly oriented inflated postglenoid process (Bisconti *et al.* 2020: ch. 156); the rounded exoccipital which is confluent with the posterior zygomatic process (Duboys de Lavigerie 2020: ch. 74); the rod-like compound posterior process which is laterally expanded and which is integrated into the skull wall (Duboys de Lavigerie 2020: ch. 188); the pars cochlearis which is not elongated, having a promontorial groove and having the endocranial opening of the facial canal, the dorsal vestibular area and the cochlear aqueduct aligned (Duboys de Lavigerie 2020: chs 144, 163 and 168); and the wide and rounded posterior temporal crest (Bisconti *et al.* 2020: ch. 107) are (amongst others) a unique combination of characters for this species.

Though the performed phylogenetic analyses yield different results, they both place the new species at or near the base of the balaenopterid lineage, giving a good indication of the phylogenetic affinities of *Persufflatius renefraaijeni* n. gen., n. sp. in relation to several other BnBB as well as a better insight into the characters that were present at the dawn of the rorqual evolution (which ultimately led to the most successful group of modern baleen whales).

The neurocranium of *Persufflatius renefraaijeni* n. gen., n. sp. is, compared to other BnBB, generally more inflated and bulbous. We could study the internal bone structure, where it is exposed in occurrence of several randomly oriented broken surfaces. On the different sections, we encountered a wide variety of types of (mainly) spongy bone. The thickness of the trabecular rods, the size and shape of the trabecular plates and cavities and the compactness varies a lot.

Some of the inflated bones (i.e. the postglenoid process, the exoccipital, the zygomatic process) do not show a different type of bone growth pattern compared to the adjacent bone and consist of spongy bone (compactness between 0.32 and 0.56), externally covered with a fine layer of cortical bone. The anteromedioventral part of the squamosal consists of a layered structure of seemingly cyclically deposited bone (consisting of alternating thin layers of trabecular and compact bone; compactness 0.44-0.66), a few centimetres thick all together. The anterior supraoccipital consists of ventrodorsally thick, compact bone (compactness 0.81 to 0.84; Table 3, 4).

Though the neurocranium of the holotype of *Persufflatius renefraaijeni* n. gen., n. sp. has a generally swollen aspect, most of the 'inflated' bone has an intermediate to low compactness. The inflated (expanded) exoccipital/postglenoid-zygomatic process has extra spongy bone. Only the anterior supraoccipital/parietal consists of a thick layer of dense bone.

As many indicative features are missing (such as the anterior zygomatic process, the condyles, the basicranium, the rostrum and the cervicals), not much can be concluded about the ecological niche and lifestyle of *Persufflatius renefraaijeni* n. gen., n. sp. The presence of a robust external occipital crest anteriorly on the dense and ventrodorsally thick supraoccipital (Fig. 8), indicates that this animal likely had strong neck muscles and therefore a manoeuvrable head, similar to extant *Eschrichtius robustus* Lilljeborg, 1861 (MB pers. obs. 2008), but without strong, rounded occipital condyles and/or robust cervicalia to confirm this, we cannot prove this assumption in any way. Undoubtedly, a more complete skeleton of *Persufflatius renefraaijeni* n. gen., n. sp., including the basicranium, the anterior elements of the skull and postcranial elements, would provide far more insight into its functional anatomy and paleoecology.

It is also stunning that after 20 years of intensive research in a broadly prospected region (southern North Sea basin), unexpected, anatomically very diverse whale species keep on being discovered, reflecting the enormously rich diversity these early late Miocene whales developed (Tortonian; Appendix 3). The extant mysticete species represent only a minute fraction of the mid-Neogene diversity. Finding out why during subsequent waves of extinction (selective extinctions; at the end of the middle Miocene, the end of the late Miocene and the end of the early Pliocene) so many of these adaptations and specialisations were eradicated, could give us a better insight in how the principle of natural selection really works (what really drives it; see for instance: Marx *et al.* 2019a; Marx & Uhen 2010) and how it shaped the actual world, teemed with the few lucky survivors of this merciless process (Marx & Fordyce 2015; Slater *et al.* 2017; Boessenecker 2013). Finding out the mechanisms, the driving force behind this selection process might help us to save the extant (whale) species, most of which so far hardly recovered from near extinction by industrial whaling (Reeves 2009; Clapham & Scott Baker 2018).

It is further interesting to note that our current knowledge of fossil whales is almost exclusively based on coastal (neritic) fossils, mainly from temperate and subtropical climate zones (Boessenecker 2013; Marx *et al.* 2019a). We may thus be missing in our fossil record circumpolar and/or tropical species, with a lifestyle similar to the extant bowhead *Balaena mysticetus,* the pigmy right whale *Caperea marginata* or Bryde's whale *Balaenoptera edeni*. Apart from that, during every selective extinction, especially small species are whiped out, without being replaced in the next radiation (Marx & Fordyce 2015; Slater *et al.* 2017; Boessenecker 2013; Marx *et al.* 2019a). The impact of climate change and the associated change in sea level and the location and shape of the coastline, is apparently having a devastating impact on (especially) small whale species (coastal ecosystems being destroyed at each transition). This could be one of the reasons why whale species have steadily increased in size over time, as maybe the larger, krill eating species, living (mainly) in a (colder) pelagic, krill-rich environment were positively selected for, over small neritic species, having a diet of small fish, molluscs and other coastal invertebrates (see also: Marx *et al.* 2019a; Marx & Fordyce 2015; Slater *et al.* 2017; Boessenecker 2013; Bisconti *et al.* 2021a).

The new species described in this publication adds up to an impressive list of (often large) late Tortonian (late Miocene; 8.1-7.5 Ma) marine tetrapods from the southern North Sea. In fact, compared to the middle Miocene and the early Pliocene (and in fact all other Neogene stages), the late Tortonian faunal assemblage of the North Sea seems to be extraordinarily rich. So far, at least 21 cetacean species have been described, along with many other large vertebrates, like pinnipeds, turtles and large-sized fishes (see Appendix 3 for a non-exhaustive list). Recent finds of almost complete skeletons of two new undescribed *Herentalia*-like species and one rather complete partial neurocranium of a *P. burtinii*-like cetothere in temporarily exposed late Tortonian outcrops (Borsbeek sand member, Deurne-Antwerp) in Belgium will probably allow us to reassess some problematic species described by Van Beneden (Bosselaers & Post 2010; Bisconti & Bosselaers 2021). These considerations and the discovery of a mandibular fragment of a Balaenidae in late Tortonian deposits in the Netherlands (Liessel) are promising and give us hope of finding some day a more complete specimen of the species described in this article and, possibly, even more new species.

Acknowledgements
We are very grateful to Felix Marx for photos, info, countless fruitful discussions, suggestions, very pleasant and inspiring cooperation; Mette Steeman for photos of and inspiring discussions on periotics; Alberto Collareta for info, suggestions, many fruitful discussions and inspiring cooperation and many years of very pleasant and inspiring cooperation; Klaas Post and Michelangelo Bisconti for discussions and many fruitful years of very pleasant and inspiring cooperation. Olivier Lambert for fruitful discussions and continuous support and very pleasant and very inspiring cooperation for many many years; Henk Jan van Vliet for reading earlier versions of the text, suggestions and countless discussions, many fruitful years of very pleasant and inspiring cooperation; Robert Marquet for confirming the determination of the shells and many years of fine cooperation; Dr Yannick Van Ael, Neurology, Monica hospital, Antwerpen-Deurne, Belgium for his comments on the brain related issues. We thank Annelise Folie, Cecilia Cousin, Alain Dreze, Julien Lalanne, Olivier Pauwels and Sébastien Bruaux for the repeated access to the IRSNB collections under their care, many years of fine cooperation and their unlimited patience. Bram Langeveld for the repeated access to the NMR collections under his care, and for many years of fine cooperation. René Fraaie for the repeated access to the MAB collections under his care, for the very pleasant reception in his museum and for many years of fine cooperation. We further owe many thanks to Alberto Collareta and Michelangelo Bisconti as their constructive reviews and positive suggestions considerably improved the manuscript.

REFERENCES

Alfsen A., Bosselaers M. & Lambert O. 2021. — New sperm whale remains from the late Miocene of the North Sea and a revised family attribution for the small crown physeteroid *Thalassocetus* Abel, 1905. *Comptes Rendus Palevol* 20 (39): 807-822. https://doi.org/10.5852/cr-palevol2021v20a39

Amson E., Muizon C. de, Laurin M., Argot C. & De Buffrénil V. 2014. — Gradual adaptation of bone structure to aquatic lifestyle in extinct sloths from Peru. *Proceedings of the Royal Society of London B: Biological Sciences* 281: 20140192: 1-6. https://doi.org/10.1098/rspb.2014.0192

Amson E., Billet G. & Muizon C. de 2018. — Evolutionary adaption to aquatic lifestyle in extinct sloths can lead to systemic alteration of bone structure. *Proceedings of the Royal Society B* 285: 20180270: 1-9. https://doi.org/10.1098/rspb.2018.0270

Baker A. E. 1985. — Pygmy right whale, *in* Ridgway S. H. & Harrison R. J. (eds), *Handbook of Marine Mammals*. Vol. 3. Academic Press, London: 345-354.

Bisconti M. & Bosselaers M. 2021. — On *Plesiocetus* Van Beneden, 1859 (Mammalia, Cetacea, Mysticeti). *Rivista Italiana di Paleontologia e Stratigrafia* 127 (2): 231-274. https://doi.org/10.13130/2039-4942/15745

Bisconti M., Lambert O. & Bosselaers M. 2013. — Taxonomic revision of *Isocetus depauwi* (Mammali, Cetacea, Mysticeti) and the Phylogenetic relationships of archaic 'cetothere' mysticetes. *Palaeontology* 56 (1): 95-127. https://doi.org/10.1111/j.1475-4983.2012.01168.x

Bisconti M., Munsterman D. K. & Post K. 2019. — A new balaenopterid whale from the late Miocene of the Southern North Sea Basin and the evolution of balaenopterid diversity (Cetacea, Mysticeti). *PeerJ* 7 (4): 6915. https//doi.org/10.7717/peerj.6915

Bisconti M., Munsterman D. K., Fraaije H. B., Bosselaers M. E. J. & Post K. 2020. — A new species of rorqual whale (Cetacea, Mysticeti, Balaenopteridae) from the late Miocene of the Southern North Sea Basin and the role of the North Atlantic in the paleobiogeography of *Archaebalaenoptera*. *PeerJ* 7: e8315. http://doi.org/10.7717/peerj.8315

Bisconti M., Pellegrino L. & Carnivale G. 2021a. — Evolution of gigantism in right and bowhead whales (Cetacea: Mysticeti: Balaenidae). *Biological Journal of the Linnean Society* 134 (2): 498-524. http://doi.org/10.1093/biolinnean/blab086

Bisconti M., Riccardo D., Damarco P., Tartarelli G., Pavia M. & Carnevale G. 2021b. — High encephalization in a fossil rorqual illuminates baleen whale brain evolution. *Brain, Behaviour and Evolution* 96 (2): 78-90. https://doi.org/10.1159/000519852

Boessenecker R. W. 2013. — Pleistocene survival of an archaic dwarf baleen whale (Mysticeti: Cetotheriidae). *Naturwissenschaften* 100: 365-371. https://doi.org/10.1007/s00114-013-1037-2

Bosselaers M. & Post K. 2010. — A new fossil rorqual (Mammalia, Cetacea, Balaenopteridae) from the Early Pliocene of the North Sea, with a review of the rorqual species described by Owen and Van Beneden. *Geodiversitas* 32 (2): 331-363. https://doi.org/10.5252/g2010n2a6

Bouetel V. & Muizon C. de 2006. — The anatomy and relationships of *Piscobalaena nana* (Cetacea, Mysticeti), a Cetotheriidae s.s. from the early Pliocene of Peru. *Geodiversitas* 28 (2): 319-395.

Breathnach A. S. 1955. — The surface features of the brain of the humpback whale (*Megaptera novaeangliae*). *Journal of Anatomy* 89 (3): 343-354. https://www.ncbi.nlm.nih.gov/pmc/articles/PMC1244762/ (last accessed march 1st 2022).

Clapham P. J. & Scott Baker C. 2018. — Modern Whaling, *in* Perrin W. F., Würsig B. & Thewissen J. G. M. (eds), *Encyclopedia of Marine Mammals*. 3rd edition. Academic Press, San Diego: 1070-1074.

De Buffrénil V. & Casinos A. 1995. — Observations histologiques sur le rostre de *Mesoplodon densirostris* (Mammalia, Cetacea, Ziphiidae) : le tissu osseux le plus dense connu. *Annales des Sciences naturelles – Zoologie et Biologie animale, 13e série* 16: 21-32.

De Buffrénil V. & Lambert O. 2011. — Histology and growth pattern of the pachy-osteosclerotic premaxillae of the fossil beaked whale *Aporotus recurvirostris* (Mammalia, Cetacea, Odontoceti). *Geobios* 44: 45-56. https://doi.org/10.1016/j.geobios.2010.09.001

De Buffrénil V., De Ricqlès A., Ray C. E. & Domning D. P. 1990. — Bone histology of the ribs of the archaeocetes (Mammalia, Cetacea). *Journal of Vertebrate Paleontology* 10: 455-466. https://doi.org/10.1080/02724634.1990.10011828

De Buffrénil V., Zylberberg L., Traub W. & Casinos A. 2000. — Structural and mechanical characteristics of the hyperdense bone of the rostrum of *Mesoplodon densirostris* (Cetacea, Ziphiidae): summary of recent observations. *Historical Biology* 14: 57-65. https://doi.org/10.1080/10292380009380555

De Ricqlès A. & De Buffrénil V. 2001. — Bone histology, heterochronies and the return of tetrapods to life in water: where are we. *in* Mazin J.-M. & De Buffrénil V. (eds), *Secondary Adaptation of Tetrapods to Life in Water*. Verlag Dr Friedrich Pfeil, Munchen, Germany: 289-310.

De Verteuil L. & Norris G. 1996. — Miocene dinoflagellate stratigraphy and systematics of Maryland and Virginia. *Micropaleontology* 42 (Suppl.): 1-172. https://doi.org/10.2307/1485926

Dewaele L., Amson E., Lambert O. & Louwye S. 2017a. — Reappraisal of the extinct seal "*Phoca*" *vitulinoides* from the Neogene of the North Sea Basin, with bearing on its geological age, phylogenetic affinities, and locomotion. *PeerJ* 5: e3316. https://doi.org/10.7717/peerj.3316

Dewaele L., Lambert O. & Louwye S. 2017b. — On *Prophoca* and *Leptophoca* (Pinnipedia, Phocidae) from the Miocene of the North Atlantic realm: redescription, phylogenetic affinities and paleobiogeographic implications. *PeerJ* 5: e3024. https://doi.org/10.7717/peerj.3024

Dewaele L., Lambert O. & Louwye S. 2018. — A critical revision of the fossil record, stratigraphy and diversity of the Neogene seal genus *Monotherium* (Carnivora, Phocidae). *Royal Society Open Science* 5: 171669. https://doi.org/10.1098/rsos.171669

Dewaele L., Lambert O., Laurin M., De Kock T., Louwye S. & De Buffrénil V. 2019. — Generalized osteosclerotic condition in the skeleton of *Nanophoca vitulinoides*, a dwarf seal from the Miocene of Belgium. *Journal of Mammalian Evolution*: 1-27. https://doi.org/10.1007/s10914-018-9438-9

Dewaele L., Gol'din P., Marx F. G., Lambert O., Laurin M., Obada T. & De Buffrénil V. 2021. — Hypersalinity drives convergent bone mass increases in Miocene marine mammals from the Paratethys. *Current Biology* 32: 1-8. https://doi.org/10.1016/j.cub.2021.10.065

Duboys de Lavigerie G., Bosselaers M., Goolaerts S., Park T., Lambert O. & Marx F. G. 2020. — New Pliocene right whale from Belgium informs balaenid phylogeny and function. *Journal of Systematic Palaeontology*. https://doi.org/10.1080/14772019.2020.1746422

Dybkjær K. & Piasecki S. 2010. — Neogene dinocyst zonation for the eastern North Sea Basin, Denmark. *Review of Palaeobotany and Palynology* 161: 1-29. https://doi.org/10.1016/j.revpalbo.2010.02.005

Ekdale E. G., Berta A. & Deméré T. A. 2011. — The Comparative Osteology of the Petrotympanic Complex (Ear Region) of Extant Baleen whales (Cetacea, Mysticeti). *Plos One* 6: e21311. https://doi.org/10.1371/journal.pone.0021311

Fensome R. A., Williams G. L. & Macrae R. A. 2019. — The Lentin and Williams Index of Fossil Dinoflagellates 2019 edition. *AASP Contributions Series* 50: 1-1173.

Fettuccia D. C., Da Silva M. F. & Simões-Lopes P. C. 2013. — Osteological alterations in the tucuxi *Sotalia fluviatilis* (Cetacea, Delphinidae). *Iheringia, Série Zoologia, Porto Alegre* 103 (3): 255-259. https://doi.org/10.1590/S0073-47212013000300007

Geisler J. H., McGraven M. R., Yang G. & Gatesy J. 2011. — A supermatrix analysis of genomic, morphological, and paleontological data from crown Cetacea. *Biomedcentral Evolutionary Biology* 2011 (11): 112. https://doi.org/10.1186/1471-2148-11-112

Girondot M. & Laurin M. 2003. — Bone profiler: A tool to quantify, model and statistically compare bone-section compactness profiles. *Journal of Vertebrate Paleontology* 23 (2): 458-461. https://www.jstor.org/stable/4524331

Gol'din P. 2014. — 'Antlers inside': are the skull structures of beaked whales (Cetacea: Ziphiidae) used for echoic imaging and visual display? *Biological Journal of the Linnean Society* 113: 510-515. https://doi.org/10.1111/bij.12337

Houssaye A., Tafforeau P., Muizon C. de & Gingerich P. D. 2015. — Transition of Eocene whales from land to sea: evidence from bone microstructure. *Plos One* 10: e0118409. https://doi.org/10.1371/journal.pone.0118409

Kazár E. & Hampe O. 2014. — A new species of *Kentriodon* (Mammalia, Odontoceti, Delphinoidea) from the Middle/Late Miocene of Groß Pampau (Schleswig-Holstein, North Germany). *Journal of Vertebrate Paleontology* 34 (5): 1216-1230. https://doi.org/10.1080/02724634.2014.857347

Kellogg R. 1968. — Fossil Marine Mammals from the Miocene Calvert Formation of Maryland and Virginia. *Bulletin of the United States National Museum* 247 (5-8): 103-201.

Kemper C. 2008. — Pygmy Right Whale, *in* Perrin W., Wursig B. & Thewissen J. G. M. (eds), *Encyclopedia of Marine Mammals*. 2nd Edition. Academic Press, San Diego: 939-941.

Kompanje E. J. O. 1999. — Considerations on the comparative pathology of the vertebrae in Mysticeti and Odontoceti; evidence for the occurrence of discarthrosis, zygarthrosis, infectious spondylitis and spondyloarthritis. *Zoologische Mededelingen Leiden* 73: 99-130.

Koretsky I. A. & Peters A. M. M. 2008. — *Batavipusa* (Carnivora, Phocidae, Phocinae): a new genus from the eastern shore of the North Atlantic Ocean (Miocene seals of the Netherlands, Part II). *Deinsea* 12: 53-62.

Köthe A. 2012. — A revised Cenozoic dinoflagellate cyst and calcareous nanoplankton zonation for the German sector of the southeastern North Sea Basin. *Newsletters on Stratigraphy* 45: 189-220. https://doi.org/10.1127/0078-0421/2012/0021

Kuhlmann G., Langereis C. G., Munsterman D. K., Van Leeuwen R.-J., Verreussel R., Meulenkamp J. E. & Wong Th. E. 2006. — Chronostratigraphy of Late Neogene sediments in the southern North Sea Basin and paleoenvironmental interpretations. *Palaeogeography, Palaeoclimatology, Palaeoecology* 239: 426-455. https://doi.org/10.1016/j.palaeo.2006.02.004

Lambert O. 2005a. — Systematics and phylogeny of the fossil beaked whales *Ziphirostrum* du Bus, 1868 and *Choneziphius* Duvernoy, 1851 (Mammalia, Cetacea, Odontoceti), from the Neogene of Antwerp (North of Belgium). *Geodiversitas* 27 (3): 443-497.

Lambert O. 2005b. — Review of the Miocene long-snouted dolphin *Priscodelphinus cristatus* Du Bus, 1872 (Cetacea, Odontoceti) and phylogeny among eurhinodelphinids. *Bulletin de l'Institut royal des Sciences naturelles de Belgique : Sciences de la Terre* 75: 211-235.

Lambert O. 2008. — Sperm whales from the Miocene of the North Sea: A re-appraisal. *Bulletin de l'Institut royal des Sciences naturelles de Belgique : Sciences de la Terre* 78: 277-316.

Lambert O. & Bianucci G. 2019. — How to break a sperm whale's teeth: dental damage in a large Miocene physeteroid from the North Sea basin. *Journal of Vertebrate Paleontology* 39 (4): e1660987. https://doi.org/10.1080/02724634.2019.1660987

LAMBERT O. & POST K. 2005. — First European pontoporiid dolphins (Mammalia: Cetacea, Odontoceti) from the Miocene of Belgium and The Netherlands. *Deinsea* 11: 7-20.

LAMBERT O., BIANUCCI G., POST K., DE MUIZON C., SALAS-GISMONDI R., URBINA M. & REUMER J. 2010. — The giant bite of a new raptorial sperm whale from the Miocene epoch of Peru. *Nature* 466: 105-108. https://doi.org/10.1038/nature09067

LAMBERT O., DE BUFFRÉNIL V. & MUIZON C. DE 2011. — Rostral density in beaked whales: diverse processes for a similar pattern. *Comptes Rendus Palevol* 10: 453-468. https://doi.org/10.1016/j.crpv.2011.03.012

LERICHE M. 1926. — Les poissons Neogènes. *Koninklijk Museum van Natuurlijke Historie, Verhandeling* 32: 369-471.

LOUWYE S., HEAD M. J. & DE SCHEPPER S. 2004. — Dinoflagellate cyst stratigraphy and palaeoecology of the Pliocene in northern Belgium, southern North Sea Basin, *Geological Magazine* 141 (3): 353-378. https://doi.org/10.1017/S0016756804009136

LOUWYE S. & DE SCHEPPER S. 2010. — The Miocene-Pliocene hiatus in the southern North Sea Basin (northern Belgium) revealed by dinoflagellate cysts. *Geological Magazine* 147: 760-776. https://doi.org/10.1017/S0016756810000191

LUO Z.-X. & GINGERICH P. D. 1999. — Terrestrial Mesonychia to aquatic Cetacea: transformation of the basicranium and evolution of hearing in whales. *University of Michigan Papers on Paleontology* 31: 1-98.

MARX F. G. & UHEN M. D. 2010. — Climate, critters, and cetaceans: Cenozoic drivers of the evolution of modern whales. *Science* 327: 993-996. https://doi.org/10.1126/science.1185581

MARX F. G. & FORDYCE R. E. 2015. — Baleen boom and bust: a synthesis of mysticete phylogeny, diversity and disparity. *Royal Society Open Science* 2: 140434. https://doi.org/10.1098/rsos.140434

MARX F., BOSSELAERS M. & LOUWYE S. 2016a. — A new species of Metopocetus (Cetacea, Mysticeti, Cetotheriidae) from the Late Miocene of the Netherlands. *PeerJ* 4: e1572. https://doi.org/10.7717/peerj.1572

MARX F., LAMBERT O. & UHEN D. 2016b. — Cetacean Paleobiology, *in* BENTON M. J. (ed.), *Topics in Paleobiology*. Wiley Blackwell, United Kingdom, 319 p.

MARX F. G., LAMBERT O. & MUIZON C. DE 2017. — A new Miocene baleen whale from Peru deciphers the dawn of cetotheriids. *Royal Society Open Science* 4: 170560. https://doi.org/10.1098/rsos.170560

MARX F. G., FITZGERALD E. M. G. & FORDYCE R. E. 2019a. — Like phoenix from the ashes: How modern baleen whales arose from a fossil "dark age". *Acta Palaeontologica Polonica* 64: 1-9. https://doi.org/10.4202/app.00575.2018

MARX F. G., POST K., BOSSELAERS M., MUNSTERMAN D. K. 2019b. — A large Late Miocene cetotheriid (Cetacea, Mysticeti) from the Netherlands clarifies the status of Tranatocetidae. PeerJ 7:e6426 https://doi.org/10.7717/peerj.6426

MOLINO G., MONTALBANO G., PONTREMOLI C., FIORILLI S. & VITALE-BROVARONE C. 2020. — Imaging techniques for the assessment of the bone osteoporosis-induced variations with particular focus on Micro-CT potential. *Applied Sciences* 10 (24): 8939. https://doi.org/10.3390/app10248939

MORGANE P. J., JACOBS M. S. & MC FARLAND W. L. 1980. — The anatomy of the brain of the bottlenose dolphin (*Tursiops truncatus*). Surface configurations of the telencephalon of the bottlenose dolphin with comparative anatomical observations in four other cetacean species. *Brain Research Bulletin* 5: 1-107. https://doi.org/10.1016/0361-9230(80)90272-5

MUNSTERMAN D. K. & BRINKHUIS H. 2004. — A southern North Sea Miocene dinoflagellate cyst zonation. *Netherlands Journal of Geosciences* 83 (4): 267-285. https://doi.org/10.1017/S0016774600020369

MUNSTERMAN D. K. 2007. — The results of age-assessment based on the palynological study of borehole Hoogdonk (B52C1978; Liessel, Peel Block, North Brabant): interval 9.2-445 m. *TNO Report* 2007-U-R0860/A.

MUNSTERMAN D. K., TEN VEEN J. H., MENKOVIC A., DECKERS J., WITMANS N., VERHAEGEN J., KERSTHOLT- BOEGEHOLD S. J., VAN DE VEN T. & BUSSCHERS F. 2019. — An updated and revised stratigraphic framework for the Miocene and earliest Pliocene strata of the Roer Valley Graben and adjacent blocks. *Netherlands Journal of Geosciences* 98: e8. https://doi.org/10.1017/njg.2019.10

ÖLSCHLÄGER H. H. A. & ÖLSCHLÄGER J. S. 2002. — Brain, *in* PERRIN W. F., WÜRSIG B. & THEWISSEN J. G. M. (eds), *Encyclopedia of Marine Mammals*. Academic Press, San Diego: 135-158.

OGG J. G., OGG G. & GRADSTEIN F. M. 2016. — *A Concise Geologic Time Scale*. Elsevier, Amsterdam, 234 p.

PETERS N. 2009. — *Brabant tussen walvissen en mastodonten, fossielen uit Liessel*. Nationaal Beiaard- en Natuurmuseum Asten en Oertijdmuseum De Groene Poort Boxtel, 110 p.

PETERS M. E., BOSSELAERS M. E. J., POST K. & REUMER W. F. 2019. — A Miocene leatherback turtle from the Westerschelde (The Netherlands) with possible cetacean bite marks: identification, taphonomy and cladistics. *Caenozoic Research* 19 (2): 121-133.

POST K., LOUWYE S. & LAMBERT O. 2017. — *Scaldiporia vandokkumi*, a new pontoporiid (Mammalia, Cetacea, Odontoceti) from the Late Miocene to earliest Pliocene of the Westerschelde estuary (The Netherlands). *PeerJ* 2017 (5): e3991. https://doi.org/10.7717/peerj.3991

POWELL A. J. 1992. — Dinoflagellate cysts of the Tertiary System, *in* POWELL A. J. (ed.), *A Stratigraphic Index of Dinoflagellate Cysts*. Chapman & Hall, London, 296 p. ISBN 0-412-36280-5

PYENSON N. D. & HOCH E. 2007. — Tortonian pontoporiid odontocetes from the Eastern North Sea. *Journal of Vertebrate Paleontology* 27 (3): 757-762. https://doi.org/d2ktvr

PYENSON N. D. & SPONBERG S. N. 2011. — Reconstructing body size in extinct crown cetacea (Neoceti) using allometry, phylogenetic methods and tests from the fossil record. *Journal of Mammalian Evolution* 18 (4): 269-288. https://doi.org/10.1007/s10914-011-9170-1

RACICOT R. A. & COLBERT M. W. 2013. — Morphology and variation in porpoise (Cetacea: Phocoenidae) cranial endocasts. *The Anatomical Record* 296: 979-992. https://doi.org/10.1002/ar.22704

RAMASSAMY B. 2016. — Description of a new long-snouted beaked whale from the Late Miocene of Denmark: evolution of suction feeding and sexual dimorphism in the Ziphiidae (Cetacea: Odontoceti). *Zoological Journal of the Linnean Society* 178 (2): 381-409. https://doi.org/10.1111/zoj.12418

REEVES R. R. 2009. — Conservation efforts, XII: Zoography of marine mammals, *in* PERRIN W. F., WÜRSIG B. & THEWISSEN J. G. M. (eds), *Encyclopedia of Marine Mammals*. Academic Press, San Diego: 294-297.

REIDENBERG J. S. & LAITMAN J. T. 2008. — Cetacean prenatal development, *in* PERRIN W. F., WÜRSIG B. & THEWISSEN J. G. M. (eds), *Encyclopedia of Marine Mammals*. 2nd edition. Academic Press, San Diego: 220-230. https://doi.org/10.1016/B978-0-12-373553-9.00056-0

SLATER G. J., GOLDBOGEN J. A. & PYENSON N. D. 2017. — Independent evolution of baleen whale gigantism linked to Plio-Pleistocene ocean dynamics. *Procedings of the Royal Society B: Biological Sciences*: 284: 20170546. https://doi.org/10.1098/rspb.2017.0546

STEEMAN M. 2009. — A new baleen whale from the Late Miocene of Denmark and early mysticete hearing. *Palaeontology* 52 (5): 1169-1190. https://doi.org/10.1111/j.1475-4983.2009.00893.x

STEEMAN M. 2010. — The extinct baleen whale fauna from the Miocene-Pliocene of Belgium and the diagnostic cetacean ear bones. *Journal of Systematic Palaeontology* 8 (1): 63-80. https://doi.org/10.1080/14772011003594961

SWOFFORD D. L. 2002. — PAUP: Phylogenetic Analysis Using Parsimony (and Other Methods), Version 4.0 Beta 10. *Sinauer Associates*, Sunderland.

THEWISSEN J. G. M., COOPER L. N., CLEMENTZ M. T., BAJPAI S., & TIWARI B. 2007. — Whales originated from aquatic artiodactyls in the Eocene epoch of India. *Nature* 450: 1190-1194. https://doi.org/10.1038/nature06343

VAN VLIET H. J., LAMBERT O., BOSSELAERS M., SCHULP A. S. & JAGT J. W. M. 2019. — A palaeogene cetacean from Maastricht, Southern Limburg The Netherlands. *Caenozoic Research* 19 (1): 95-113.

WALSH B. M. & BERTA A. 2011. — Occipital ossification of balaenopteroid mysticetes. *The Anatomical Record* 294: 391-398. https://doi.org/10.1002/ar.21340

Submitted on 24 December 2021;
accepted on 2 April 2022;
published on 27 October 2022.

APPENDICES

APPENDIX 1. — Mysticete species information, alphabetical list of fossil whale species/specimens in the text.

Atlanticetus patulus (Kellogg, 1968)	USNM 23690	holotype
Balaenoptera acutorostrata Lacépède, 1804	NMR 99903024 (juvenile specimen)	
'*Balaenoptera*' *ryani* Hanna & McLellan, 1924	CASG 1733	holotype
Brandtocetus chongulek Gol'din & Startsev, 2014	TNU Skull A	holotype
Caperea marginata Gray, 1864	NMR 9990-01449 (juvenile specimen)	
	IRSNB Reg. 1536 (adult specimen)	
Cephalotropis nectus Cope, 1896	UL 3	reffered specimen
Cetotherium rathkii Brandt, 1843	PIN 1840/1	holotype
Cetotherium riabinini Hofstein, 1943	NMNH-P 668/1	holotype
'*Diorocetus*' *chichibuensis* Yoshida, Kimura & Hasegawa, 2003	SMNH-VeF-62	holotype
Diorocetus hiatus Kellogg, 1968	USNM 16783	holotype
	3-D images: https://phenome10k.org/diorocetus-hiatus/	
'*Diorocetus*' *shobarensis* Otsuka & Ota, 2008	HMN-F00005	holotype
Herentalia nigra Bisconti, 2014	ZMA.MAM.5069, now held in Naturalis, Leiden	holotype
Heterocetus affinis (Van Beneden, 1886)	IRSNB M 605a-b	lectotype
Idiocetus longifrons Van Beneden, 1880	IRSNB M 719	lectotype
Isanacetus laticephalus Kimura & Ozawa, 2002	MFM 28501	holotype
Joumocetus shimizui Kimura & Hasegawa, 2010	GMNH-PV-2401	holotype
Tiucetus rosae Marx, Lambert & de Muizon, 2017	MNHN.F.PPI261	holotype
Mesocetus latifrons Van Beneden, 1880	IRSNB M 567	lectotype
Metopocetus hunteri Marx, Bosselaers & Louwye, 2016	NMR 9991-07729	holotype
Morenocetus parvus Cabrera, 1926	MLP 5-11	holotype
Parietobalaena campiniana Bisconti, Lambert & Bosselaers, 2013	IRSNB M 399	holotype
Parietobalaena laxata (Van Beneden, 1880)	IRSNB M 727	lectotype
Parietobalaena palmeri Kellogg, 1924	USNM 10668	holotype
	USNM 16119	referred specimen
Pelocetus calvertensis Kellogg, 1965	USNM 11976	holotype
***Persufflatius renefraaijeni* n. gen., n. sp.**	**MAB 010293**	**holotype (this publication)**
Piscobalaena nana Pilleri & Siber, 1989	SMNK PAL 4050	holotype
'*Plesiocetus*' *burtinii* Van Beneden, 1885	IRSNB M 676	lectotype

As a consequence of the revision of the genus *Plesiocetus* Van Beneden, 1859 by Bisconti & Bosselaers (2021), '*P.*' *burtinii* IRSNB M 676 is now considered a Balaenoidea indet.

'*Plesiocetus*' *dubius* Van Beneden, 1885	IRSNB M 652	lectotype

This isolated right periotic was referred to '*Aglaocetus*' *burtinii* by Steeman 2010, but differs from the latter and is therefore listed here under his original name. As a consequence of the revision of the genus *Plesiocetus* by Bisconti & Bosselaers (2021), '*P.*' *dubius* is now considered a Thalassotherii indet.

Titanocetus sammariensis Bisconti, 2006	MGB 1CMC 172 9073	holotype
Uranocetus gramensis Steeman, 2009	MSM p 813	holotype

APPENDIX 2. — Measurement of cavities, trabecular rods and trabecular plates on some bone samples of Fig. 25. Per bone sample 20 ad random measurements were performed (15 for sample 5). Abbreviations: **H**, height; **L**, length; **Nr**, number of the measurement; **plates**, trabecular plates; **rod**, trabecular rod; **T**, thickness; **W**, width.

Sample 1: anterior parietal at vertex. Cavities posterodorsal-anteroventrally oriented; on average about 3 times higher than wide. Rods on average about half as thick as the width of the cavities and slightly shorter than the hight of the cavities. Plates are on average almost as wide as high and half the hight of the cavities.

Nr	W cavity	H cavity	T rod	L rod	W plate	H plate
1	0.29	0.23	0.17	0.63	0.76	0.69
2	0.73	2.66	0.38	0.76	1.10	1.20
3	0.21	0.49	0.13	0.62	1.16	0.68
4	0.76	0.40	0.18	0.65	1.47	1.24
5	1.31	0.88	0.53	1.68	1.12	1.14
6	0.43	4.44	0.27	1.42	1.55	0.88
7	0.72	1.26	0.50	2.24	0.75	0.75
8	0.88	2.64	0.39	2.30	1.40	1.05
9	1.81	0.45	0.22	0.68	0.87	0.52
10	0.95	0.92	0.23	0.62	0.68	0.77
11	0.77	4.72	0.26	2.15	0.80	0.95
12	0.18	0.30	0.26	0.75	0.58	0.49
13	0.21	1.17	0.23	1.20	0.62	0.30
14	0.21	0.87	0.1	0.88	1.13	0.61
15	0.35	0.88	0.18	1.19	1.01	0.76
16	0.13	1.20	0.38	1.84	0.67	0.70
17	1.65	1.90	0.26	0.82	0.67	0.79
18	0.56	3.39	0.42	1.45	0.73	1.30
19	0.13	0.50	0.16	1.22	1.09	0.55
20	0.44	2.41	0.15	1.20	0.73	0.98
sum	12.72	31.71	5.61	24.30	18.89	16.35
mean	0.636	1.5855	0.2805	1.250	0.9445	0.8175

Sample 2: pterygoid-squamosal suture. Cavities mediolaterally oriented and elongated; on average about 2.5 times wider than high. Rods on average less than half as thick as the height of the cavities and elongated. Plates are on average almost as wide as high and a bit narrower than the hight of the cavities.

Nr	W cavity	H cavity	T rod	L rod	W plate	H plate
1	2.06	0.97	0.85	2.71	1.02	1.88
2	1.35	0.6	0.5	0.48	1.69	1.47
3	2.21	1.48	0.58	2.46	1.47	1.56
4	1.66	0.84	0.91	2.97	0.89	1.30
5	2.06	3.73	1.37	2.89	1.33	1.07
6	2.89	1.63	0.81	1.57	1.57	1.38
7	0.37	1.36	0.66	2.44	1.58	0.84
8	0.99	0.73	0.79	1.74	1.16	1.06
9	1.58	2.76	0.46	3.95	2.45	1.07
10	0.30	1.97	1.35	2.37	1.13	1.13
11	0.46	2.54	0.80	1.46	1.19	1.07
12	3.93	1.56	0.76	1.25	1.42	1.28
13	2.95	0.55	0.69	1.94	1.23	1.08
14	1.61	2.73	0.46	3.22	0.79	1.60
15	1.78	1.26	0.80	1.45	0.65	1.49
16	0.17	0.38	0.71	4.07	1.31	1.43
17	2.21	4.12	0.37	3.21	1.28	0.87
18	1.68	1.60	0.59	1.55	0.83	1.73
19	0.65	0.67	0.64	2.84	1.34	2.69
20	4.45	1.89	0.58	3.18	0.76	1.51
sum	35023	38.37	14.68	47.75	25.09	27.51
mean	1.7615	1.6685	0.7340	2.3875	1.2545	1.3755

Sample 3: anteroventral squamosal border. Cavities mediolaterally oriented; on average about 2.5 times wider than high. Rods thick; on average about as long as and half as thick as the width of the cavities. Plates are on average higher than wide and almost as high as the cavities.

Nr	W cavity	H cavity	T rod	L rod	W plate	H plate
1	0.31	0.18	0.74	0.21	0.82	1.74
2	2.20	0.49	0.46	3.87	0.68	0.61
3	1.25	0.52	0.56	2.39	0.58	0.91
4	2.86	0.52	0.42	2.82	0.54	0.94
5	1.60	0.53	0.38	1.73	0.66	0.84
6	1.85	1.03	0.42	4.72	0.74	0.94
7	3.42	0.83	0.46	2.73	0.87	0.95
8	0.50	0.59	0.91	0.15	0.85	1.05
9	1.15	0.27	1.79	0.57	0.84	0.96
10	3.04	2.42	0.44	2.70	0.66	1.06
11	5.12	1.18	0.31	5.04	1.09	0.63
12	2.61	0.70	0.30	3.22	0.58	1.18
13	3.00	1.06	0.47	2.73	0.75	1.47
14	5.18	1.22	0.74	2.56	0.86	1.20
15	1.19	1.45	1.41	0.45	0.87	0.58
16	0.41	0.32	0.21	1.29	0.57	0.90
17	1.98	0.71	0.17	1.93	0.65	1.07
18	0.89	1.24	0.30	2.49	0.89	1.09
19	3.86	0.89	0.50	3.59	0.87	1.22
20	0.41	0.33	1.20	0.42	0.79	0.94
sum	42.83	16.48	7.94	49.60	15.14	19.48
mean	2.1415	0.8240	0.3970	2.4800	0.7570	0.9740

Sample 5: posterolateral postglenoid process. Cavities slightly wider than high; rather small. Rods very thin and elongated; mainly horizontally oriented Plates very small and slightly wider than high

Nr	W cavity	H cavity	T rod	L rod	W plate	H plate
1	0.48	0.76	0.12	.065	0.45	0.42
2	1.02	0.87	0.21	0.99	0.41	0.32
3	0.87	0.43	0.24	0.85	0.43	0.40
4	0.71	0.94	0.14	0.71	0.33	0.29
5	0.54	0.30	0.14	0.79	0.43	0.31
6	1.16	0.61	0.14	1.52	0.32	0.49
7	0.80	0.84	0.13	1.30	0.56	0.38
8	0.79	0.82	0.10	1.95	0.71	0.30
9	1.44	0.67	0.15	0.90	0.34	0.33
10	1.70	0.75	0.11	1.01	0.27	0.29
11	1.21	1.07	0.12	0.91	0.23	0.37
12	0.92	1.30	0.09	0.97	0.42	0.52
13	1.23	0.93	0.11	1.18	0.46	0.24
14	1.64	0.62	0.13	1.04	0.62	0.37
15	0.63	0.57	0.13	0.59	0.21	0.51
sum	15.14	11.48	2.06	15.36	6.19	5.54
mean	1.0093	0.7653	0.1373	1.0240	0.4127	0.3693

APPENDIX 2. — Continuation.

Sample 7B: middle part of the anterior supraoccipital (at the longitudinal axis). Cavities dorsoventrally oriented; on average about 2.5 times higher than wide. Rods thick and on average 4 times longer than thick. Plates are on average almost as wide as high and 3 times wider than the rods.

Nr	W cavity	H cavity	T rod	L rod	W plate	H plate
1	0.45	1.89	0.74	3.04	1.14	2.29
2	0.57	2.07	0.68	2.98	1.46	0.88
3	0.64	1.72	0.25	1.52	1.54	1.14
4	1.59	0.83	2.65	0.42	2.85	2.07
5	2.44	0.74	0.67	3.01	1.09	0.90
6	1.09	2.15	0.69	2.53	2.04	1.22
7	0.72	3.05	0.18	1.83	0.94	1.35
8	0.40	2.39	0.45	2.43	1.17	0.89
9	0.27	2.32	0.72	2.54	0.85	0.84
10	0.25	0.57	0.74	2.96	1.04	0.61
11	0.86	3.68	0.77	3.02	–	–
12	0.0	1.02	0.43	0.91	–	–
13	0.59	4.79	0.68	4.04	–	–
14	0.40	1.51	0.23	1.61	–	–
15	0.77	2.46	0.25	2.00	–	–
16	2.16	1.04	0.53	1.21	–	–
17	0.24	2.32	0.37	0.72	–	–
18	0.27	1.14	1.00	0.48	–	–
19	0.21	0.39	0.38	2.48	–	–
20	1.05	0.61	0.44	0.59	–	–
sum	15.47	36.69	10.10	43.07	14.12	12.19
mean	0.7735	1.8345	0.5050	2.1535	1.412	1.219

Sample 8: base of zygomatic process. On average all features are much smaller in this section than in all the others. Cavities criss-cross oriented; on average slightly higher than wide. Rods relatively elongated and on average 4.5 times longer than thick. Plates are slightly higher than wide.

Nr	W cavity	H cavity	T rod	L rod	W plate	H plate
1	0.64	0.54	0.18	0.67	0.26	0.31
2	0.15	0.68	0.15	0.53	0.24	0.31
3	0.34	0.47	0.13	0.66	0.27	0.39
4	0.40	0.46	0.13	0.46	0.26	0.34
5	0.19	0.44	0.55	0.13	0.29	0.35
6	0.63	0.42	0.24	0.65	0.24	0.38
7	0.10	0.51	0.15	0.68	0.27	0.36
8	0.47	0.54	0.12	0.49	0.39	0.70
9	0.20	0.54	0.15	0.62	0.24	0.33
10	0.66	0.61	0.14	0.40	0.39	0.28
11	0.15	0.71	0.21	0.40	0.39	0.28
12	0.44	0.50	0.52	0.12	0.22	0.24
13	0.20	0.53	0.74	0.14	0.34	0.27
14	0.08	0.09	0.09	0.76	0.23	0.24
15	0.67	0.50	0.14	0.73	0.20	0.29
16	0.28	0.58	0.80	0.14	0.19	0.33
17	0.25	0.42	0.31	0.51	0.24	0.39
18	0.35	0.31	0.15	0.76	0.20	0.28
19	0.53	0.43	0.13	1.25	0.39	0.27
20	0.34	0.30	0.10	0.57	0.37	0.32
sum	7.070	9.560	2.870	12.900	5.480	6.820
mean	0.3535	0.4780	0.1435	0.6450	0.2740	0.3410

APPENDIX 3. — Late Tortonian faunal assemblage (not exhaustive) of (some) bigger marine vertebrates (except Selachii) in the Low Countries (Belgium and the Netherlands), Germany and Denmark.

Species	Superfamily	Group/family	Locality	Current taxonomic status
Acipenser sp. Linaeus, 1758	Acipenseriformes	Acipenseridae	Antwerp, Belgium; Liessel, the Netherlands	Peters 2009
Lophius sp. Linaeus, 1758	Lophioidea	Lophiidae	Liessel, the Netherlands	Peters 2009
Molidae sp. Bonaparte, 1832	Tetraodontoidei	Molidae	Antwerp, Belgium	Leriche 1926
Chelonia sp. Brongniart, 1800	Chelonioidea	Cheloniidae	Antwerp, Belgium	(undescribed)
Psephophorus polygonus von Meyer, 1847	Chelonioidea	Dermochelyidae	Western Scheldt River, the Netherlands; Borsbeek, Belgium	Peters *et al.* 2019
Batavipusa neerlandica Koretsky & Peters, 2008	Pinnipedia	Phocidae	Liessel, the Netherlands	Koretsky & Peters 2008
Frisiphoca aberatum Van Beneden, 1876	Pinnipedia	Phocidae	Borgerhout-Antwerp, Belgium	Dewaele *et al.* 2018
Frisiphoca affine Vanden Broeck, 1874	Pinnipedia	Phocidae	Deurne-Antwerp, Belgium	Dewaele *et al.* 2018
Nanophoca vitulinoides (Van Beneden, 1871)	Pinnipedia	Phocidae	Deurne/Borgerhout; Antwerp, Belgium	Dewaele *et al.* 2017a
Leptophoca proxima (Van Beneden, 1877)	Pinnipedia	Phocidae	Liessel, the Netherlands (Antwerp, Borgerhout, Borsbeek), Belgium	Dewaele *et al.* 2017b
Monotherium delognii Van Beneden, 1876	Pinnipedia	Phocidae	Deurne, Antwerp, Belgium	Dewaele *et al.* 2018
Choneziphius planirostris Cuvier, 1824	Odontoceti	Ziphiidae	Antwerp, Belgium; Western Scheldt River, the Netherlands	Lambert 2005a
Dagonodum mojnum Ramassamy, 2016	Odontoceti	Ziphiidae	Denmark	Ramassamy 2016
Kentriodon hoepfneri Kazár & Hampe, 2014	Odontoceti	Kentriodontidae	Germany	Kazár & Hampe 2014
? *Physeterula dubusi* Van Beneden, 1877	Odontoceti	Physeteroidea	Borsbeek, Belgium	Lambert 2008
cf. *Pontistes* Burmeister, 1885	Odontoceti	Pontoporiidae	Eastern North Sea	Pyenson & Hoch 2007
Protophocaena minima Abel, 1905	Odontoceti	Pontoporiidae	Southern North Sea	Lambert & Post 2005
'*Scaldicetus*' *caretti* Du Bus, 1867 IRSNB M512	Odontoceti	Physeteroidea	Antwerp, Belgium Liessel, the Netherlands	Lambert & Bianucci 2019
Scaldiporia vandokkumi Post, Louwye & Lambert, 2017	Odontoceti	Pontoporiidae	Western Scheldt River, the Netherlands	Post *et al.* 2017
Thallasocetus sp. Abel, 1905	Odontoceti	Physeteroidea	Antwerp, Belgium	Alfsen *et al.* 2021
Xiphiacetus cristatus Du Bus, 1872	Odontoceti	Eurhinodelphinidae	Borsbeek, Belgium	Lambert 2005b
Ziphirostrum Marginatum Du Bus, 1868	Odontoceti	Ziphiidae	Borsbeek, Deurne, Antwerp, Belgium/Scheldt River, the Netherlands	Lambert 2005a
Archaebalaenoptera liesselensis Bisconti, Munsterman, Fraaije, Bosselaers & Post, 2020	Mysticeti	Balaenopteridae	Liessel	Bisconti *et al.* 2020
Nehalaennia devossi Bisconti, Munstermann & Post, 2019	Mysticeti	Balaenopteridae	Western Scheldt River, the Netherlands	Bisconti *et al.* 2019
aff. '*Parietobalaena*' (*Heterocetus*) *affinis* (Van Beneden, 1880)	Mysticeti	Cetotheriidae	Borsbeek, Belgium	*sensu* Steeman 2010
Tranatocetus argillarius Roth, 1978	Mysticeti	Cetotheriidae	Gram, Denmark	Marx *et al.* 2019
Tranatocetus maregermanicum Marx, Post, Bosselaers & Munstermann, 2019	Mysticeti	Cetotheriidae	Western Scheldt River	Marx *et al.* 2019
Uranocetus gramensis Steeman, 2009	Mysticeti	Cetotheriidae	Gram, Denmark	Marx & Fordyce 2015

APPENDIX 4. — Measurements (in mm) of the cranium and the vertebral bodies (corpus) of the adult specimen of *Caprerea marginata* (Gray, 1846) (IRSNB Reg. 1536). Abbreviations: **Ca**, caudal vertebrae; **Cerv**, cervical vertebrae; **H**, height; **L**, length; **Lu**, lumbar vertebrae; **Th**, thoracic vertebrae; **W**, width; height and width were measured at the posterior side of the vertebral corpus, the length was measured ventrally. Total body length of the specimen (as mounted): 5995 mm.

***Caperea marginata* IRSNB Reg. 1536 (in mm)**

Cranium		Vertebrae	Cerv 1-6	Cerv 7
Height cranium (posterior)	330	H corpus posterior	66	78
bizygomatic width	725	W corpus posterior	175	90
Length cranium; condylobasal length (CBL)	1400	L corpus ventral	120	45

***Caperea marginata* IRSNB Reg. 1536 (in mm)**

Th 1	Th 2	Th3	Th 4	Th 5	Th6	Th 7	Th 8	Th 9	Th 10	Th 11	Th 12	Th 13	Th 14	Th 15	Th 16	Th 17
80	79.3	80.9	74.0	76.4	73.1	79.2	82.2	84.2	85.1	89.6	90.2	90.7	94.1	95.2	98.0	100.3
97.7	93.7	103.0	101.0	97.5	99.9	96.0	98.7	100.9	101.7	101.9	109.8	110.1	109.1	111.3	116.2	119.4
47	57.7	65.0	75.0	92.7	102.7	108.7	124.7	128.5	133.5	138.7	145.0	149.2	152.0	165.0	173.0	178.0

***Caperea marginata* IRSNB Reg. 1536 (in mm)**

Lu 1	Sacr 1	Ca 1	Ca 2	Ca 3	Ca 4	Ca 5	Ca 6	Ca 7	Ca 8	Ca 9	Ca 10	Ca 11	Ca 12	Ca 13	Ca 14	Ca 15
103.1	124.0	126.0	135.3	130.1	137.8	125.1	107.5	98.0	91.2	76.0	73.6	58.2	44.0	35.0	26.0	15.5
113.6	121.6	115.0	111.9	112.1	110.1	102.9	95.0	82.5	88.4	81.6	63.6	57.0	49.0	36.8	32.0	23.8
185.0	185.0	185.0	173.0	163.0	152.0	139.0	125.5	96.5	66.8	59.0	57.7	55.8	46.0	39.3	29.0	22.5

APPENDIX 5. — Modified matrix after Bisconti *et al.* 2020: https://doi.org/10.5852/geodiversitas2022v44a30_s1

APPENDIX 6. — Modified matrix after Duboys de Lavigerie *et al.* 2020: https://doi.org/10.5852/geodiversitas2022v44a30_s2